Experimental and Numerical Comparison of Flexural Capacity of Light Gage Cold Formed Steel Roof Deck

by

Dawid Gwozdz

A Report Submitted to the Faculty of the

Milwaukee School of Engineering

in Partial Fulfillment of the

Requirements for the Degree of

Master of Science in Civil Engineering

Milwaukee, Wisconsin

August 2017

Abstract

This paper presents an analysis of experimental data and compares it to two numerical analysis methods of light gage cold formed steel roof deck. The flexural capacity was determined upon the first failure mode of the light gage cold formed steel roof deck. A comparison of the experimental data was made to both the effective width method and the direct strength method. The objective of the comparison was to have a physical test provide the actual behavior of the light gage cold formed steel roof deck and grade how well the numerical analysis, effective width and direct strength methods, compare against the results. Material testing samples were taken from the steel roof deck and evaluated for the actual yield stress. This allowed for the most accurate comparison between the experimental results with the numerical analysis since the exact yield strength was used in calculation. It was found that the effective width method and the direct strength method vary in their prediction of the nominal moment capacity across material grades and deck thickness but tend to converge to a constant ratio, Mn_{DSM}/Mn_{EWM}, at higher deck gages. The effective width method was found to be more accurate for thinner gage steel roof deck, while the direct strength method was more found to be more accurate for thicker gage steel roof deck. The effective width method was great at extracting the most strength out of steel roof deck, particularly the thinner gage ones, while the direct strength method was a much quicker process to find the flexural capacity of the deck. Both methods can be used to determine the capacity of the deck and it is up to the end user to determine which method is appropriate for the given application.

Acknowledgments

The advisor on this project is Dr. Christopher Raebel. Dr. Raebel has been an immense help in coordinating, advising and assisting with testing on this project. Dr. James Fisher and Dr. Tom Sputo have also assisted in this project with advice on testing configurations and methods of analysis. Additional thanks to Joshua Buckholt from CSD Structural Engineers for his expertise in the analysis of cold formed steel shapes and both the Effective Width Method and the Direct Strength Method.

NRCA has generously donated to the funding for this project. The SDI had also donated funding to aid in this project's success. The process of getting steel deck donated for this project was coordinated with SDI, specifically with the help of Dr. Tom Sputo and Mark Graham. Additionally, AISI also generously contributed funding for this project.

Finally, a generous donation of steel roof deck from CANAM Group made this project viable as this was the critical component to the success of this study.

Table of Contents

List of Figures

List of Tables

Nomenclature

Symbols

Degrees	=	measure of the angle between the flange and web
F_y	=	yield stress of material (ksi)
ksi	=	kips per square inch
kip	=	kip
kips	=	kips
kip-ft	=	kip-feet
kip-in.	=	kip-inch
lb	=	pound
M_{crd}	=	critical elastic distortional buckling moment (k-in.)
M_{cre}	=	critical elastic lateral-torsional buckling moment (k-in.)
M_{crl}	=	critical elastic local buckling moment (k-in.)
M_n	=	nominal flexural strength (k-in.)
M_{nd}	=	nominal flexural strength for distortional buckling (k-in.)
M_{ne}	=	nominal flexural strength for lateral-torsional buckling (k-in.)
M_{nl}	=	nominal flexural strength for local buckling (k-in.)
M_y	=	yield moment (S_gF_y) (k-in.)
Mn_{DSM}	=	nominal flexural strength using Direct Strength Method (kip-in.)
Mn_{EWM}	=	nominal flexural strength using Effective Width Method (kip-in.)
Radians	=	measure of the angle between the flange and web
S_g	=	elastic section modulus of gross section (kip-in.)

Abbreviations

AISI	=	American Iron and Steel Institute
CSEC	=	Construction Science and Engineering Center
CUFSM	=	Cornell University Finite Strip Method
DL	=	Dead Load
DSM	=	Direct Strength Method
EWM	=	Effective Width Method
HSS	=	Hollow Structural Section
LVDT	=	Linear Variable Differential Transformer
MSOE	=	Milwaukee School of Engineering
MTS	=	MTS Systems Corporation

Glossary

Linear Variable Differential Transformer (LVDT) – a type of electrical transformer used for measuring linear displacement.

MTS System (MTS) – a data collection system that applies a specified load using hydraulic rams and collects force and displacement readings.

Chapter 1.

Introduction, Literature Review and Numerical Analysis Methods

1.0 Introduction

1.0.1 Project Origin

This project stemmed from a proposal for testing steel roof deck for membrane fastener pullout. Mechanically attached roofing membranes load the steel roof deck in uplift in a more severe manner than uniformly adhered membranes. Quantifying the additional usable strength of the deck will improve the overall competitiveness of steel deck roofs. The project evolved into a larger project where the flexural capacity of the roof deck would be evaluated and compared to numerical results. A prior study conducted at the University of Florida [1] on the application of the Direct Strength Method (DSM) and Effective Width Method (EWM) to metal roof deck showed differing results, and more investigation was necessary to identify the source of discrepancy and the accuracy of the numerical models as compared to in-situ testing.

1.0.2 Description of the Project

The current research initiative intents to close the loop by testing the flexural strength of thin gage, cold formed steel deck roof panels and comparing the results from the experimental study to the capacities predicted by both DSM and EWM results. The current study will set the stage for additional steel deck flexural studies, particularly those related to floor deck panels with different profiles than those used for roof deck.

1.0.3 Justification of the Project

Studies conducted at the University of Florida [1] uncovered discrepancies between numerical results found using the DSM and EWM when evaluating roof deck in flexure. Future studies were recommended as a conclusion of that project. The current research initiative follows that recommendation and adds to the body of knowledge of the flexural capacity of light gage roof deck. The author hopes that the results of this study could impact current provisions in the American Iron and Steel Institute (AISI) S100 Standard.

1.1 Literature Review

There have been many studies [1, 2, 3, 4, 5] conducted on the behavior of cold formed steel shapes in recent years and many new developments have been made to more quickly and accurately numerically determine the capacity of these different shapes.

The cross-sections typically used in cold-formed steel member design are thin, light and efficient [4]. These shapes allow for economy in construction, being able to provide a substantial strength-to-weight ratio and ease of manufacturing. The design cost that often comes with these shapes is that their thin elements buckle in more complex fashions then heavier, hot-rolled shapes [4]. There are a few key buckling modes that cold-formed steel cross-sections exhibit, including local buckling, distortional buckling and lateral-torsional buckling. Local buckling is where an individual plate element within the shape's cross-section buckles when a compressive stress is applied to the cross-section. Distortional buckling is when a local rotation is observed in one or more of the plate elements within the cross-section. Lateral torsional buckling occurs when the entire

cross-section is affected and a global rotation occurs, often with no other local deformations on the cross-sectional shape [5].

These complex failure modes happen at different half wavelengths. The half wavelengths are the length of the buckled area along the length of the member. The buckle length is half of a typical sine wave, which is where the name is derived. For local buckling this length is often short in length, as the name implies. The length of these half wavelengths increases as one goes from local buckling to distortional buckling and finally to lateral torsional buckling [4].

Attempting to determine the flexural capacity of these shapes and being able to evaluate all failure modes can be mathematically complex. The unique challenge with cold-formed steel is that the entire cross-section will not be able to contribute equally to the strength. The different plate elements that make up the cross-section may become ineffective at, for example, the middle of a wider section or at the end of an unstiffened edge. This leads to consuming more exhaustive analysis of cross-sections prone to local failures. Fortunately, through the aid of recent software advances, one can efficiently determine a cross-section's capacity.

One such software is the Cornell University Finite Strip Method (CUFSM) [4]. The finite strip method divides the cross-section into small strips like that of a finite element analysis. Figure 1 shows an illustrated view of how a typical cross-section is divided into strips, the degrees of freedom that each of the strips are allowed to have and how a "traction edge vector" applies. This illustration is from a conventional finite strip method example; however, the CUFSM is based on this method and adds the feature of decomposing the different buckling modes allowing for a more detailed solution.

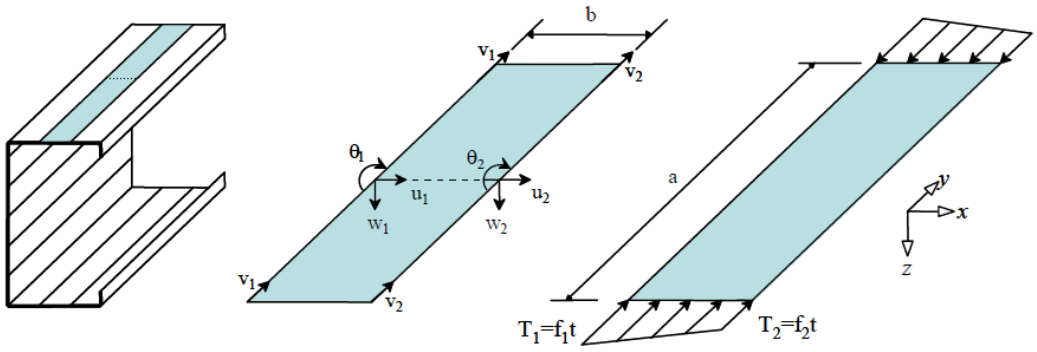

Figure 1: Finite Strip Method Example [4].

The finite strip method is similar to a finite element analysis with fewer degrees of freedom. A finite element analysis model is possible to do for a cold-formed steel cross-section. Typical difficulties arise, such as selection of an appropriate element type to represent the steel deck. Using a finite strip effectively solves issues such as these and reduces the size of the model.

1.1.1 General CUFSM Analysis Procedure

The software package utilized in the current research is, coincidentally, also called CUFSM [2]. This software employs the direct strength method of analysis which uses cross-section elastic buckling solutions as the primary input to the strength prediction. This software is utilized to develop a numerical solution of steel deck's flexural capacity. The title screen for the software is shown in Figure 2 (in order to show the version and reference for the program).

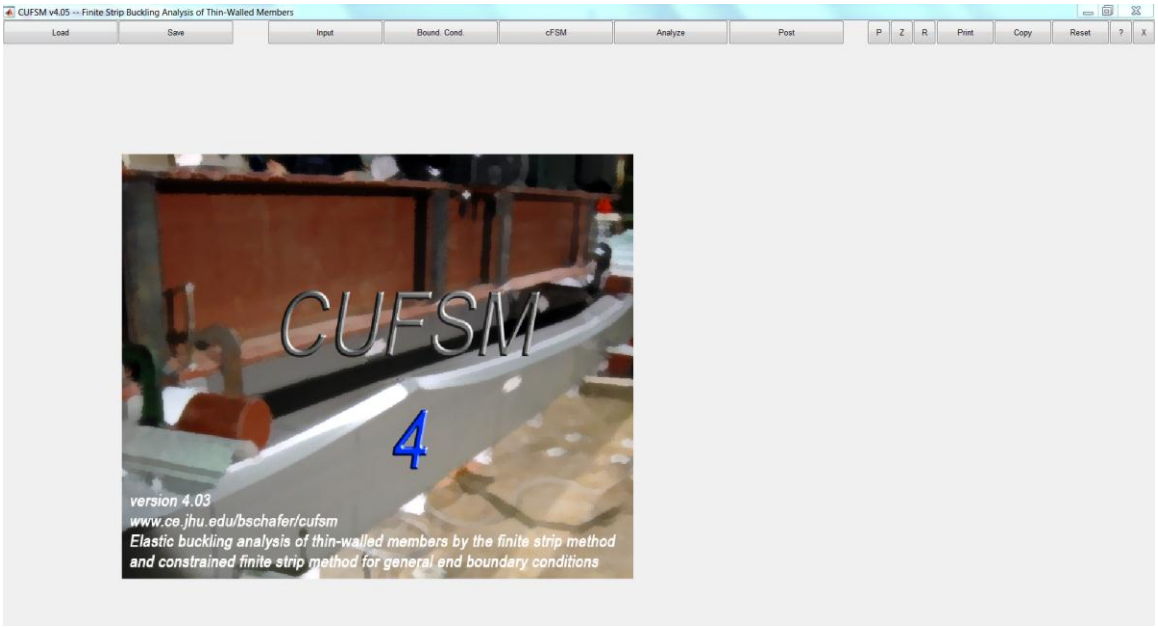

Figure 2: CUFSM Main Menu.

The user inputs a geometry using nodes, elements and material types into the user interface. Figure 3 shows the general input menu (i.e., preprocessor) of the CUFSM software.

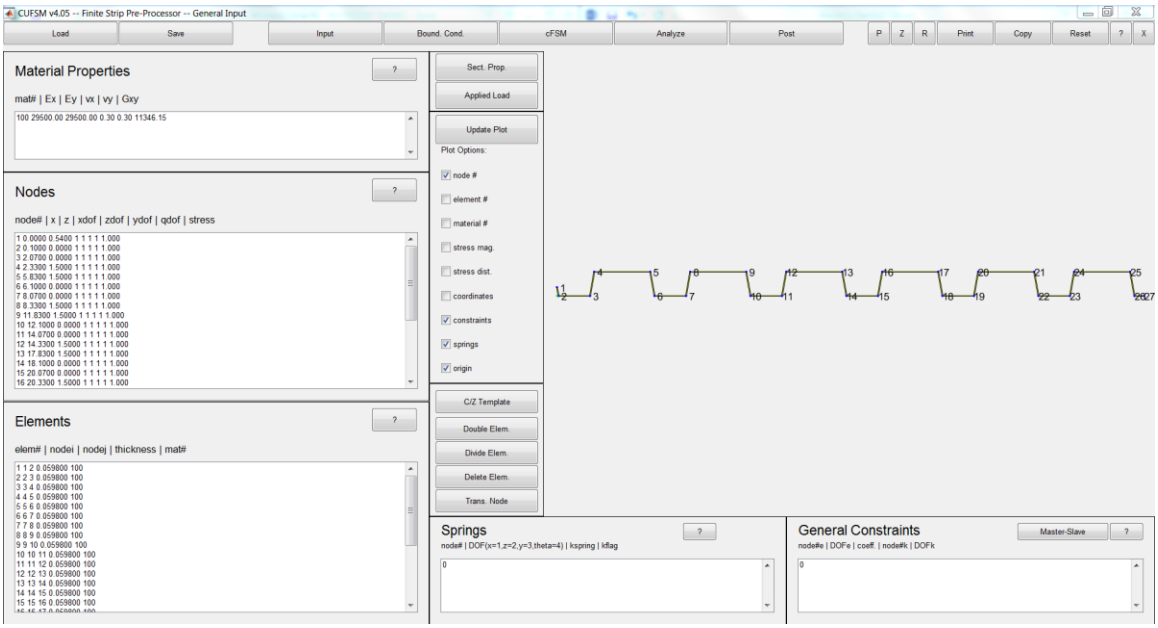

Figure 3: Cross-Section Definition (Input).

The user can then define a loading on the cross-section in the form of a stress distribution. This covers the possibilities of using shapes as tension, compression or flexural members. The software allows a yield stress to be input and a maximum moment that would cause initial yield. Figure 4 illustrates the sub-menu in the input section.

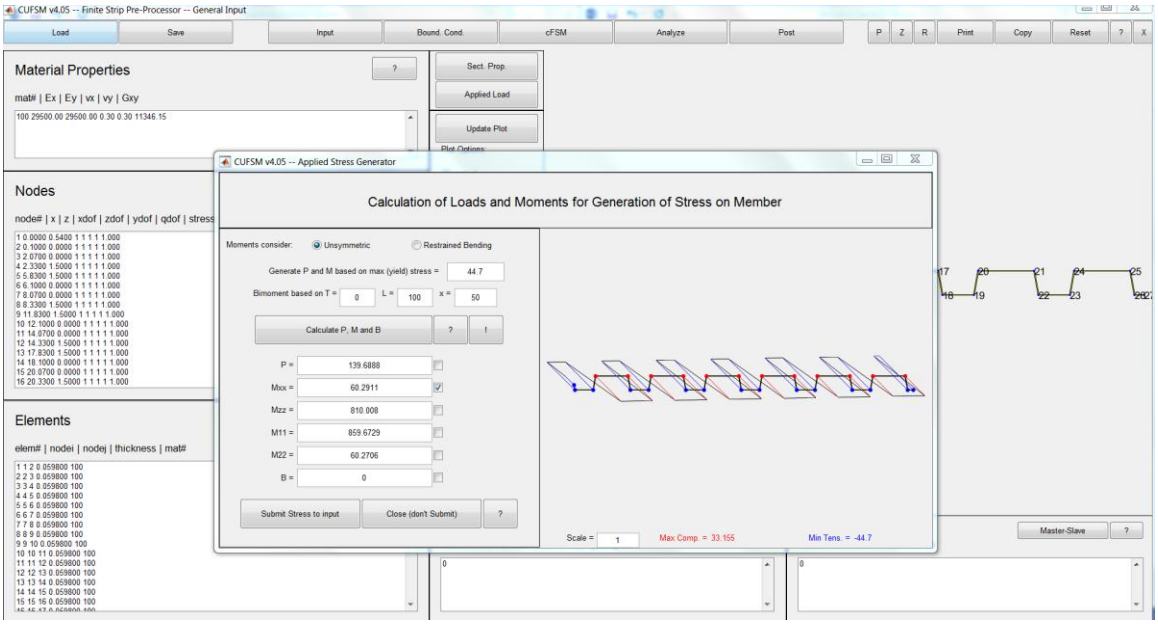

Figure 4: Stress Distribution Input.

The next step is to input the half wavelength that the software will use to determine when the failure mode will occur. For the current research, a preprocessor was utilized that generates half wavelengths for the user to input into CUFSM [1]. Figure 5 illustrates the input of these values. The number and difference between values is important here as the more values input, the greater the accuracy of the final answer as the software can analyze buckling over more lengths.

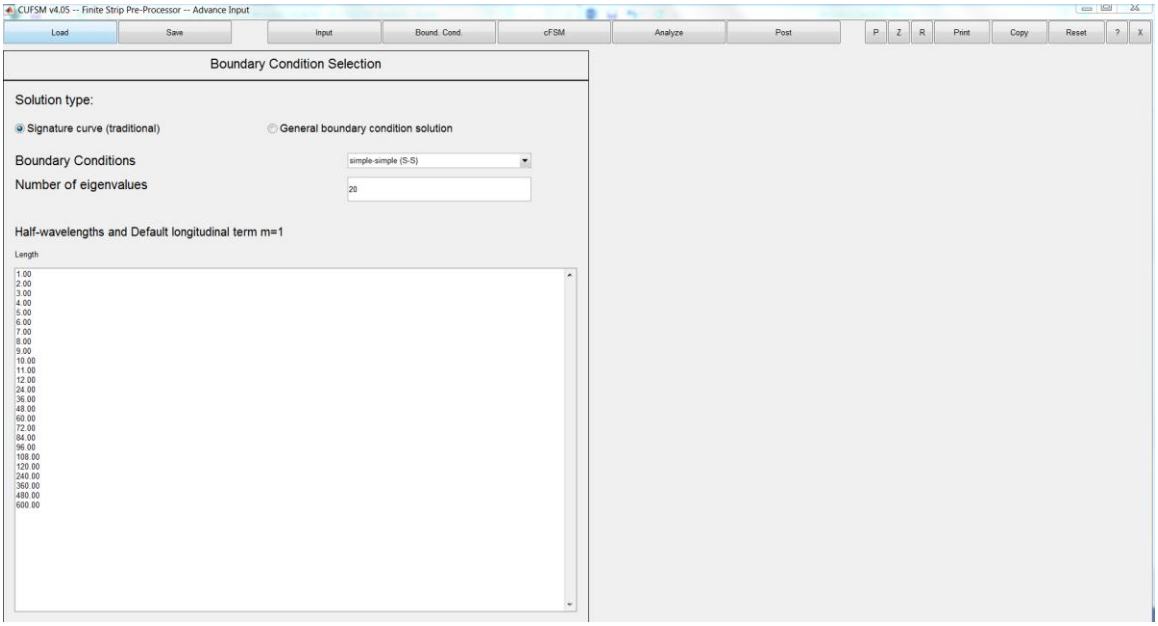

Figure 5: Half Wavelength Input.

The final step before analyzing the shape is to turn on the base vectors so all the different failure modes (local, distortional, global) can be classified in post processing if so desired. The base vectors are the normalized version of each buckling types (global, distortional, local and other) [2]. This is done so that the results can be compared correctly in the signature curve. The software can automatically determine these vectors based on the geometry input before and the density of the mesh. Figure 6 shows how the base vectors are input to the program.

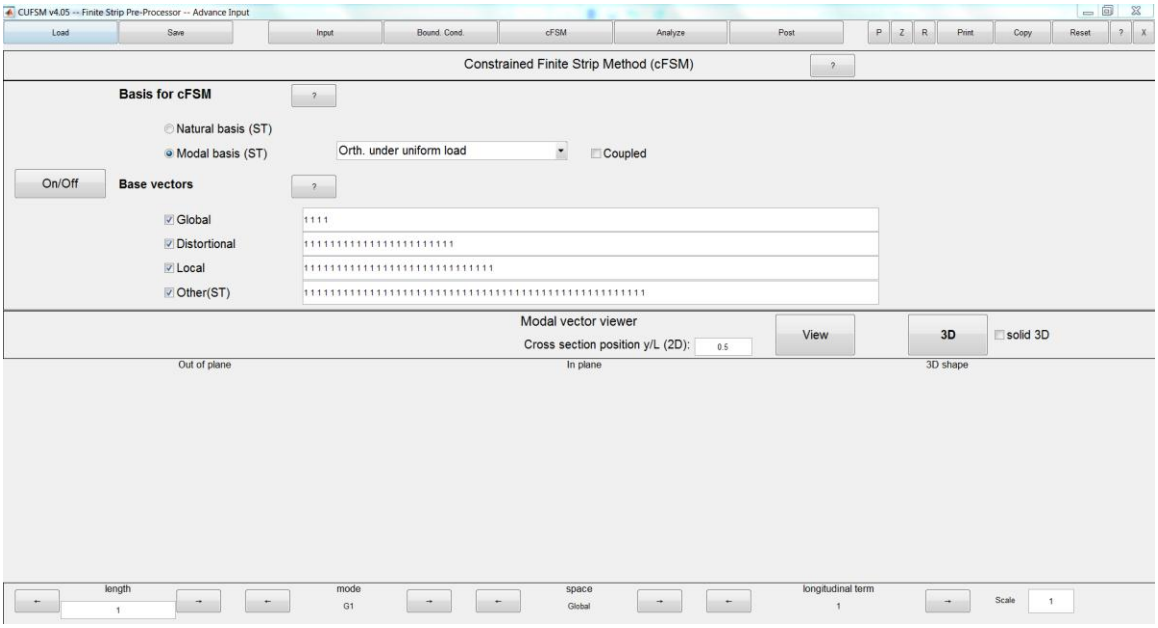

Figure 6: Base Vector Input.

Once the user has completed all of these steps, the model can be analyzed.

1.2 Effective Width Method

The Effective Width Method can be used to analyze a cold formed steel shape. The concept behind the effective width method is that not all of the cross-section is effective and contributing equally, or even significantly, to the flexural capacity [1]. For example, the top of the flute in a cross-section of steel roof deck that is not stiffened is so thin and flexible that it does not completely contribute to the flexural strength when a compressive stress is applied to it. The areas that are more effective are typically around the corners and bends of a shape as the corner is much stiffer then the midspan of the flute. Figures 7 and 8 illustrate how the stress is theoretically distributed across the cross-section.

Figure 7: Effective Compression Flange [1].

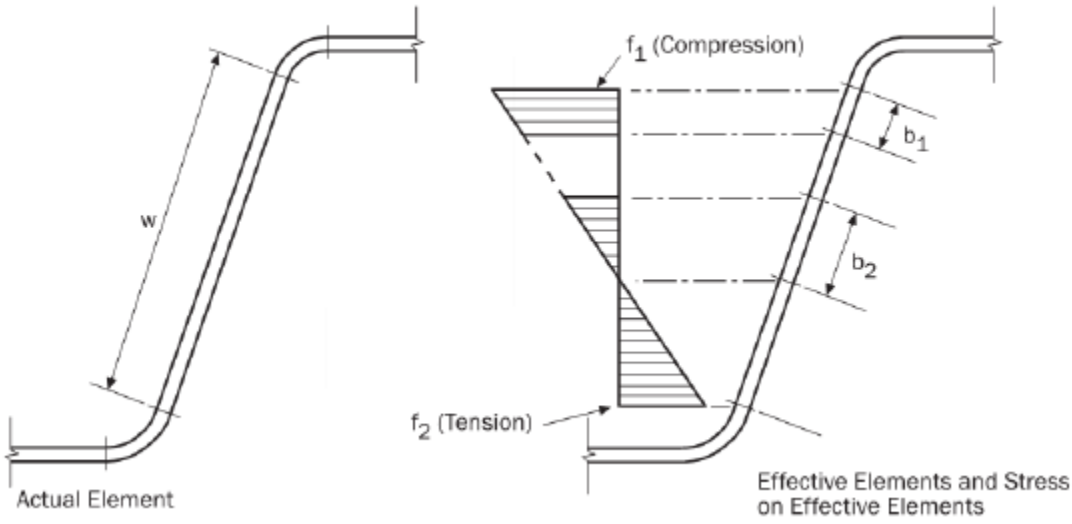

Figure 8: Effective Web Sections [3].

Figures 7 and 8 show the effective width of the compression flange and how the stresses are concentrated around the corners. A similar approach is applied to the web, where only a portion of the web is considered effective. The stress is a linear distribution along the entire depth of the section where either the extreme tension or compression fiber are at first yield. The portion of the web that is in compression has two areas that can be considered as effective. The first area is right next to the bend that leads to the compression flange. The other area is just above the neutral axis of the stress distribution. Finally, the portion of the cross-section that is in tension is fully effective since there is

no buckling in this region because the entire section is in tension. Since the lengths of the effective width in the web portion of the shape are based on the location of the neutral axis, the location of the neutral axis is assumed and then verified by comparing the total tension and compression force couple. This is an iterative process of assuming a location for the neutral axis, solving for the effective widths and subsequent areas from the assumed neutral axis and comparing the resultant tension force with the compression force. Once the forces balance, it is assumed that the correct neutral axis location has been determined and the resulting flexural capacity can be accurately calculated.

1.3 Direct Strength Method

Once the CUFSM software analyzed the cross-section a signature curve was produced. A signature curve is a graph that lists points of interest where a particular failure mode exists. The horizontal coordinate is the half wavelength at which the failure occurs and the vertical coordinate is a load factor that is used in equations that evaluate the different buckling and yield failure modes [1, 6]. Figure 9 illustrates an example of a signature curve for typical 16 gage steel roof deck.

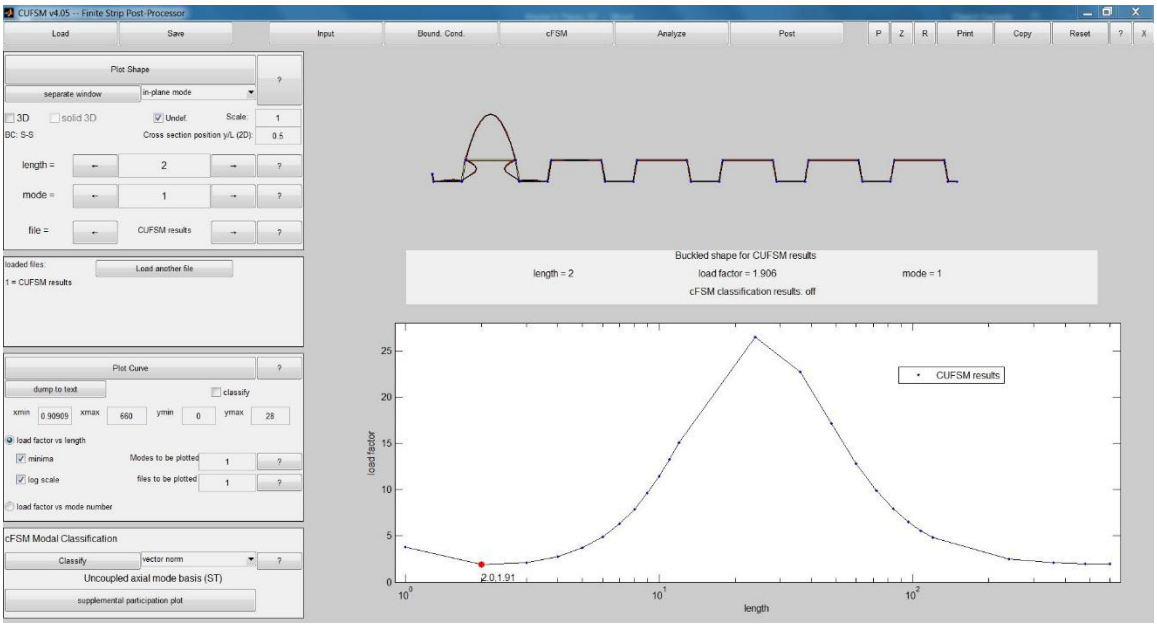

Figure 9: Example of a Signature Curve for 16 Gage Deck Signature Curve.

The results from the finite strip analysis are used to determine a flexural capacity based on lateral torsional buckling, local buckling, yielding and distortional buckling. For the limit state of yielding,

$$M_y = F_y S_{\pm} \tag{1}$$

where

$F_y = yield\ strength\ from\ material\ testing\ [ksi]$,

$S_{\pm} = positive\ or\ negative\ elastic\ section\ modulus\ [in^3]$.

The next step is to extract the values from the signature curve and use them in their respective capacity calculations. The third minima value from the signature curve is typically used in the calculation of lateral torsional buckling; however, since lateral-torsional buckling not a realistic failure mode due to the wide, flat shape of the deck, the highest value from the signature curve can also be taken. The load factor is input to the equation for critical elastic moment:

$$M_{cre} = Load\ Factor_{LTB} \times M_y. \quad (2)$$

Next, some comparisons are made to apply the correct formula to calculate the actual flexural capacity with respect to lateral torsional buckling:

$For\ M_{cre} < 0.56 \times M_y,$

$$M_{ne} = M_{cre}. \quad (3)$$

$For\ 2.78 \times M_y \geq M_{cre} \geq 0.56 \times M_y,$

$$M_{ne} = \frac{10}{9} \times M_y \times \left(1 - \frac{10 \times M_y}{36 \times M_{cre}}\right). \quad (4)$$

$For\ M_{cre} > 2.78 \times M_y,$

$$M_{ne} = M_y. \quad (5)$$

The next capacity calculation is for local buckling. The local buckling load factor is the first minima value from the signature curve. Therefore:

$$M_{crl} = Load\ Factor_{LOCAL} \times M_y. \quad (6)$$

Next, determine which equation is used to determine the local buckling strength:

$For\ \lambda_l \leq 0.776,$

$$M_{ne} = M_{crl}. \quad (7)$$

$For\ \lambda_l > 0.776,$

$$M_{nl} = \left(1 - 0.15 \times \left(\frac{M_{crl}}{M_{ne}}\right)^{0.4}\right) \times \left(\frac{M_{crl}}{M_{ne}}\right)^{0.4} \times M_{ne}, \quad (8)$$

$$where\ \lambda_l = \sqrt{\frac{M_{ne}}{M_{crl}}}. \quad (9)$$

Finally, the distortional buckling strength is calculated. Its load factor is typically the second minima on the signature curve. Similar to lateral torsional buckling, this is

also typically an unrealistic failure mode for steel roof deck so the highest value on the signature curve can be taken as the load factor. Thus,

$$M_{crl} = Load\ Factor_{DIST} \times M_y.$$

And (10)

$For\ \lambda_d \leq 0.673,$

$$M_{nd} = M_y. \quad (11)$$

$For\ \lambda_d > 0.673,$

$$M_{nl} = \left(1 - 0.22 \times \left(\frac{M_{crd}}{M_y}\right)^{0.5}\right) \times \left(\frac{M_{crd}}{M_y}\right)^{0.5} \times M_y, \quad (12)$$

$$where\ \lambda_l = \sqrt{\frac{M_y}{M_{crd}}}. \quad (13)$$

The flexural capacity is the minimum of M_{nd}, M_{ne} and M_{nl}.

Now, the results from the finite strip analysis shown in Figure 9 are used to determine a flexural capacity based on lateral torsional buckling, local buckling, yielding and distortional buckling. For the limit state of yielding,

$$M_y = F_y S_{\pm}. \quad (1)$$

This example will use a yield stress of 44.7 ksi. This yield stress magnitude was determined through material testing. Details related to the material testing results will be discussed later in this report.

The positive or negative elastic section modulus are taken from the CANAM steel roof deck catalog [7] for the steel roof deck used in the experimental program. For this example, a value of 1.23 in.^{3} is used. Therefore, the yield moment would equal:

$$M_y = (44.7ksi)(1.23in.^3), \quad (1)$$

$$M_y = 54.98\ kip - in.$$

The third minima value from the signature curve is typically used in the calculation of lateral torsional buckling; however, since lateral-torsional buckling not a realistic failure mode due to the wide, flat shape of the deck, the highest value from the signature curve is taken at 26.464. The load factor is input to the equation for critical elastic moment:

$$M_{cre} = Load\ Factor_{LTB} \times M_y, \tag{2}$$

$$M_{cre} = 26.464 \times 54.98\ kip - in.,$$

$$M_{cre} = 1{,}455\ kip - in.$$

Next, some comparisons are made to apply the correct formula to calculate the actual flexural capacity with respect to lateral torsional buckling:

$$For\ M_{cre} < 0.56 \times M_y,$$

$$M_{ne} = M_{cre}. \tag{3}$$

$$For\ 2.78 \times M_y \geq M_{cre} \geq 0.56 \times M_y,$$

$$M_{ne} = \frac{10}{9} \times M_y \times \left(1 - \frac{10 \times M_y}{36 \times M_{cre}}\right). \tag{4}$$

$$For\ M_{cre} > 2.78 \times M_y,$$

$$M_{ne} = M_y. \tag{5}$$

In this case, Equation (1) controls and the lateral torsional buckling capacity is the same as that for yielding. The local buckling load factor is the first minima value from the signature curve at 1.91. Therefore:

$$M_{crl} = Load\ Factor_{LOCAL} \times M_y, \tag{6}$$

$$M_{crl} = 1.91 \times 54.98\ kip - in,$$

$$M_{crl} = 105\ kip - in.$$

Next, determine which equation is used to determine the local buckling strength:

$For\ \lambda_l \leq 0.776,$

$$M_{ne} = M_{crl}. \tag{7}$$

$For\ \lambda_l > 0.776,$

$$M_{nl} = \left(1 - 0.15\times\left(\frac{M_{crl}}{M_{ne}}\right)^{0.4}\right)\times\left(\frac{M_{crl}}{M_{ne}}\right)^{0.4}\times M_{ne}, \tag{8}$$

$$where\ \lambda_l = \sqrt{\frac{M_{ne}}{M_{crl}}}. \tag{9}$$

In this case, lambda (λ) is less than 0.776, so the local buckling strength is equal to the yield strength, M_{ne}.

The distortional buckling strength load factor is typically the second minima on the signature curve. Similar to lateral torsional buckling, this also would not control as a rotation in the cross-section would be needed. Therefore, the highest value on the signature curve was taken as the load factor:

$$M_{crl} = Load\ Factor_{DIST}\times M_y, \tag{10}$$

$For\ \lambda_d \leq 0.673,$

$$M_{nd} = M_y. \tag{11}$$

$For\ \lambda_d > 0.673,$

$$M_{nl} = \left(1 - 0.22\times\left(\frac{M_{crd}}{M_y}\right)^{0.5}\right)\times\left(\frac{M_{crd}}{M_y}\right)^{0.5}\times M_y, \tag{12}$$

$$where\ \lambda_l = \sqrt{\frac{M_y}{M_{crd}}}. \tag{13}$$

In this case, λ_d was less than 0.673, so the distortional buckling strength is equal to the yield strength, M_{ne}.

The flexural capacity is the minimum of M_{nd}, M_{ne} and M_{nl}. Since all the different checks for the different buckling modes resulted in the yield strength controlling the flexural capacity, the actual flexural capacity is:

$$M_n = 54.98\ kip - in.$$

1.4 Comparing DSM and EWM Results

A prior study by Dudenbostel [1] considered the flexural capacity of 1.5B deck using both the DSM and the EWM. Roof deck gages 16, 18, 20, 22 and 24 were included in the study. Table 1 shows a comparison between the nominal moment capacity using the DSM and EWM for 40 ksi steel roof deck. Both the positive and negative moment capacities are included in the table. Table 2 shows a similar comparison for 50 ksi roof deck.

Table 1: Nominal Moment Capacity - DSM and EWM Comparison (F_y = 40 ksi) [1].

Deck	Orientation	DSM M_n(kip-in.)	EWM M_n (kip-in.)
1.5WR22	Positive	16.86	20.29
1.5WR20	Positive	23.16	25.36
1.5WR18	Positive	36.45	34.69
1.5WR16	Positive	47.26	44.71
1.5WR22	Negative	23.52	22.21
1.5WR20	Negative	28.53	27.46
1.5WR18	Negative	37.62	36.22
1.5WR16	Negative	47.26	45.50

Table 2: Nominal Moment Capacity - DSM and EWM Comparison (F_y = 50 ksi) [1].

Deck	Orientation	DSM M_n (kip-in.)	EWM M_n (kip-in.)
1.5WR22	Positive	19.50	24.04
1.5WR20	Positive	26.86	31.20
1.5WR18	Positive	42.43	42.74
1.5WR16	Positive	59.08	55.22
1.5WR22	Negative	27.41	26.91
1.5WR20	Negative	35.66	34.32
1.5WR18	Negative	47.02	45.27
1.5WR16	Negative	59.08	56.88

The yield stresses that were used by Dudenbostel were 40 and 50 ksi, which are industry standards and commonly available [7]. The results of the DSM and EWM nominal moment capacity was then plotted as a ratio of capacity to the thickness of the steel roof deck. Figures 10 and 11 illustrate the trends of how the two analysis methods compare to one another over various material thicknesses.

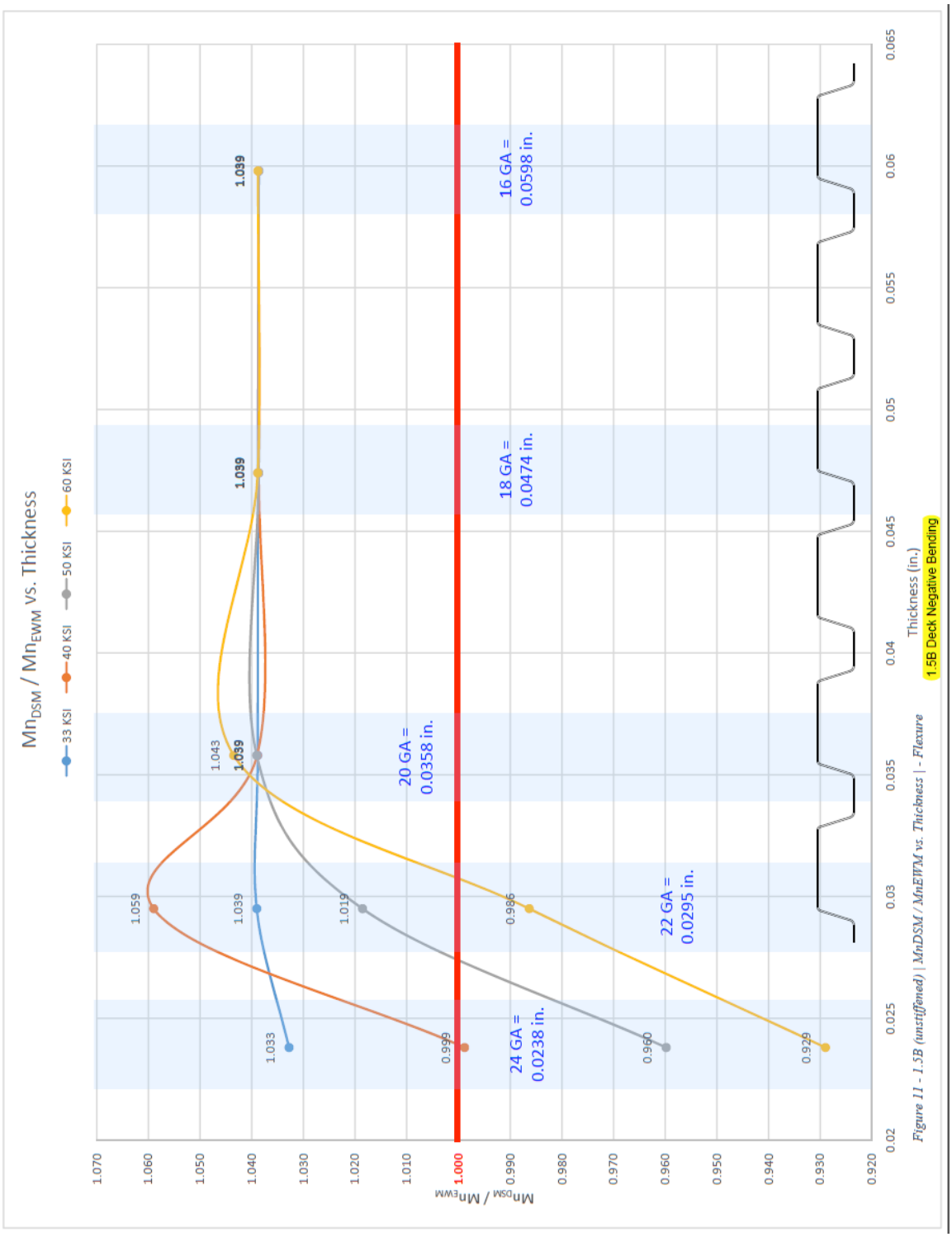

Figure 10: Mn_{DSM}/Mn_{EWM} for Negative Bending [1].

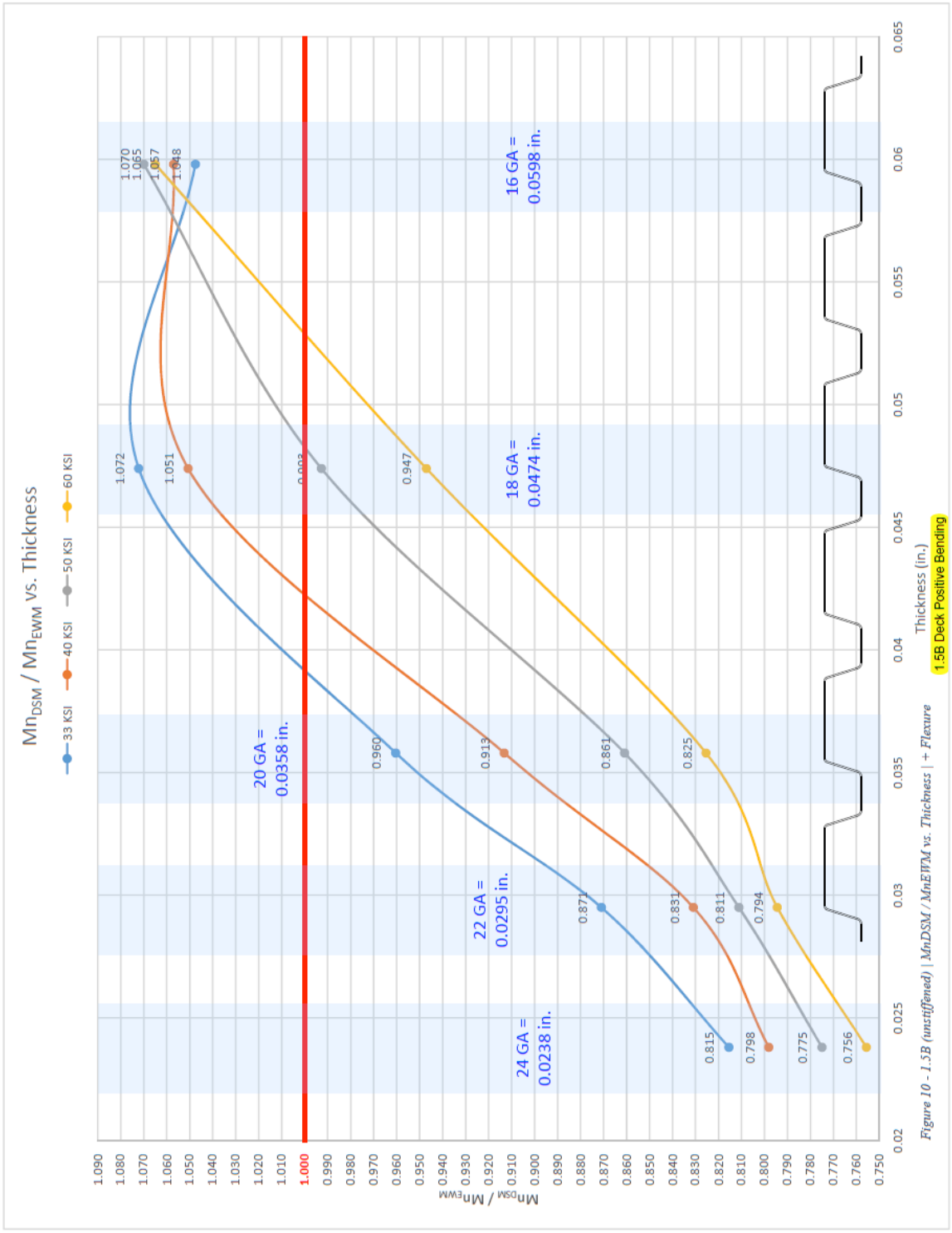

Figure 11: Mn_{DSM}/Mn_{EWM} for Positive Bending [1].

The general trend for negative bending is that the thinner gage decks have a varying Mn_{DSM}/Mn_{EWM} ratio from about 0.9 to 1.033 across the different yield strengths. As the deck becomes thicker, the yield strength makes less of an impact on the ratio. The ratio ends up converging on 1.039.

The general trend for positive bending shows that there is much more variation between different material strengths for the same steel deck thickness and ends up converging at the thicker gage deck. For the thinner gage decks, the EWM reported a higher nominal moment strength than the DSM. Between the 20 gage and 18 gage thicknesses, the ratio switches and the DSM reports a higher nominal moment strength then the EWM. All the different material strengths trend at the same rate and eventually approaches convergence at 16 gage thickness. At a ratio between 1.07 and 1.05 the DSM reports a higher value for the nominal moment strength then the EWM. With this variance between different yield strengths and material thickness, this study will be able to determine which analysis method more closely matches the experimentally measured moment capacity.

As previously discussed, the theoretical yield stress values were used in Dudenbostel's study. There can be a significant variance from the theoretical yield stress to the actual yield stress of the steel roof deck. The measured tensile stress was found to be anywhere from 26% higher to 66% higher [3] than the nominal tensile stress. This is a very significant difference and needs to be incorporated in the numerical analyses. Even though this is the tensile stress, having such a disparity in this aspect of a material property lead to the need to have the more significant yield stress evaluated. Material samples were taken from the steel deck that was tested in the laboratory and the yield

stress determined from material testing was used for the DSM and EWM in subsequent calculations for accurate comparisons between analytical and numerical results.

Chapter 2: Experimental Program

2.0 Testing Setup

2.0.1 Test Frame and Apparatus

Testing was conducted in the Construction Science and Engineering Center (CSEC) at the Milwaukee School of Engineering (MSOE). An existing self-reacting test frame (Figure 12) was used. The test frame houses two MTS hydraulic actuators, of which one was used for the current project. The MTS actuator has the ability to measure force and displacement.

Figure 12: Existing Test Frame.

The test configuration is for a two-point bending setup. This consisted of a six-foot simply supported deck span and a rectangular steel load frame that, when pulled upward by the MTS actuator, applied a symmetrical line load application at two points

near the mid-span of the deck. The spacing between the lines of load was 18 in. Figure 13 illustrates the testing setup for the two-point bending tests.

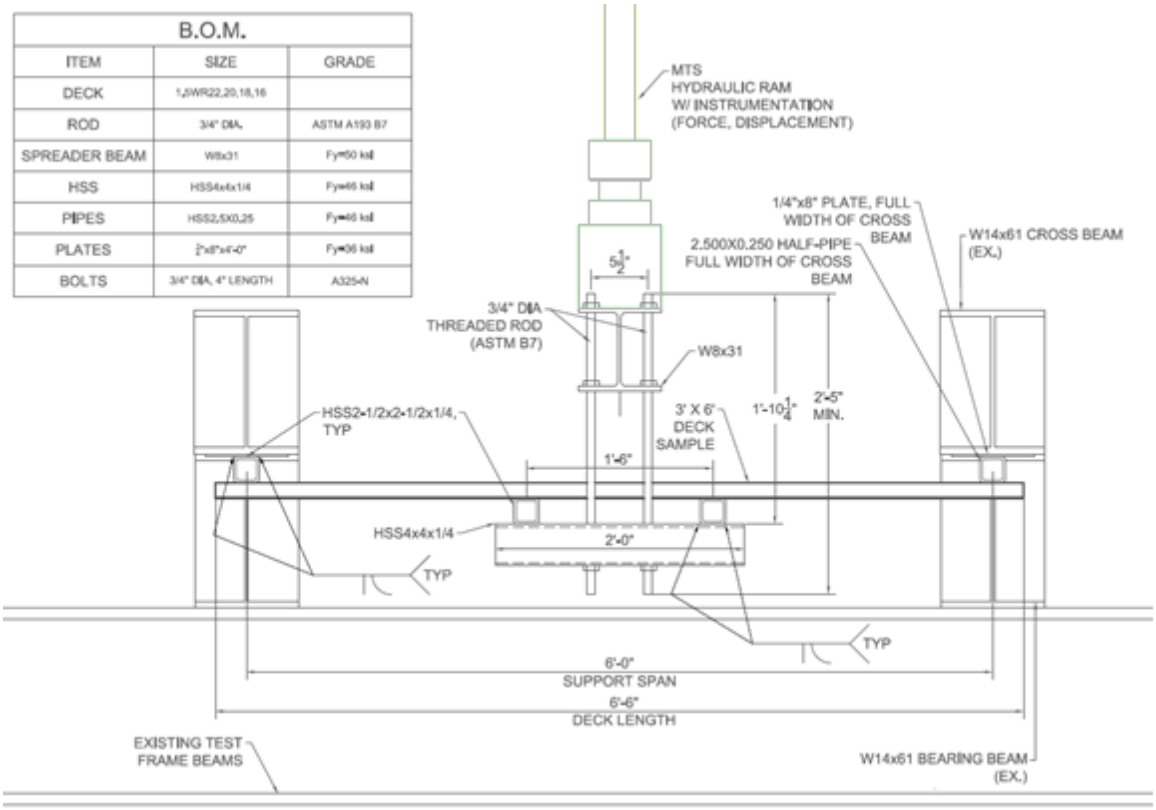

Figure 13: Four Point Bending Test Setup.

The roof deck was simply supported by HSS tubes strapped parallel to the length of the W14×61 cross beams. The W14×61 cross beams are bolted to the W14×61 bearing beams and the bearing beams are bolted to the test frame. The two HSS tubes strapped to the W14×61 cross beams allowed for adjustability to fine-tune the span to be exactly six feet between supports.

The load frame was fabricated out of larger HSS sections to apply the hydraulic actuator's load onto the roof deck. The 18 in. spacing between the lines of load created a constant moment region at the midspan of the deck. A photograph of the load frame is shown in Figure 14.

Figure 14: Load Frame.

The load frame was suspended from a spreader beam by ¾ in. diameter threaded rod from a spreader beam that was bolted to the hydraulic actuator. The threaded rod allows for adjustability to level the load frame. A photograph of the fully assembled load frame, threaded rod and cross beam as installed beneath the MTS actuator is shown in Figure 15.

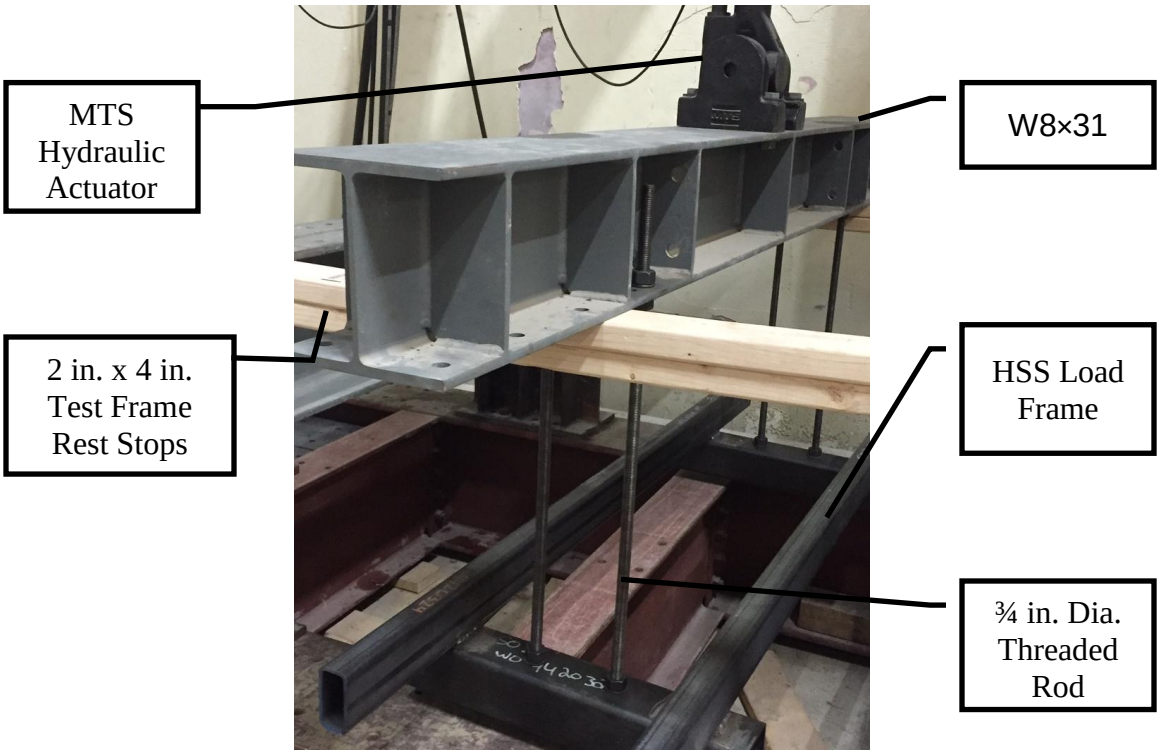

Figure 15: Fully Assembled Load Frame.

2.0.2 Methods of Data Collection

The methods of data collection consisted of numerical data sets, photographs and video. The numerical data consisted of displacement measurements obtained by means of LVDTs placed adjacent to the load frame to measure the deck displacement at different points throughout the duration of the test. The displacement measurements were recorded simultaneously with the force and displacement measurements taken through the MTS hydraulic actuator. Figure 16 shows a deck sample fully instrumented with all LVDTs in place and read for the test to begin.

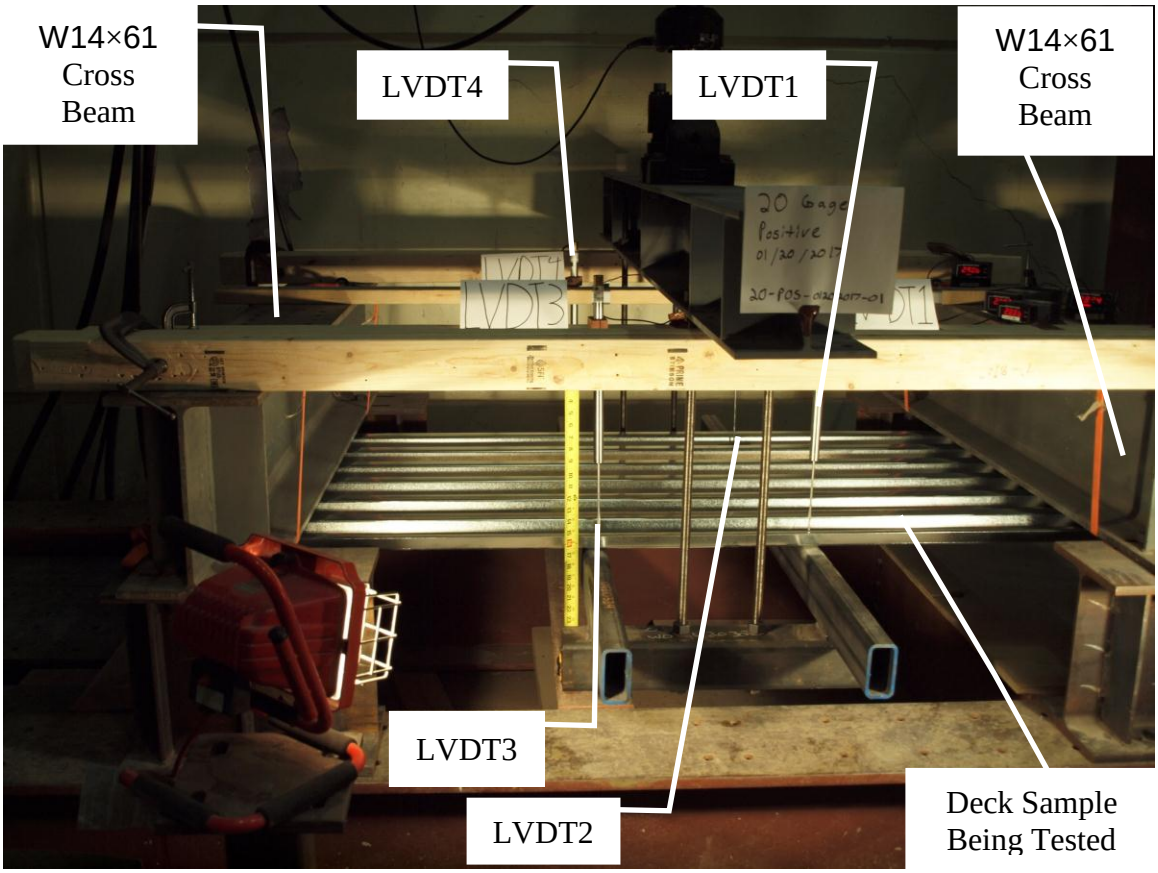

Figure 16: Test Frame with Full Instrumentation in Place.

Photographs and video were taken during each test. These are used to better identify the point of initial failure for each specimen. Photographs were also used to illustrate the progression of failure and to document the initial cause of failure. The video is a real time documentation of the test. The initial actuator force and displacement are read aloud at the beginning of the test and the final force and displacement magnitudes are read aloud at the end of the test.

2.0.3 Experimental Program

The experimental program included 24 total tests of four different gages of steel roof deck. Each of the four deck gages (16, 18, 20 and 22) were tested three times in both the positive and negative position. Table 3 summarizes the tests performed.

Table 3: Summary of Tests.

Deck	Orientation	Number of Tests	Size
1.5WR22	Positive	3	3’-0” x 6’-6”
1.5WR20	Positive	3	3’-0” x 6’-6”
1.5WR18	Positive	3	3’-0” x 6’-6”
1.5WR16	Positive	3	3’-0” x 6’-6”
1.5WR22	Negative	3	3’-0” x 6’-6”
1.5WR20	Negative	3	3’-0” x 6’-6”
1.5WR18	Negative	3	3’-0” x 6’-6”
1.5WR16	Negative	3	3’-0” x 6’-6”

The actuator was run in displacement mode, applying a uniform displacement of 5.5 inches in 10 minutes. Two initial tests were run slower with incremental displacement in order to learn about the deck’s behavior prior to running multiple tests, and these two tests slightly deviated from the typical displacement rate. The slow displacement of the actuator allowed for the roof deck to accrue load slowly, and it resulted in a smooth collection of data and an opportunity to capture good quality photos and video during the test. The test was terminated when of any one of the four LVDT’s maximum stroke was reached (about 6 inches total stroke). Readings of force and displacement were manually recorded at the start and end of the test, and maximum force was noted during the test. This was done to confirm recorded data and to identify when key photographs were taken. Post-test photographs were taken both while the deck was still in the test frame and after it had been removed from the frame.

The test frame and testing setup was designed to apply the load to the steel roof deck as a tension load on the actuator. There was concern that, with higher loadings present especially in the 18 and 16 gage steel roof deck, stability issues for the testing apparatus may lead to results that are not representative of the actual failure. The testing apparatus could potentially displace laterally in the event the steel roof deck deforms in

an uneven manner. Applying the load as a tensile load eliminated the potential for this sort of instability.

The actuator has a clevis mount at the point where the cross beam mounts to it, as well as where the actuator itself mounts to the overall test frame. The clevis is attached to the actuator with a ball-and-socket connection, allowing the clevis to rotate about all three primary axes. This protects the actuator while it is applying a load and allows it to continue to apply an axial deformation to the test subject.

Efforts were made to install all frames, support points and deck samples symmetrically and with level alignment in order to minimize eccentricity. This helped to provide quality data consistent with the intent of the experimental setup, and allowed the experimental data to be compared accurately to the results from the computer model.

Web crippling and crushing was a concern at the beginning of the project. The expected loading that would be required to cause the deck to buckle was in the thousands of pounds and the concentrated forces at the reaction points was an area of concern. Originally, a pipe or an angle piece was to be clamped to the W14×61 cross beam but that was thought to not have enough bearing area, and localized force concentrations may artificially affect results. The final design used an HSS square tube as the reaction point where the deck is supported as it provides a sufficient bearing area so that localized concentrated loads would not occur. The HSS tube still allowed the end of the deck to rotate freely as a true pin support should.

Web crippling check was checked using provisions from the AISI S100-2007 specification [1]. Equation (14) (Eq. C3.4.1-1 from AISI S100) was used to calculated the force required to fail one web element in the deck:

$$P_n = Ct^2 F_y \sin\theta \left(1 - C_R\sqrt{\frac{R}{t}}\right)\left(1 + C_N\sqrt{\frac{N}{t}}\right)\left(1 - C_h\sqrt{\frac{h}{t}}\right), \quad (14)$$

where

P_n = Nominal web crippling strength, ksi

C = Coefficient from Table C3.4.1-5 [6]

t = web thickness, in.

F_y = Yield Stress, ksi

θ = Angle between plane of web and plane of bearing surface, degrees

C_R = inside bend radius coefficient

R = inside bend radius, in.

C_N = bearing length coefficient from Table C3.4.1-5 [6]

N = bearing length, in.

C_h = web slenderness coefficient from Table C3.4.1-5 [6]

h = flat dimension of web measured in plane of web, in.

Tables 4 through 7 show the parameters used to calculate web crippling capacities for the different deck gages. The web crippling limit differs depending on whether the load is applied at the end or middle of the steel roof deck sample. Table 8 summarizes the web crippling capacity versus demand for each deck gage.

Table 4: 22 Gage Web Crippling.

Exterior (End)			Interior (Load Point)		
C	3	-	C	8	-
t	0.0295	in.	t	0.0295	in.
F_y	44.5	ksi	F_y	44.5	ksi
θ	72.5	degrees	θ	72.5	degrees
θ	1.265364	radian	θ	1.265364	radian
C_R	0.04	-	C_R	0.1	-
R	0.2179	in.	R	0.2179	in.
C_N	0.29	-	C_N	0.17	-
N	2	in.	N	2	in.
C_h	0.028	-	C_h	0.004	-
h	1.3	in.	h	1.3	in.
P_n	0.27238	kips/web	P_n	0.502638	kips/web
Total P_n	3.27	kips	Total P_n	6.03	kips

Table 5: 20 Gage Web Crippling.

Exterior (End)			Interior (Load Point)		
C	3	-	C	8	-
t	0.0358	in.	t	0.0358	in.
F_y	47.25	ksi	F_y	47.25	ksi
θ	72.5	degrees	θ	72.5	degrees
θ	1.26536	radian	θ	1.26536	radian
C_R	0.04	-	C_R	0.1	-
R	0.2179	in.	R	0.2179	in.
C_N	0.29	-	C_N	0.17	-
N	2	in.	N	2	in.
C_h	0.028	-	C_h	0.004	-
h	1.3	in.	h	1.3	in.
P_n	0.4112	kips/web	P_n	0.77124	kips/web
Total P_n	4.93	kips	Total P_n	9.25	kips

Table 6: 18 Gage Web Crippling.

Exterior (End)			Interior (Load Point)		
C	3	-	C	8	-
t	0.0474	in.	t	0.0474	in.
F_y	43.45	ksi	F_y	43.45	ksi
θ	72.5	degrees	θ	72.5	degrees
θ	1.26536	radian	θ	1.26536	radian
C_R	0.04	-	C_R	0.1	-
R	0.2179	in.	R	0.2179	in.
C_N	0.29	-	C_N	0.17	-
N	2	in.	N	2	in.
C_h	0.028	-	C_h	0.004	-
h	1.3	in.	h	1.3	in.
P_n	0.6284	kips/web	P_n	1.20548	kips/web
Total P_n	7.54	kips	Total P_n	14.47	kips

Table 7: 16 Gage Web Crippling.

Exterior (End)			Interior (Load Point)		
C	3	-	C	8	-
t	0.0598	in.	t	0.0598	in.
F_y	44.7	ksi	F_y	44.7	ksi
θ	72.5	degrees	θ	72.5	degrees
θ	1.26536	radian	θ	1.26536	radian
C_R	0.04	-	C_R	0.1	-
R	0.2179	in.	R	0.2179	in.
C_N	0.29	-	C_N	0.17	-
N	2	in.	N	2	in.
C_h	0.028	-	C_h	0.004	-
h	1.3	in.	h	1.3	in.
P_n	0.98326	kips/web	P_n	1.92046	kips/web
Total P_n	11.80	kips	Total P_n	23.04	kips

Table 8: Web Crippling Capacity versus Demand.

Deck	Orient.	Ext. Cap. (kips)	Int. Cap. (kips)	Ext. Dem. (kips)	Int. Dem. (kips)
1.5WR22	Positive	3.27	6.03	0.84	0.84
1.5WR20	Positive	4.93	9.25	1.05	1.05
1.5WR18	Positive	7.54	14.47	1.63	1.63
1.5WR16	Positive	11.80	23.04	2.22	2.22
1.5WR22	Negative	3.27	6.03	0.85	0.85
1.5WR20	Negative	4.93	9.25	1.06	1.06
1.5WR18	Negative	7.54	14.47	1.67	1.67
1.5WR16	Negative	11.80	23.04	2.29	2.29

Table 8 suggests that the testing setup proposed and the expected loadings will not exceed the capacity of the webs of the steel roof deck. The failure is expected to be within the constant moment region, which is between the load points from the test frame.

The support points of the steel roof deck specimens were inspected for signs of localized damage (buckling or crippling). There was no observable damage at these locations for any of the tests.

Chapter 3: Results and Discussion

3.0 Numerical Results

Preliminary estimates of the flexural capacity of the steel roof deck were generated prior to testing using the effective width method. These values, along with their equivalent actuator loads, are presented in Table 9.

Table 9: Predicted Load Magnitude at Flexural Yield.

Deck	Orientation	Total Load (lb)	Moment (kip-in.)
1.5WR22	Positive	1,780	24.00
1.5WR20	Positive	2,310	31.20
1.5WR18	Positive	3,170	42.70
1.5WR16	Positive	4,090	55.20
1.5WR22	Negative	1,990	26.90
1.5WR20	Negative	2,540	34.30
1.5WR18	Negative	3,350	45.20
1.5WR16	Negative	4,210	56.90

Again, these predicted results are from the effective width method and a simple support of the deck with two concentrated load points. Figure 17 is a simple diagram illustrating the setup for which the resulting nominal moment was calculated for.

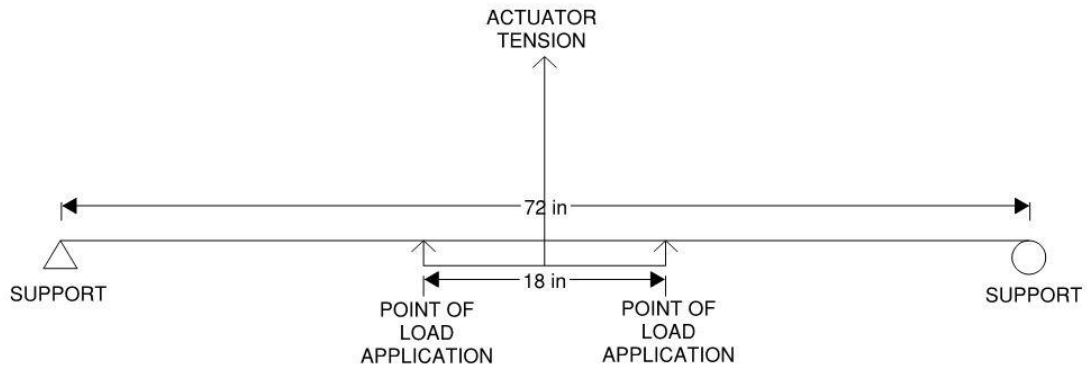

Figure 17: Preliminary Loading Diagram.

3.0.1 Material Testing Results

The steel roof deck that was donated from CANAM Group had additional samples cut from both the web and flute. These were then sent to a material test lab, which were subsequently cut into dog bone coupons and tested for yield and tensile limits using ASTM A1008. The results are summarized in Table 10 with the average column containing the average between the web and the flute that was used for calculations.

Table 10: Material Testing Results.

Deck	Flute Yield (ksi)	Flange Yield (ksi)	Average Yield (ksi)
1.5WR22	47.10	41.90	44.50
1.5WR20	48.60	45.90	47.25
1.5WR18	42.60	44.30	43.45
1.5WR16	44.90	44.50	44.7

3.0.2 Effective Width Results

The Effective Width Method was used to calculate the nominal moment capacity of the deck for initial comparison to the experimental results. Tables 11 and 12 show a comparison between the results from Dudenbostel [1] and current calculations. The moment capacities calculated are based on a 3 foot wide cross-section. Although both Dudenbostel's calculations and the current calculations used a 1.5B nominal roof deck, the current calculations were based on the measured profile of the deck whereas Dudenbostel used a typical profile as published in manufacturers' data.

Table 11: EWM Comparison Fy = 40 ksi (Dudenbostel versus Gwozdz).

Deck	Orientation	Dudenbostel EWM M_n (kip-in.)	Gwozdz EWM Mn (kip-in.)
1.5WR22	Positive	20.29	18.46
1.5WR20	Positive	25.36	23.41
1.5WR18	Positive	34.69	33.88
1.5WR16	Positive	44.71	45.08
1.5WR22	Negative	22.21	21.54
1.5WR20	Negative	27.46	27.34
1.5WR18	Negative	36.22	39.15
1.5WR16	Negative	45.50	49.58

Table 12: EWM Comparison Fy = 50 ksi (Dudenbostel versus Gwozdz).

Deck	Orientation	Dudenbostel EWM M_n (kip-in.)	Gwozdz EWM Mn (kip-in.)
1.5WR22	Positive	24.04	23.07
1.5WR20	Positive	31.20	29.27
1.5WR18	Positive	42.74	42.36
1.5WR16	Positive	55.22	56.36
1.5WR22	Negative	26.91	26.92
1.5WR20	Negative	34.32	34.17
1.5WR18	Negative	45.27	48.94
1.5WR16	Negative	56.88	61.98

Table 13 summarizes the results of the EWM for each of the different deck gages in both positive and negative flexural orientation. These calculations used the actual yield stress as determined from material testing.

Table 13: Summary of Results Using Effective Width Method.

Deck	Orientation	Yield Stress (ksi)	EWM Mn (kip-in.)	Expected Load (lbs)*
1.5WR22	Positive	44.50	20.53	1521
1.5WR20	Positive	47.25	27.66	2049
1.5WR18	Positive	43.45	36.81	2726
1.5WR16	Positive	44.70	50.38	3732
1.5WR22	Negative	44.50	23.96	1775
1.5WR20	Negative	47.25	32.29	2392
1.5WR18	Negative	43.45	42.53	3150
1.5WR16	Negative	44.70	55.41	4104

** The "expected" load can be compared to the applied actuator load from Table 1. It is the load necessary to generate the nominal moment, Mn, in the four-point bending configuration used in experimental tests.*

The results were compared to the effective sections that Dudenbostel found using the EWM [1]. While not perfectly comparable since Dudenbostel used theoretical yield stresses of 40 ksi and 50 ksi, the comparison could be used to benchmark the current EWM calculations. The results (Table 14) fell in between the 40 ksi and 50 ksi results found by Dudenbostel, which is to be expected since the yield strength from material testing fell between those magnitudes.

Table 14: EWM Comparison (As Tested versus Theoretical).

Deck	Orientation	Yield Stress (ksi)	EWM M_n (kip-in.) Fy=40ksi	EWM Mn (kip-in.) Fy=As Tested	EWM M_n (kip-in.) Fy=50ksi
1.5WR22	Positive	44.50	20.29	20.53	24.04
1.5WR20	Positive	47.25	25.36	27.66	31.20
1.5WR18	Positive	43.45	34.69	36.81	42.74
1.5WR16	Positive	44.70	44.71	50.38	55.22
1.5WR22	Negative	44.50	22.21	23.96	26.91
1.5WR20	Negative	47.25	27.46	32.29	34.32
1.5WR18	Negative	43.45	36.22	42.53	45.27
1.5WR16	Negative	44.70	45.50	55.41	56.88

3.0.3 Direct Strength Results

Similar to the EWM comparisons, Tables 15 and 16 show a comparison between Dudenbostel's DSM calculations and the current DSM calculations. The tables report a moment capacity based on a 3 foot width of steel roof deck.

Table 15: DSM Comparison Fy = 40 ksi (Dudenbostel versus Gwozdz).

Deck	Orientation	Dudenbostel DSM M_n (kip-in.)	Gwozdz DSM M_n (kip-in.)
1.5WR22	Positive	16.86	15.50
1.5WR20	Positive	23.16	22.10
1.5WR18	Positive	36.45	34.90
1.5WR16	Positive	47.26	49.20
1.5WR22	Negative	23.52	19.00
1.5WR20	Negative	28.53	24.50
1.5WR18	Negative	37.62	37.00
1.5WR16	Negative	47.26	49.20

Table 16: DSM Comparison Fy = 50 ksi (Dudenbostel versus Gwozdz).

Deck	Orientation	Dudenbostel DSM M_n (kip-in.)	Gwozdz DSM M_n (kip-in.)
1.5WR22	Positive	19.50	18.00
1.5WR20	Positive	26.86	27.50
1.5WR18	Positive	42.43	43.60
1.5WR16	Positive	59.08	61.50
1.5WR22	Negative	27.41	22.20
1.5WR20	Negative	35.66	30.60
1.5WR18	Negative	47.02	46.20
1.5WR16	Negative	59.08	61.50

Table 17 summarizes the results from the Direct Strength Method for determining the nominal moment capacity of the four different deck types in both positive and negative orientation.

Table 17: Summary of Results Using Direct Strength Method.

Deck	Orientation	Yield Stress (ksi)	DSM Mn (kip-in.)	Expected Load (lbs)*
1.5WR22	Positive	44.50	16.67	1235
1.5WR20	Positive	47.25	23.98	1853
1.5WR18	Positive	43.45	37.93	2809
1.5WR16	Positive	44.70	54.98	4072
1.5WR22	Negative	44.50	20.53	1520
1.5WR20	Negative	47.25	28.92	2141
1.5WR18	Negative	43.45	40.23	2979
1.5WR16	Negative	44.70	54.98	4072

** The "expected" load can be compared to the applied actuator load from Table 1. It is the load necessary to generate the nominal moment, Mn, in the four-point bending configuration used in experimental tests.*

Table 18 further compares the Direct Strength Method results to Dudenbostel's results at two different yield strengths.

Table 18: Summary of Results Using Direct Strength Method.

Deck	Orientation	Yield Stress (ksi)	DSM Mn (kip-in.) Fy=40ksi	DSM Mn (kip-in.) Fy=As Tested	DSM Mn (kip-in.) Fy=50ksi
1.5WR22	Positive	44.50	16.86	16.67	19.50
1.5WR20	Positive	47.25	23.16	23.98	26.86
1.5WR18	Positive	43.45	36.45	37.93	42.43
1.5WR16	Positive	44.70	47.26	54.98	59.08
1.5WR22	Negative	44.50	23.52	20.53	27.41
1.5WR20	Negative	47.25	28.53	28.91	35.66
1.5WR18	Negative	43.45	37.62	40.22	47.02
1.5WR16	Negative	44.70	47.26	54.98	59.08

** The "expected" load can be compared to the applied actuator load from Table 1. It is the load necessary to generate the nominal moment, Mn, in the four-point bending configuration used in experimental tests.*

The nominal strength determined using the tested yield stress fell between the 40 ksi and 50 ksi magnitudes as calculated by Dudenbostel, with the exception of the 22 gage deck that fell just below the results for the 40 ksi deck. The lower capacity could be attributed to the differences between the deck cross-sections used. The values are still very similar.

The deck geometry used in the results discussed above was a simple model using straight elements with the appropriate deck thickness. The elements connected to one another using a single node at the corners based on the measured deck geometry. This was mentioned that it is taxing on the capacity of the deck that CUFSM returns to the user [1, 2]. Therefore, another set of models was created in an effort to better capture the capacity of the steel roof deck. The enhanced geometry included the corners more accurately modeled with small elements connecting between tightly spaced nodes to better simulate a corner of the deck. Table 19 shows the results using the better defined geometry.

Table 19: Summary of Results Using Direct Strength Method (Refined Geometry).

Deck	Orientation	DSM Mn (kip-in.)	Expected Load (lbs)*
1.5WR22	Positive	16.55	1226
1.5WR20	Positive	24.62	1824
1.5WR18	Positive	37.11	2749
1.5WR16	Positive	54.98	4073
1.5WR22	Negative	14.20	1052
1.5WR20	Negative	19.70	1459
1.5WR18	Negative	31.86	2357
1.5WR16	Negative	46.33	3432

** The "expected" load can be compared to the applied actuator load from Table 1. It is the load necessary to generate the nominal moment, Mn, in the four-point bending configuration used in experimental tests.*

It was observed that, in many cases, the nominal moment capacity was reduced from that of the simple model. Possible explanations for this reduction will be provided in the discussion section of this report.

3.1 Experimental Results

3.1.1 Graphical Results

The experimental results are displayed over the next several pages in a graphical format, as the graphs show measured load versus measured displacement throughout the duration of each test. The following naming scheme was used:

"(Gage of Deck)-(Positive or Negative Orientation)-(MMDDYYY)-(Test Number)".

For example, test 16-NEG-02102017-01 would identify the first 16 gage deck in its negative bending position conducted on February 10, 2017. The following graphs are the results of each of the four point moment testing done for each of the different steel roof deck gages. Figures 18, 19 and 20 show the results for the 16 gage roof deck tests for negative bending.

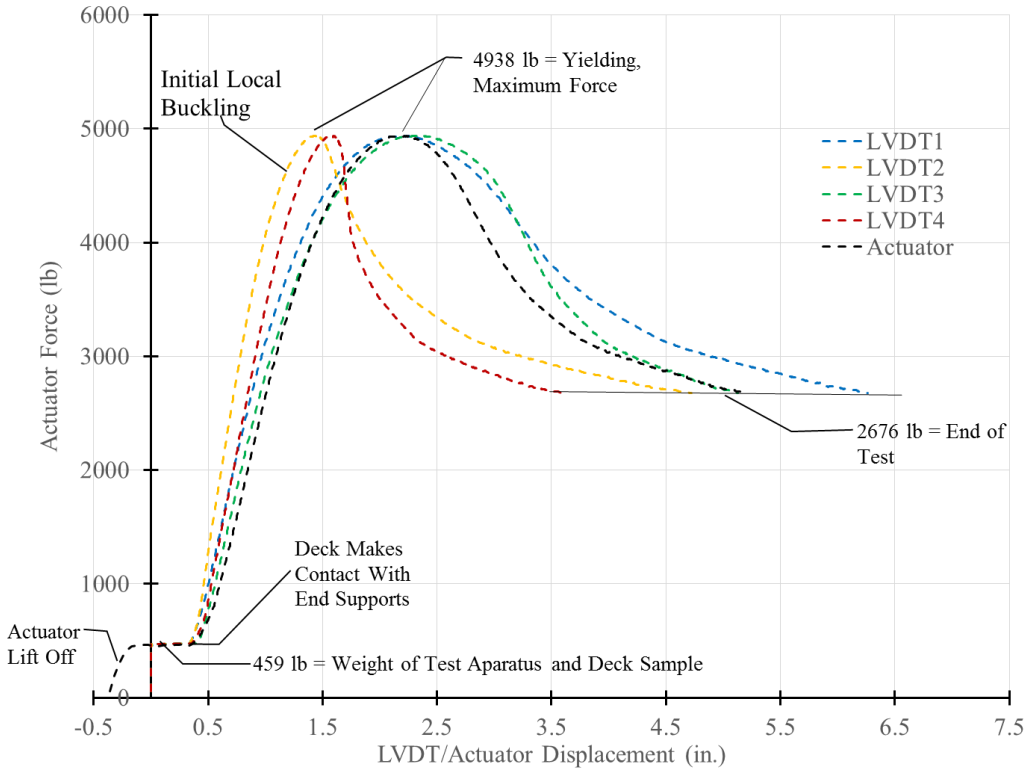

Figure 18: Results for Test 16-NEG-02102017-01.

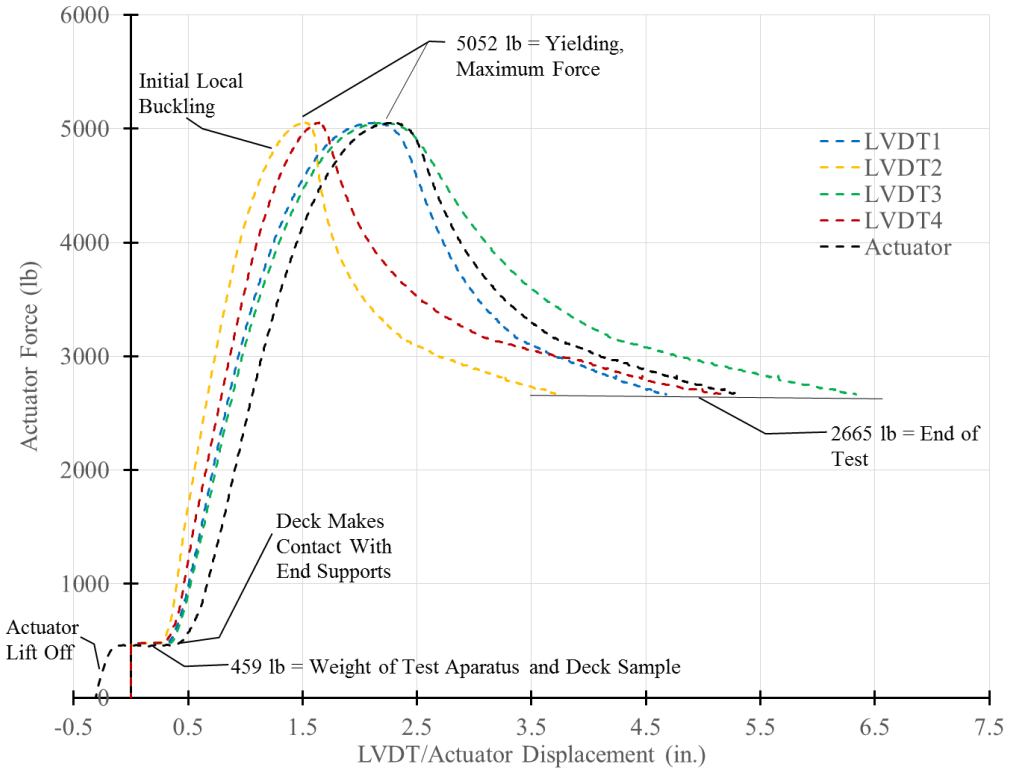

Figure 19: Results for Test 16-NEG-02222017-02.

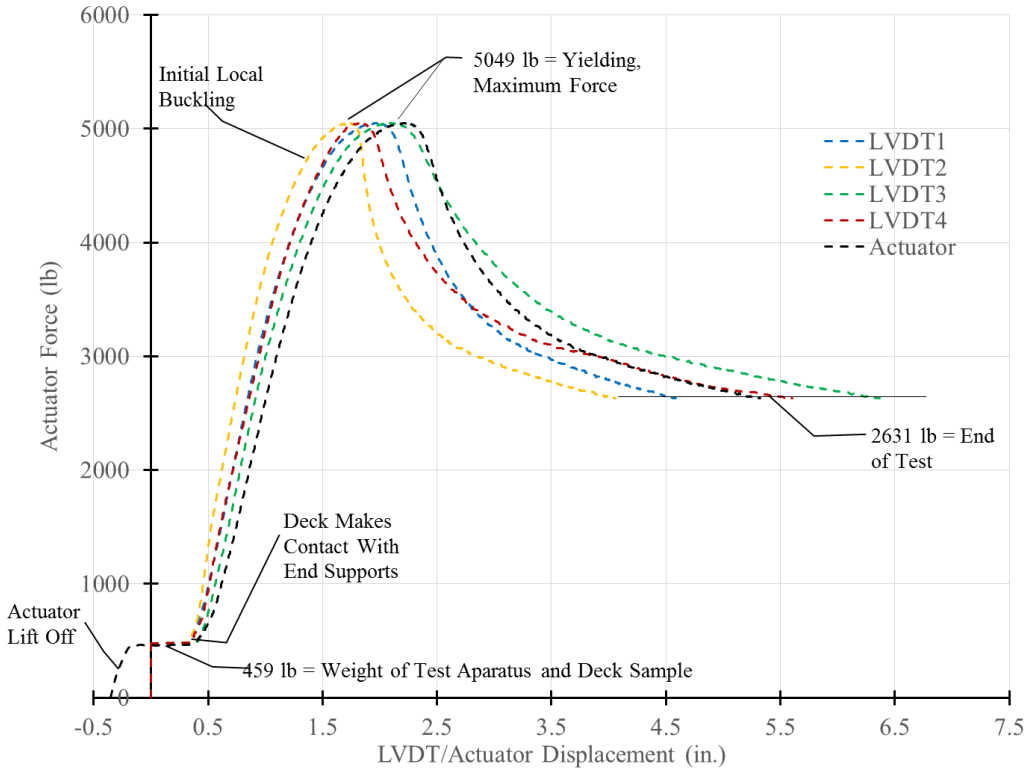

Figure 20: Results for Test 16-NEG-02222017-03.

Figure 21 shows the results from each of the three 16 gage negative tests overlaid on one another. There is excellent consistency among results. The overlay plot shows measured force versus measured displacement at the actuator (typical for all overlay plots in this section of the report).

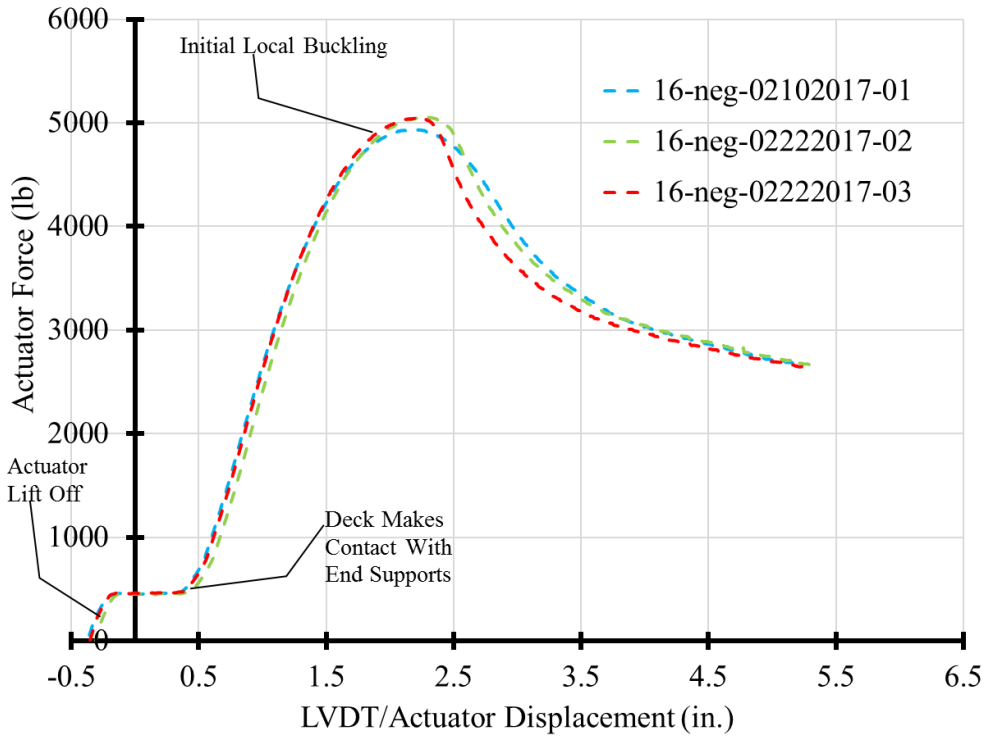

Figure 21: Overlay of 16 Gage Negative Test Results.

Figure 22 is a photograph of the 16 gage deck in negative bending showing the early signs of local buckling. Notice the webs starting to buckle laterally.

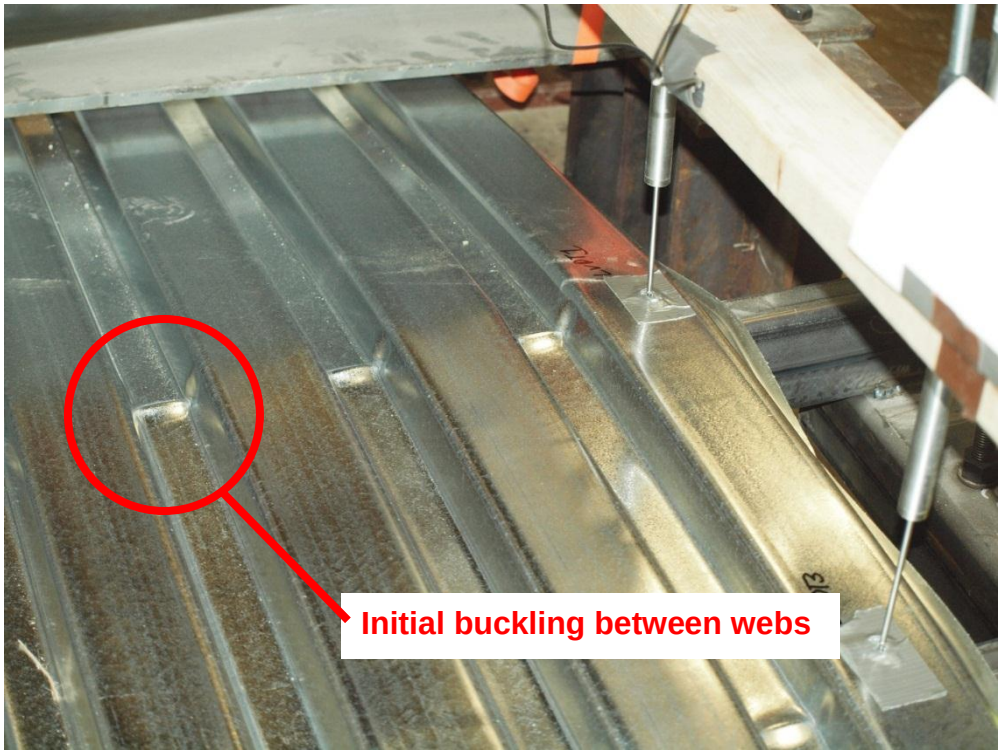

Figure 22: 16 Gage Deck Negative Bending - Initial Buckling.

Figure 23 is a photograph of the 16 gage deck in negative bending close to the maximum applied load. Notice the ribs severely buckle, particularly at the edge of the deck.

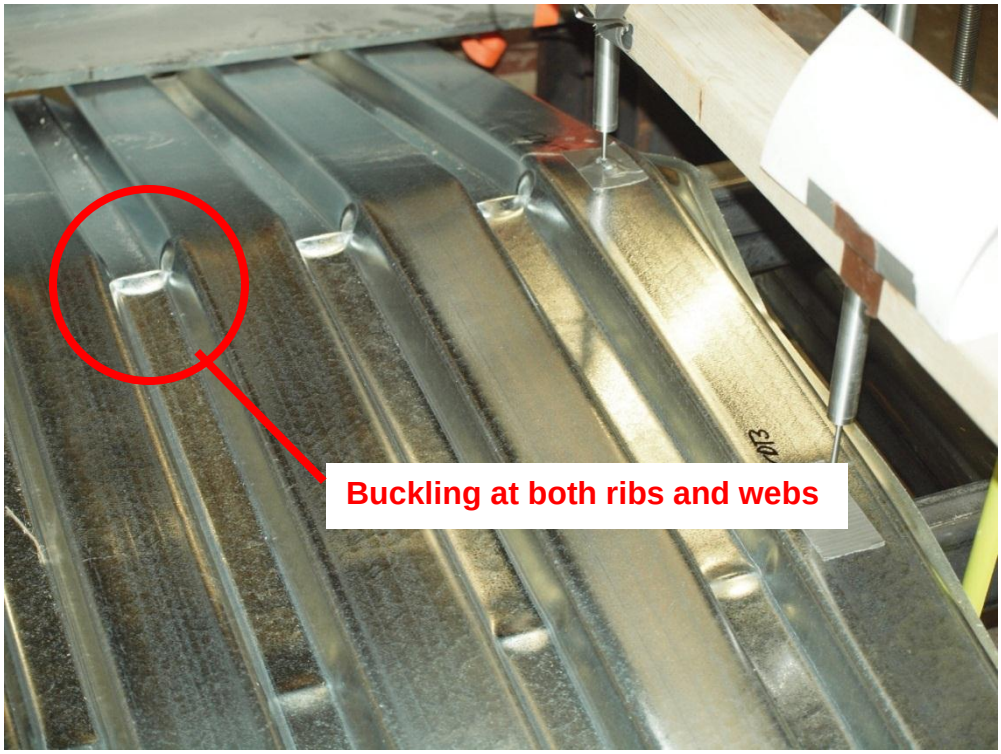

Figure 23: 16 Gage Deck Negative Bending - Further Buckling.

Figures 24 and 25 are photographs showing the final state of a 16 gage deck in negative bending. Note that the configuration is similar to that seen in Figure 23, only with more deformation.

Figure 26 is a photograph of the deck after it has been removed from the test frame. The deck is permanently deformed with both local and global buckling remaining visible.

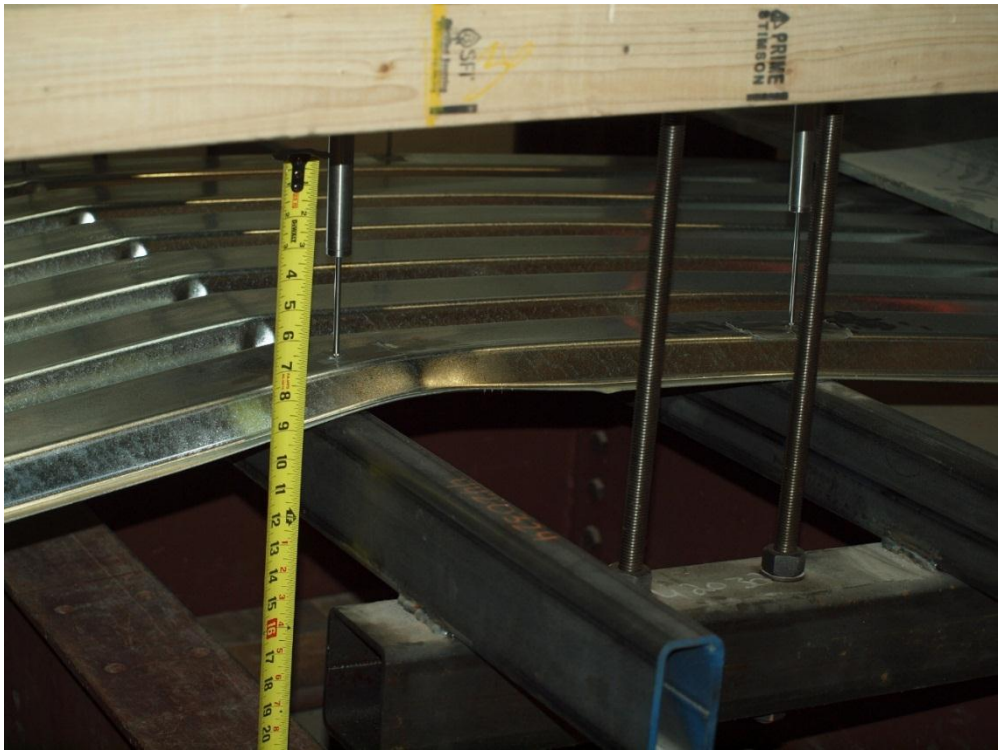

Figure 24: 16 Gage Deck Negative Bending - Final State.

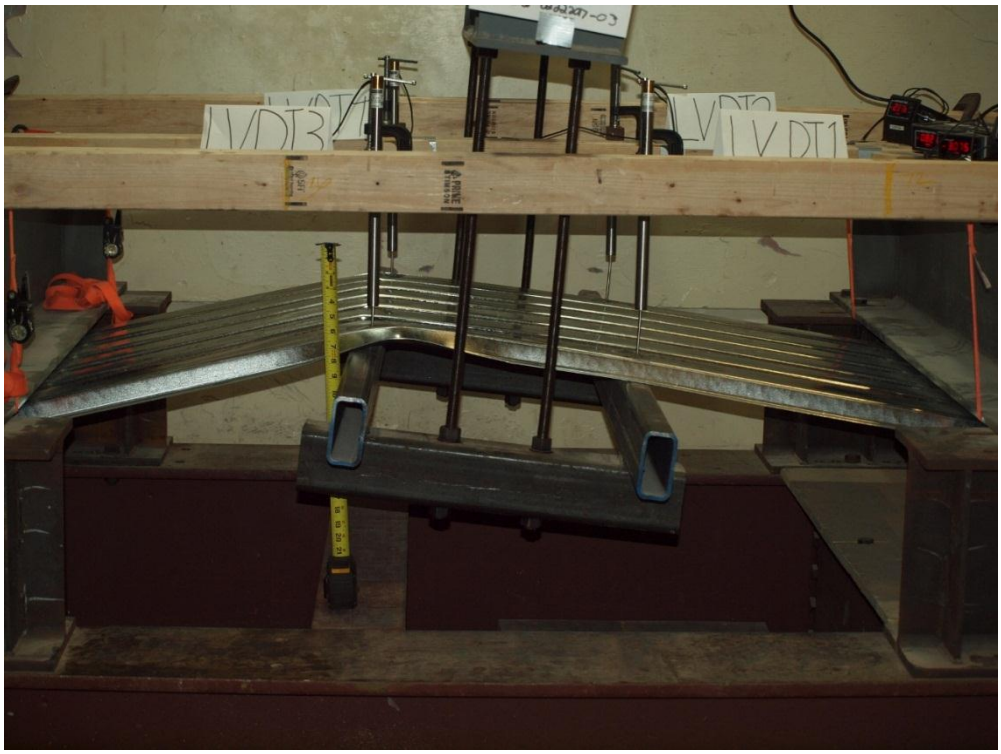

Figure 25: 16 Gage Deck Negative Bending – End of Test.

Figure 26: 16 Gage Deck Negative Bending – Specimen Removed.

Figures 27, 28 and 29 show the results for the 16 gage roof deck tests for positive bending.

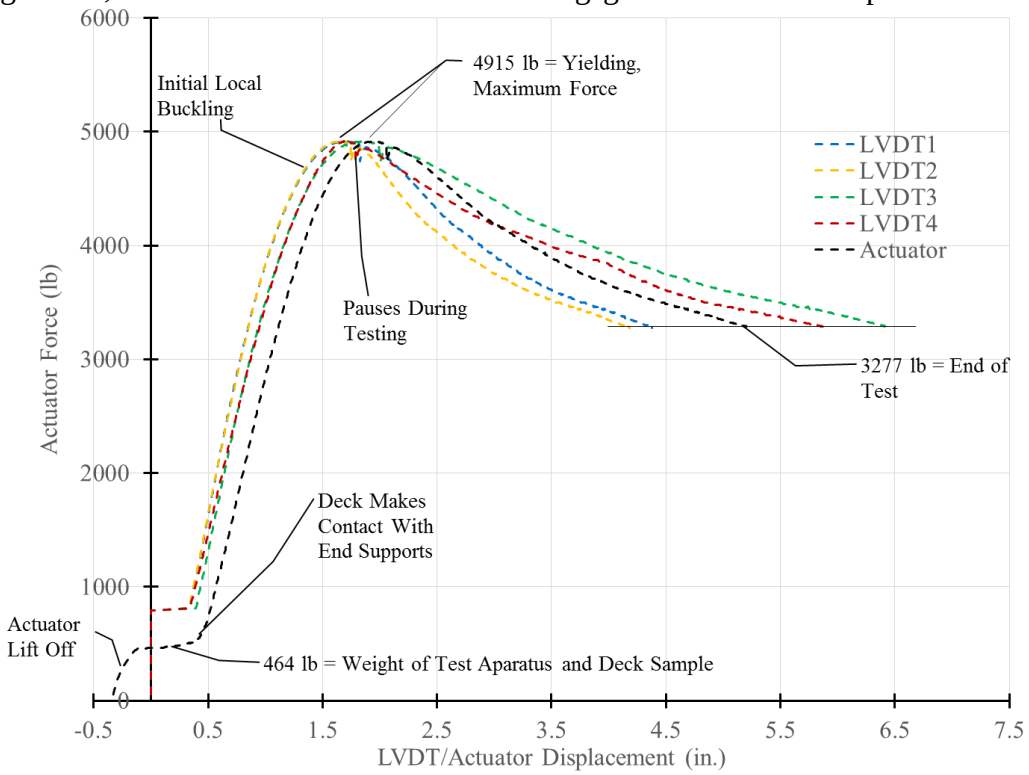

Figure 27: Results for Test 16-POS-02102017-01.

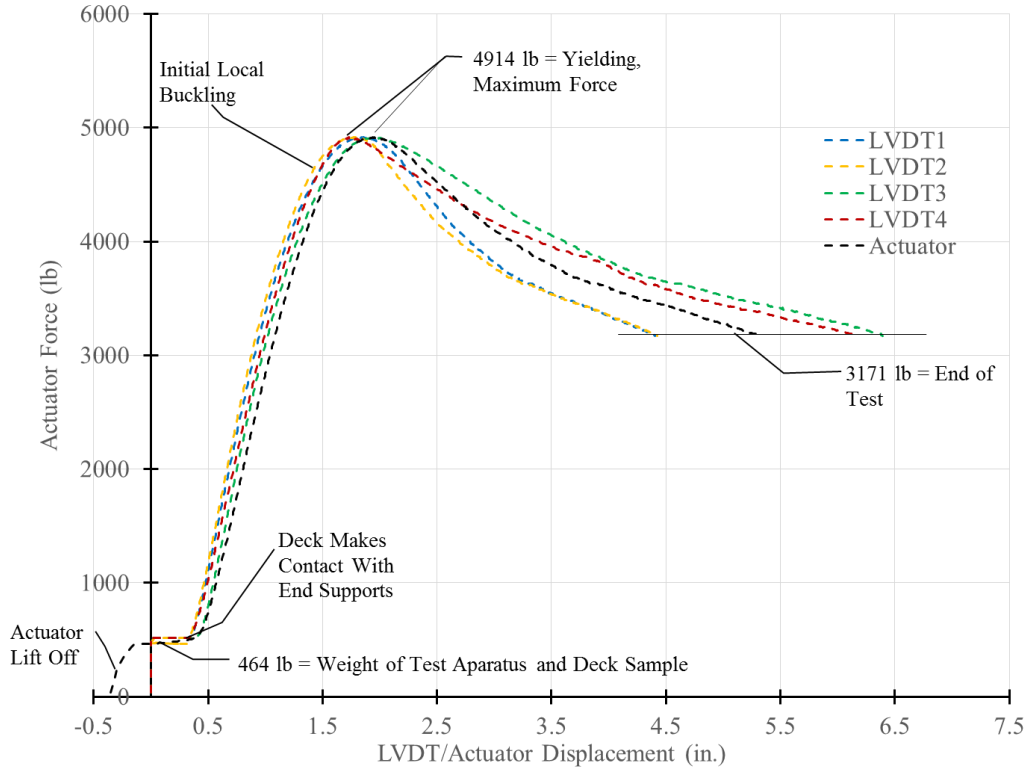

Figure 28: Results for Test 16-POS-02172017-02.

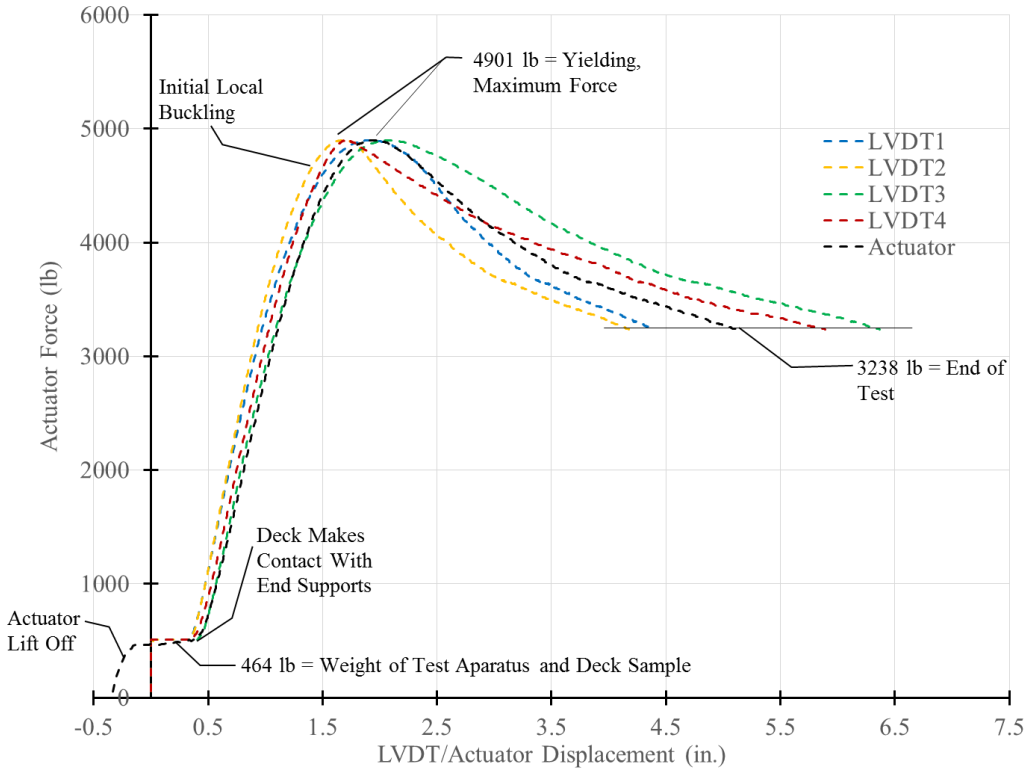

Figure 29: Results for Test 16-POS-02172017-03.

Figure 30 shows the results from each of the three 16 gage positive tests overlaid on one another. As with the negative tests, there is excellent consistency among the results.

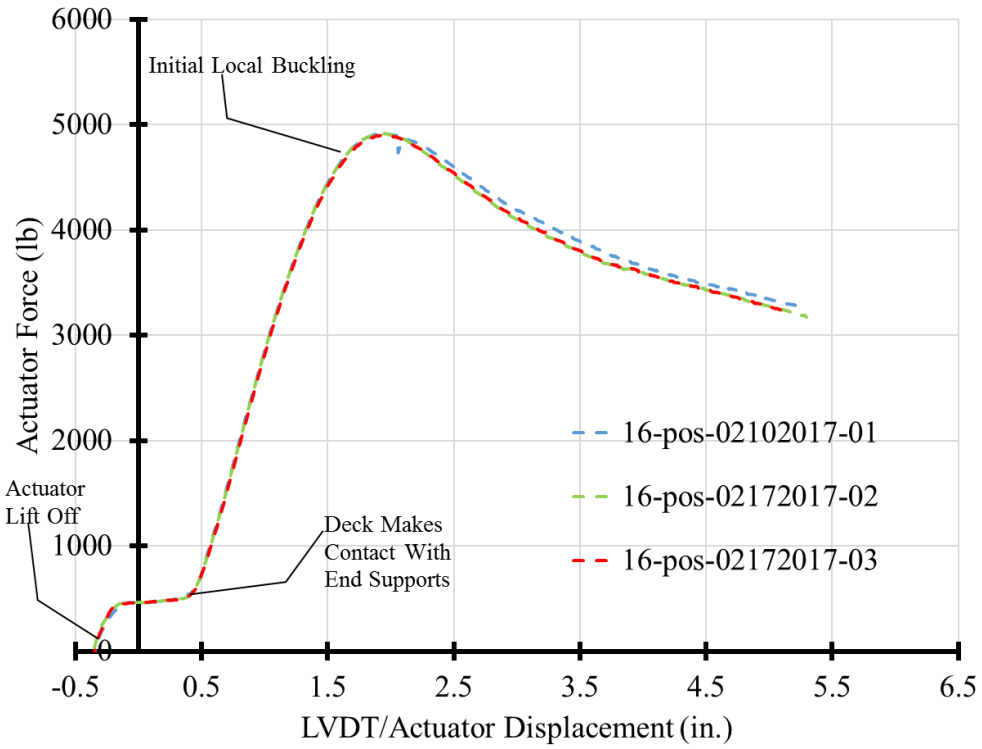

Figure 30: Overlay of 16 Gage Positive Test Results.

Figure 31 is a photograph of 16 gage deck in positive bending showing the early signs of local buckling within the ribs.

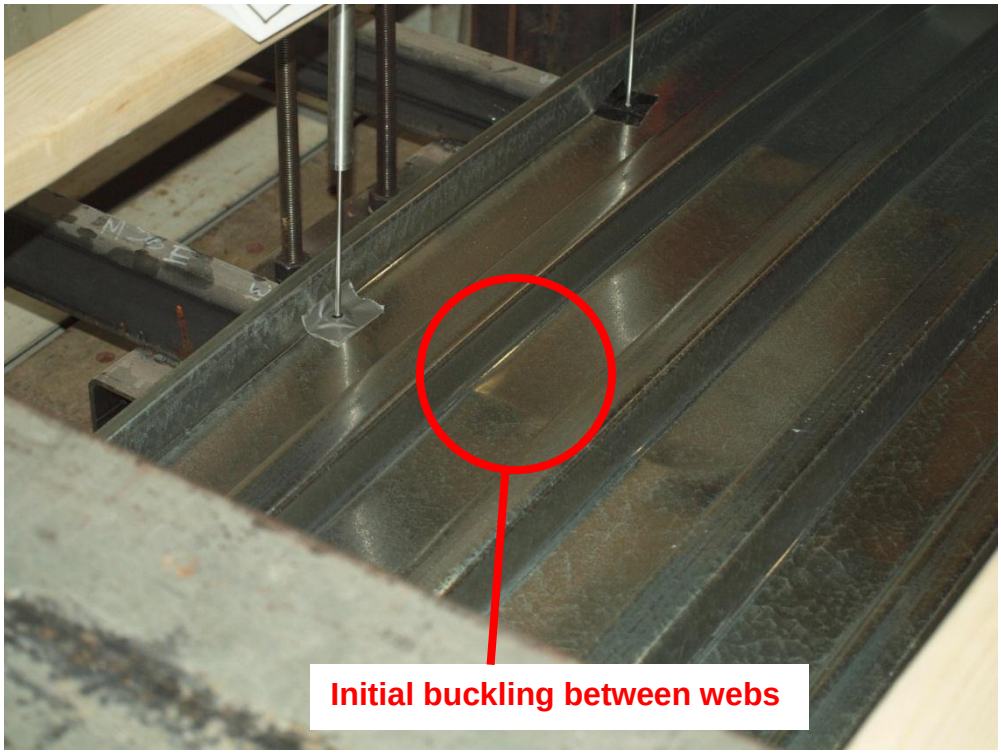

Figure 31: 16 Gage Deck Positive Bending - Initial Buckling.

Figure 32 is a photograph of 16 gage deck in positive bending showing additional deformation in the ribs and the webs.

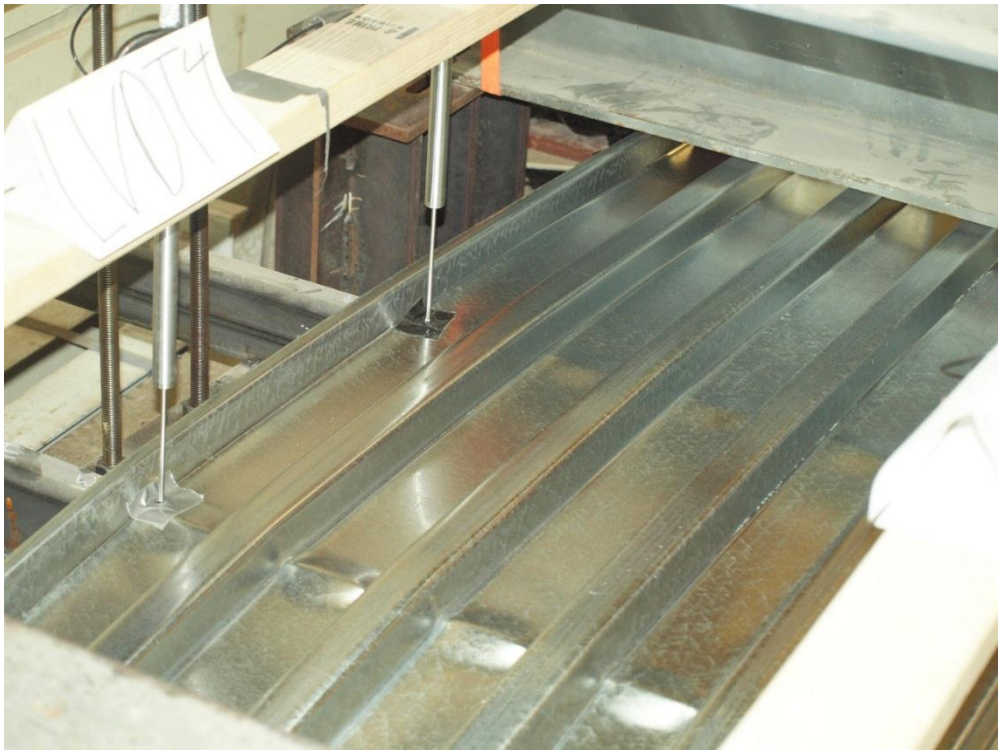

Figure 32: 16 Gage Deck Positive Bending - Further Buckling.

Figure 33 is a photograph of 16 gage deck in positive bending showing the webs severely buckled along with the ribs.

Figure 33: 16 Gage Deck Positive Bending – Both Ribs and Webs Buckling.

Figure 34 is a photograph of 16 gage deck in positive bending removed from the test frame in its final state.

Figure 34: 16 Gage Deck Positive Bending - Final State.

Figures 35, 36 and 37 show the results for the 18 gage roof deck tests for negative bending.

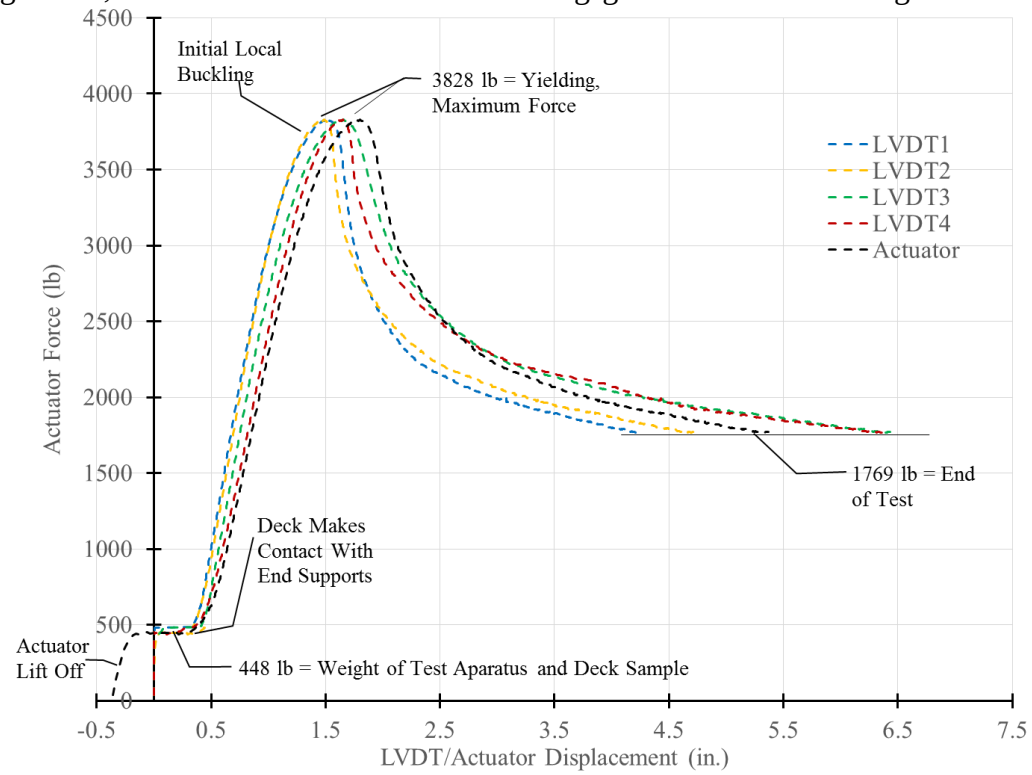

Figure 35: Results for Test 18-NEG-02172017-01.

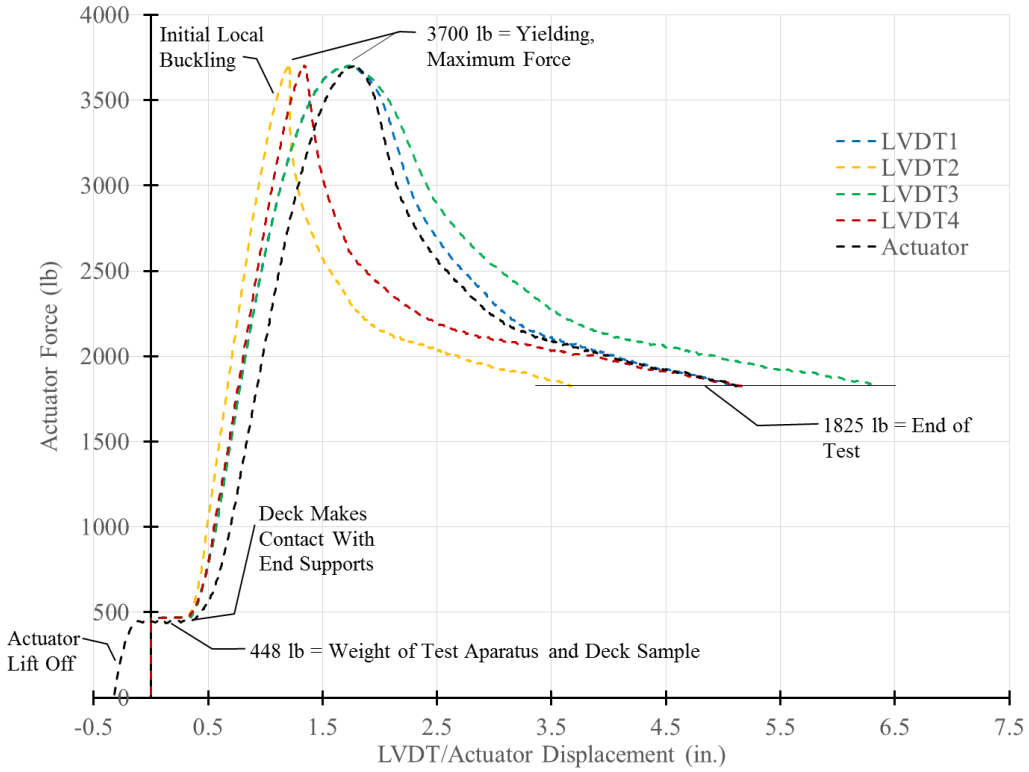

Figure 36: Results for Test 18-NEG-02222017-02.

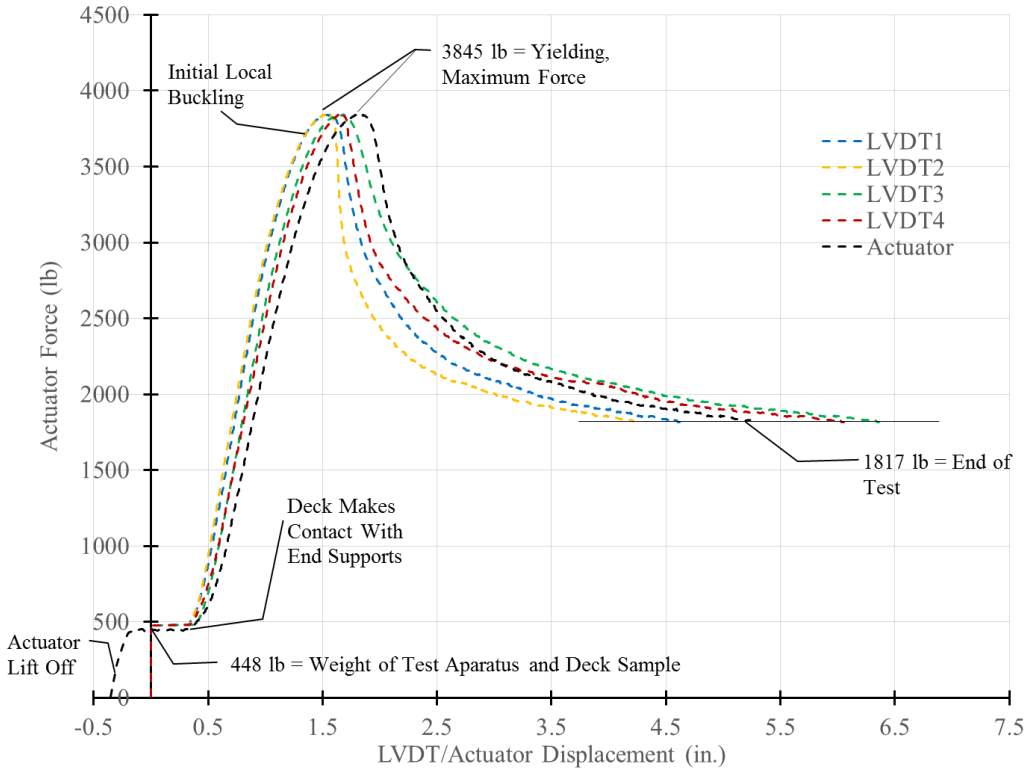

Figure 37: Results for Test 18-NEG-02222017-03.

Figure 38 shows the results from each of the three 18 gage negative tests overlaid on one another. As with the 16 gage tests, there is excellent consistency among results.

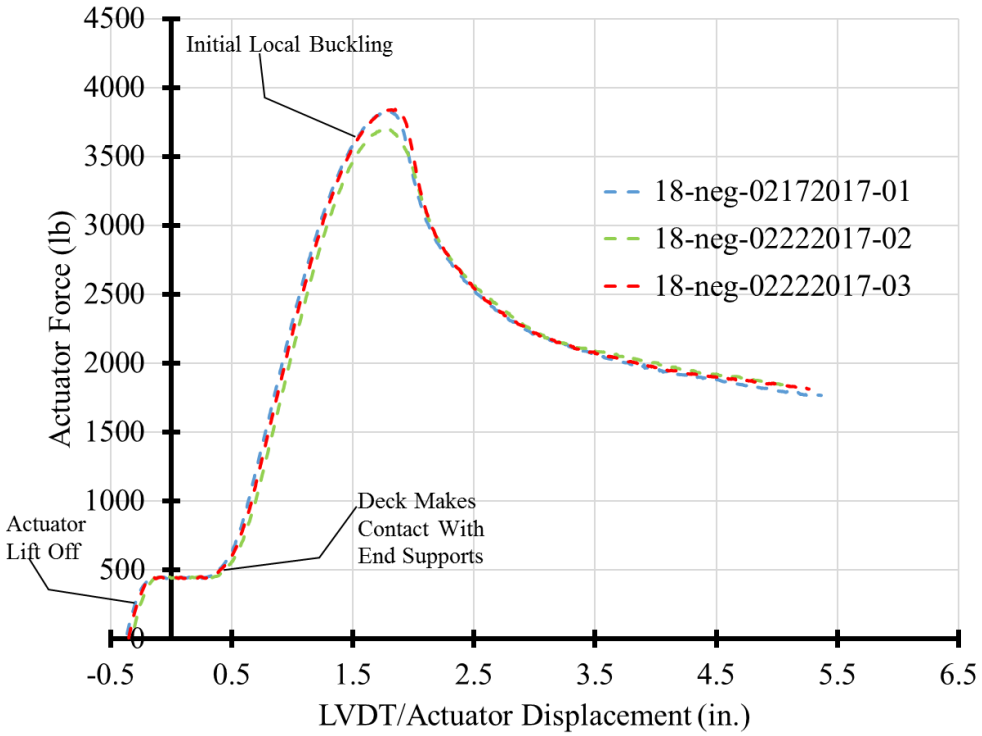

Figure 38: Overlay of 18 Gage Negative Test Results.

Figure 39 is a photograph of 18 gage deck in negative bending showing the initial signs of local buckling in the ribs and the webs.

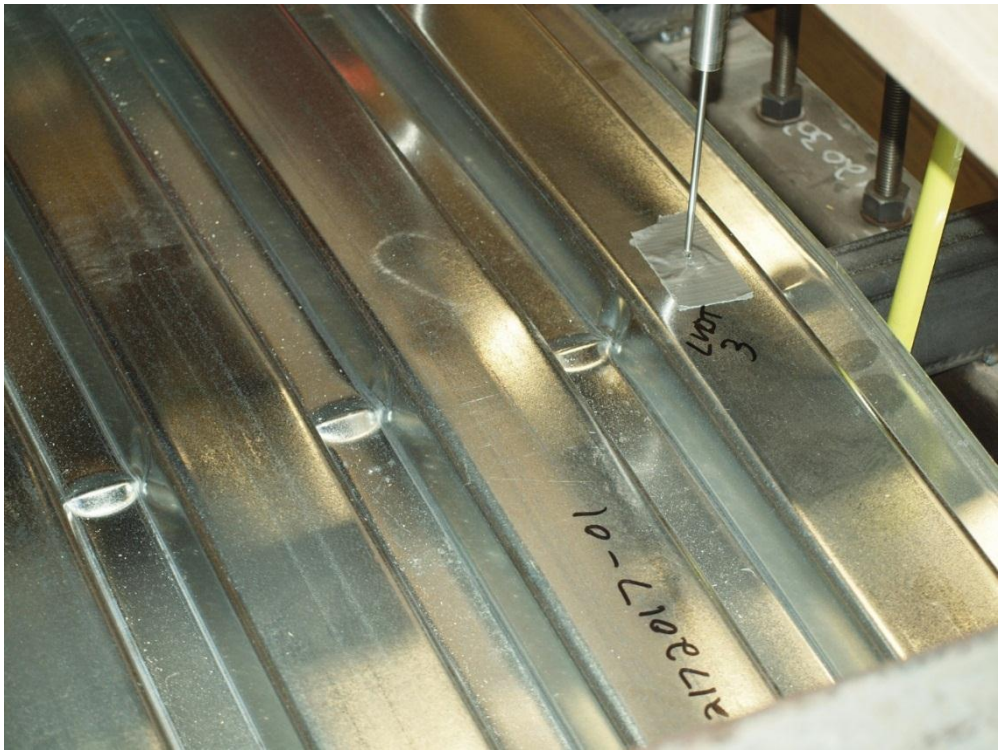

Figure 39: 18 Gage Deck Negative Bending - Initial Buckling.

Figure 40 is a photograph of 18 gage deck in negative bending severely deformed from local buckling and nearing the end of the test.

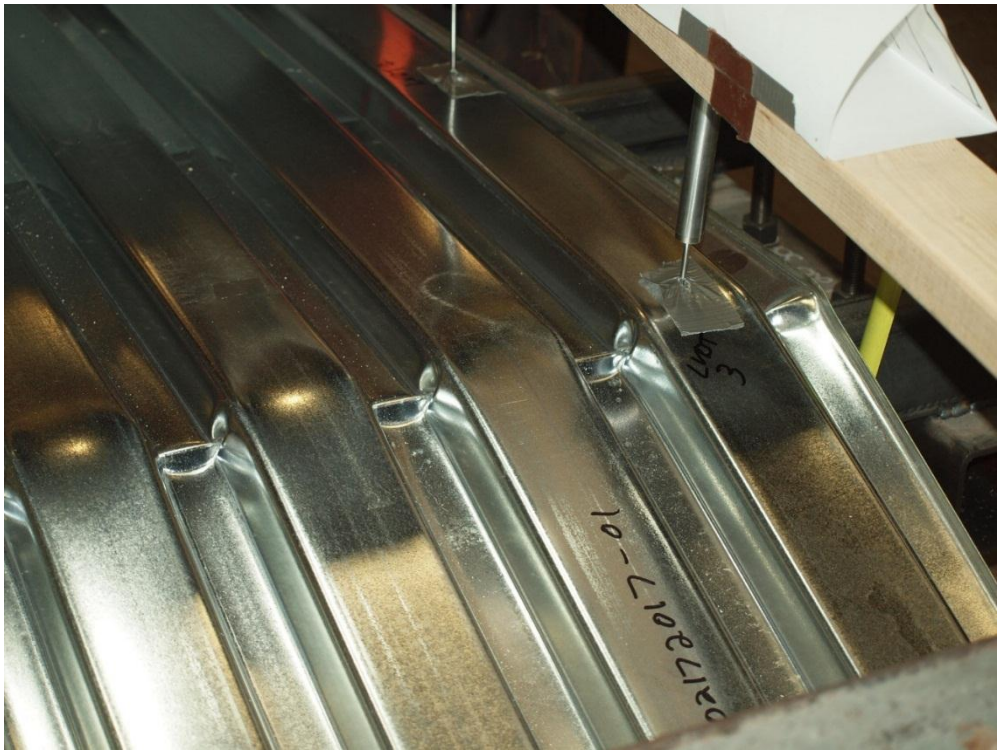

Figure 40: 18 Gage Deck Negative Bending - Further Buckling.

Figure 41 is a photograph of 18 gage deck in negative bending after being removed from the test frame in its final state.

Figure 41: 18 Gage Deck Negative Bending - Final State.

Figures 42, 43 and 44 show the results for the 18 gage roof deck tests for positive bending.

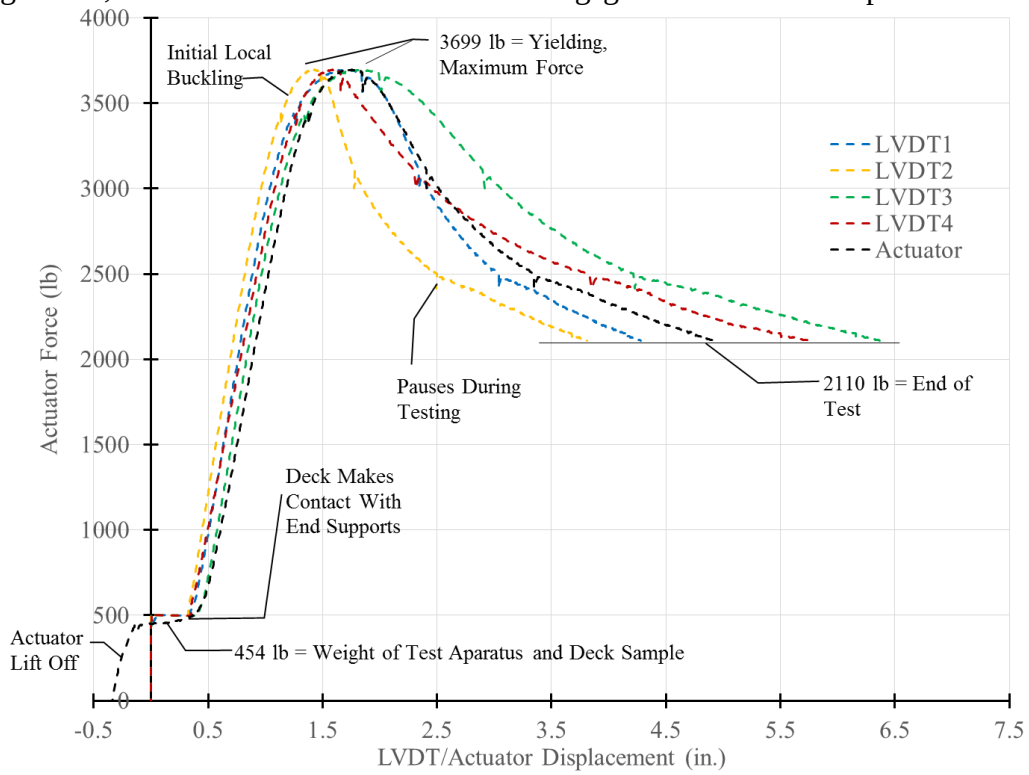

Figure 42: Results for Test 18-POS-02102017-01.

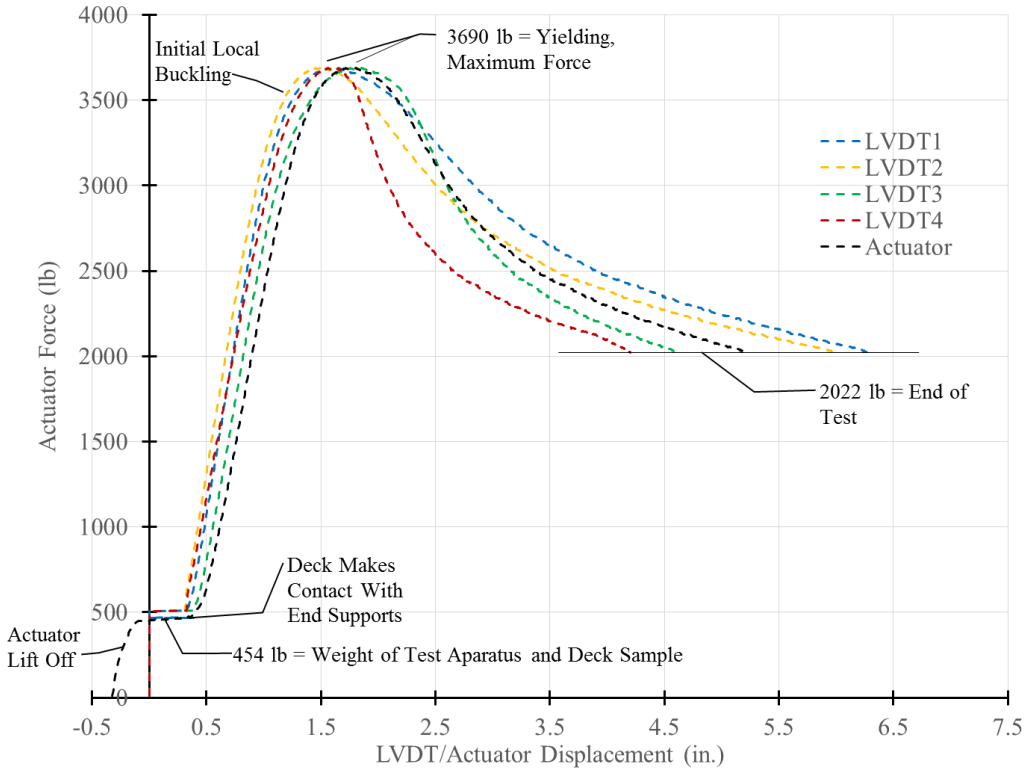

Figure 43: Results for Test 18-POS-02172017-02.

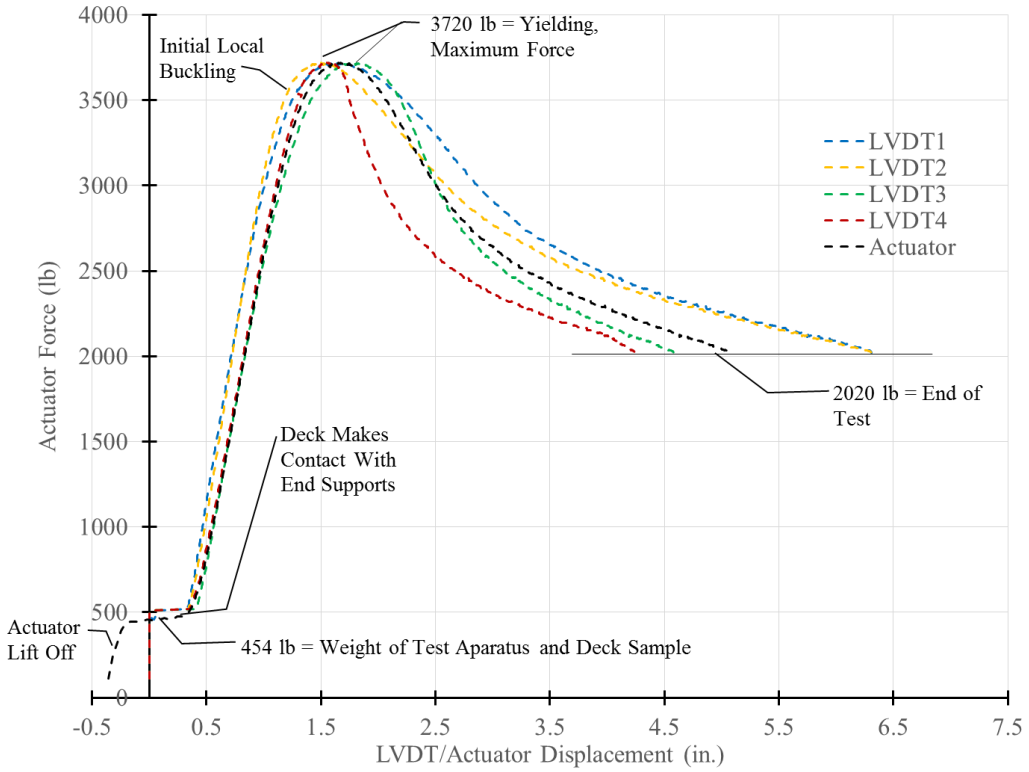

Figure 44: Results for Test 18-POS-02172017-03.

Figure 45 shows the results from each of the three 16 gage positive tests overlaid on one another. Once again, the plots show excellent consistency among tests.

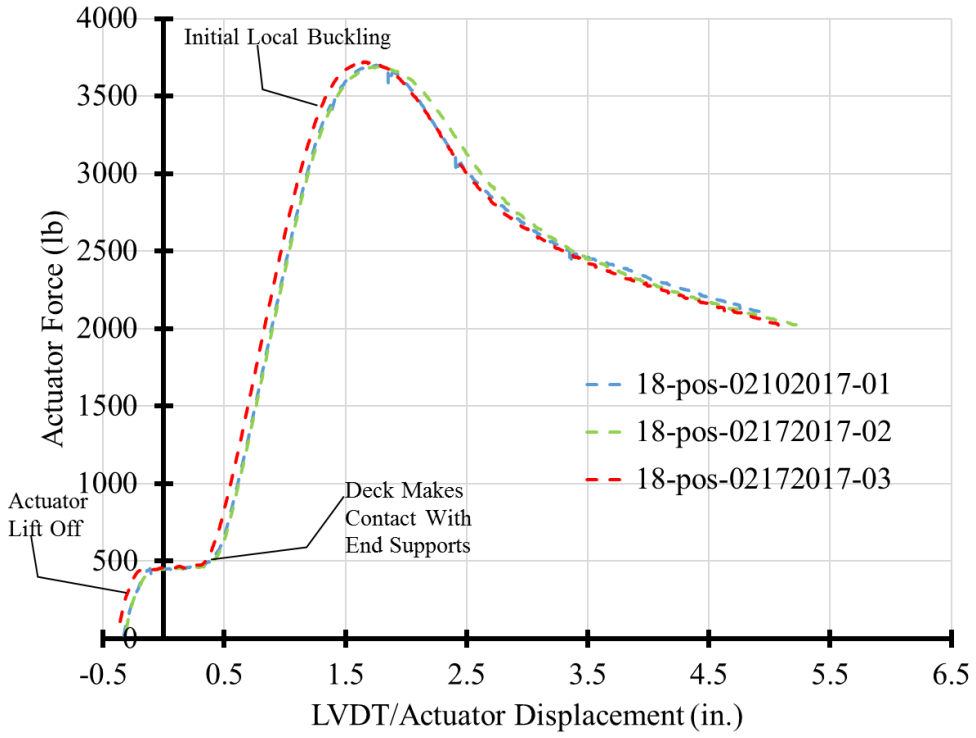

Figure 45: Overlay of 18 Gage Positive Test Results.

Figure 46 shows a photograph of 18 gage deck in positive bending test in place prior to testing.

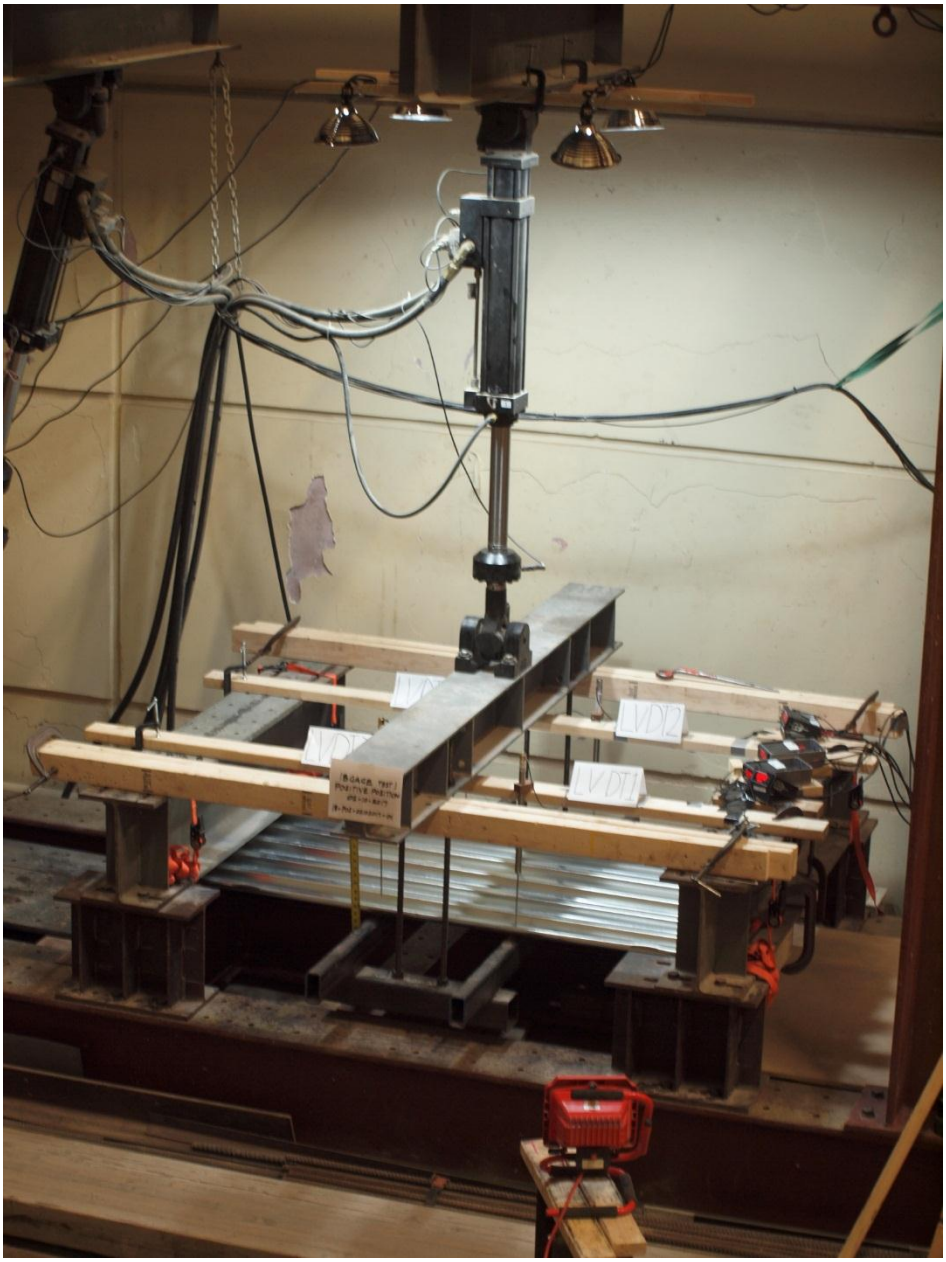

Figure 46: 18 Gage Deck Positive Bending - Initial Setup.

Figure 47 is a photograph of 18 gage deck in positive bending with slight local buckling beginning in the webs and the ribs.

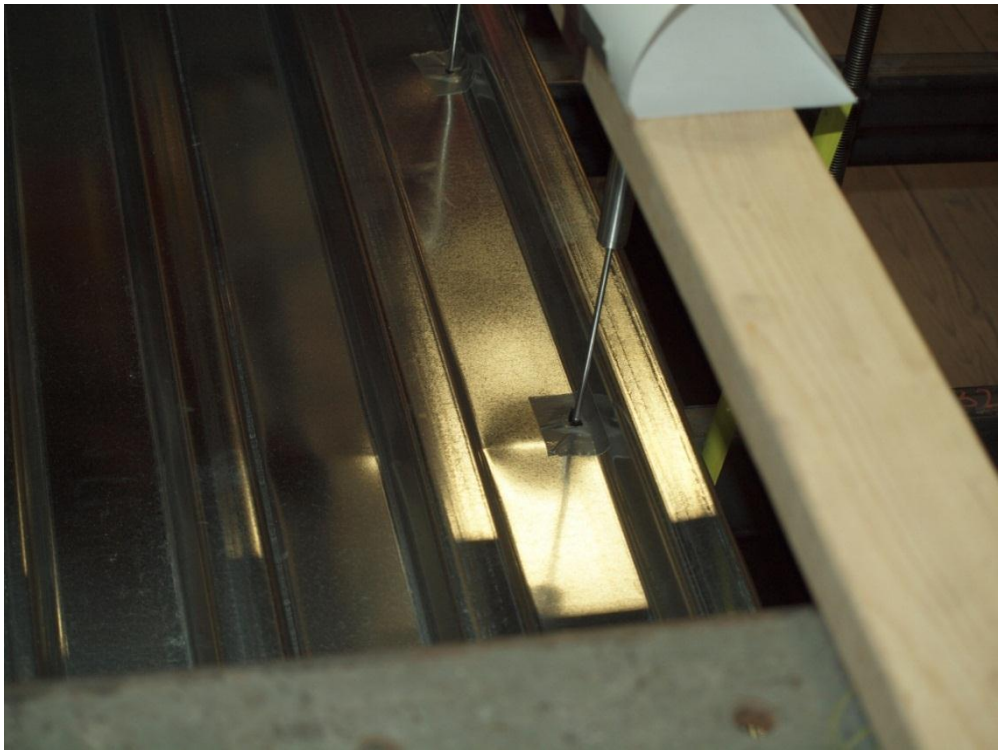

Figure 47: 18 Gage Deck Positive Bending - Initial Buckling.

Figure 48 is a photograph of 18 gage deck in positive bending with more severe local buckling and deformation. Notice the ribs at the application of the load have severely buckled.

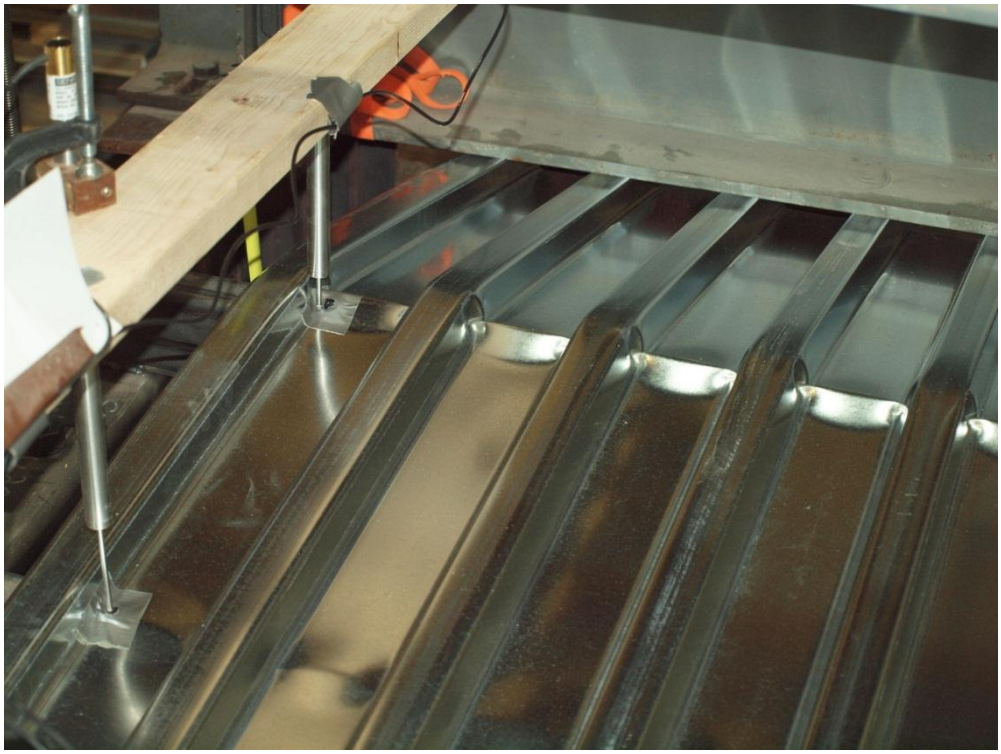

Figure 48: 18 Gage Deck Positive Bending - Further Buckling.

Figures 49, 50 and 51 show the results for the 20 gage roof deck tests for negative bending.

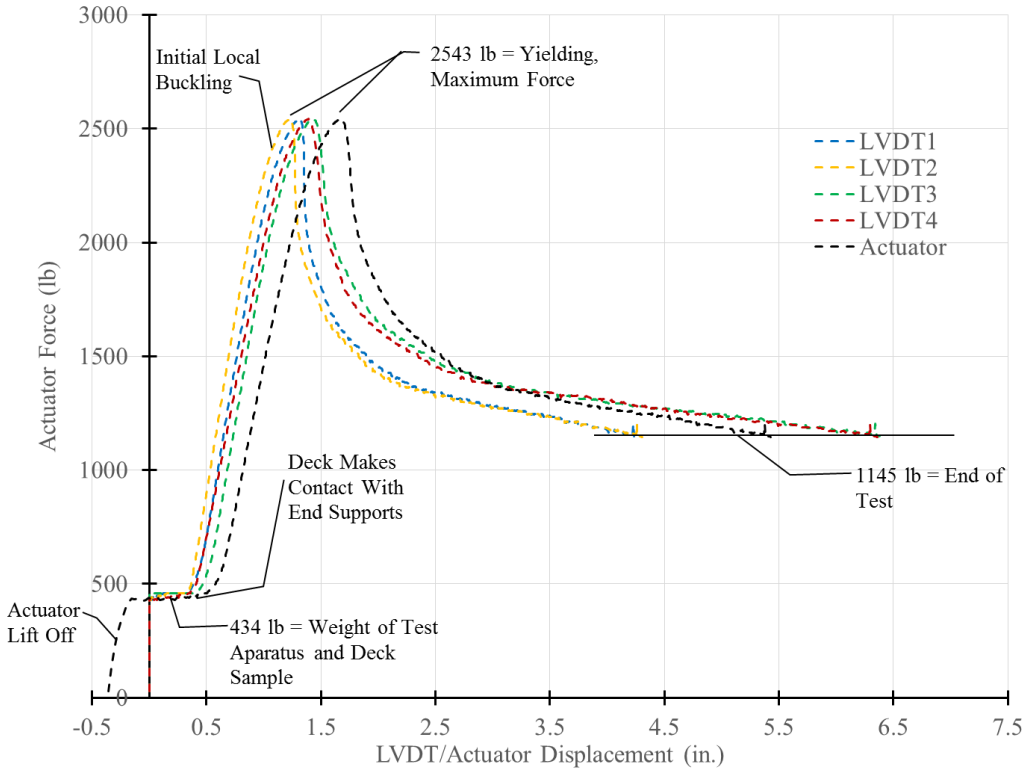

Figure 49: Results for Test 20-NEG-02172017-01.

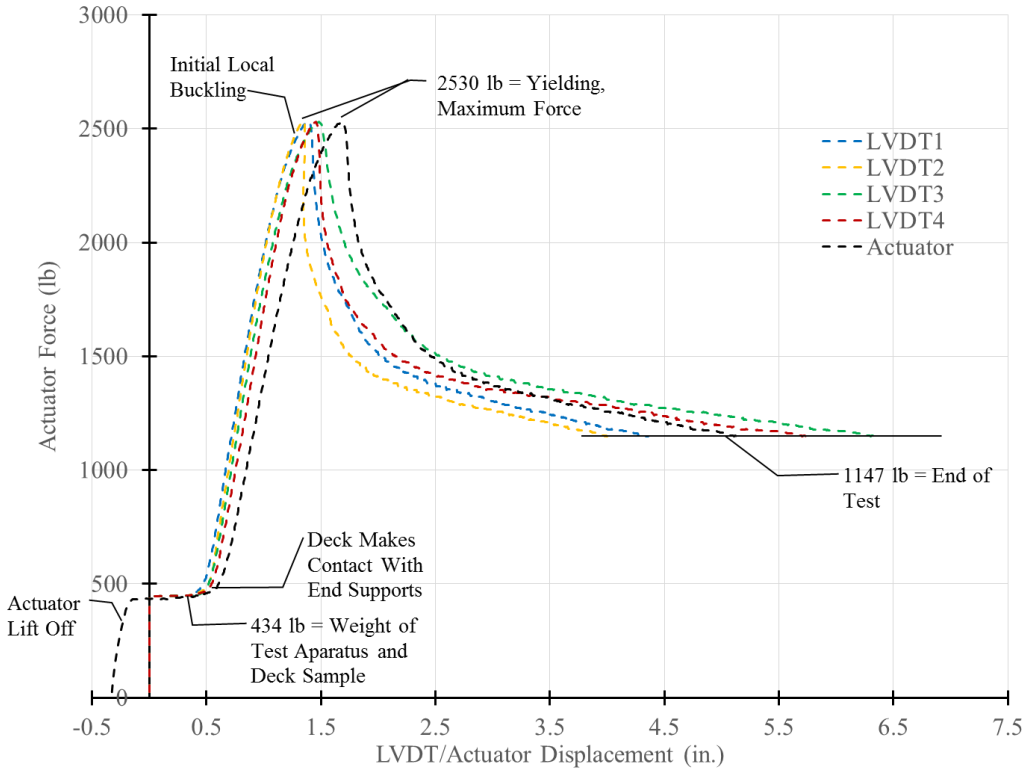

Figure 50: Results for Test 20-NEG-02222017-02.

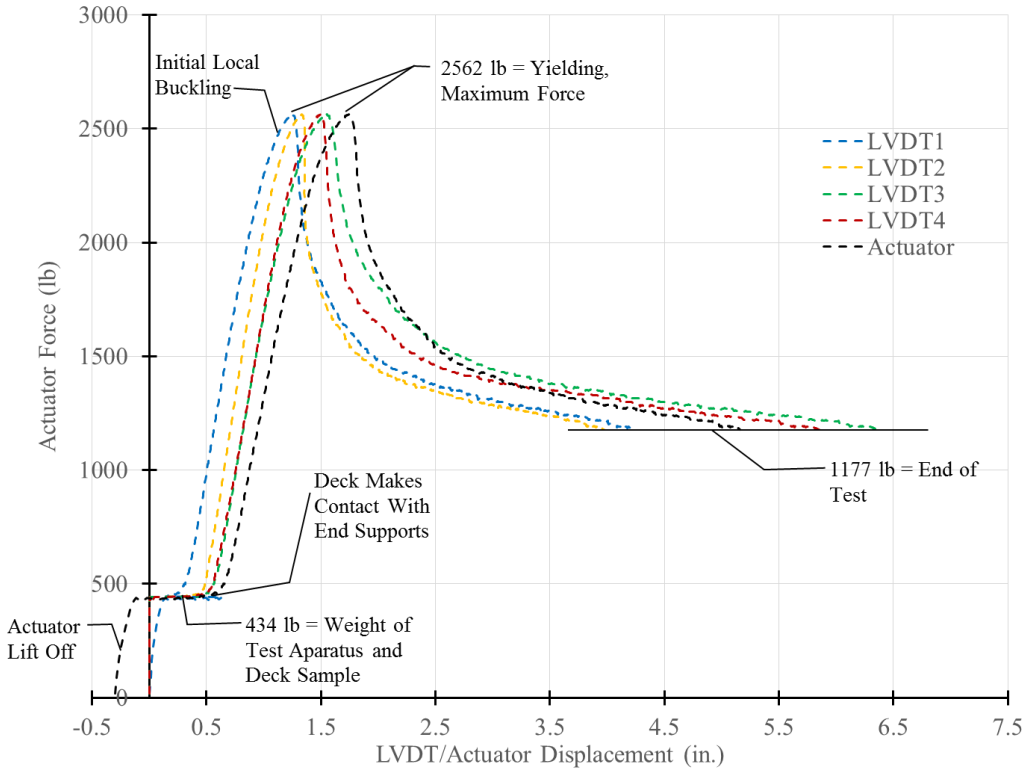

Figure 51: Results for Test 20-NEG-02222017-03.

Figure 52 shows the results from each of the three 20 gage negative tests overlaid on one another. Results among tests are consistent.

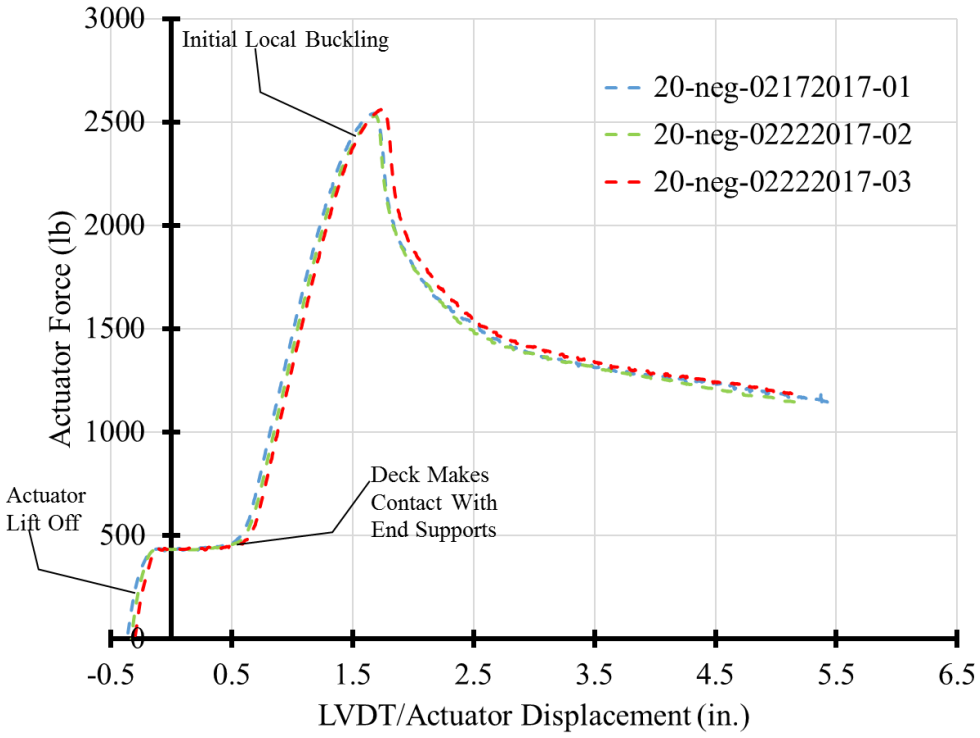

Figure 52: Overlay of 20 Gage Negative Test Results.

Figure 53 is a photograph of 20 gage deck in negative bending showing the initial signs of local buckling. This is typical after reaching the highest force reading and starting to decrease in applied load.

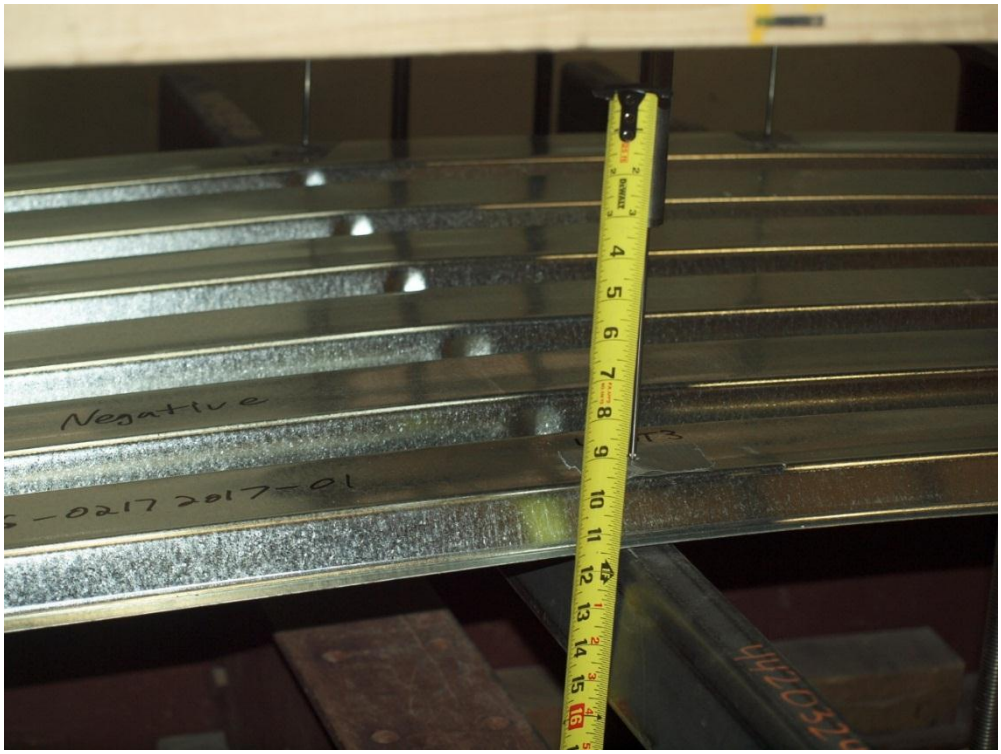

Figure 53: 20 Gage Deck Negative Bending - Initial Buckling.

Figure 54 is a photograph of 20 gage deck in negative bending with severe local buckling nearing the end of the test.

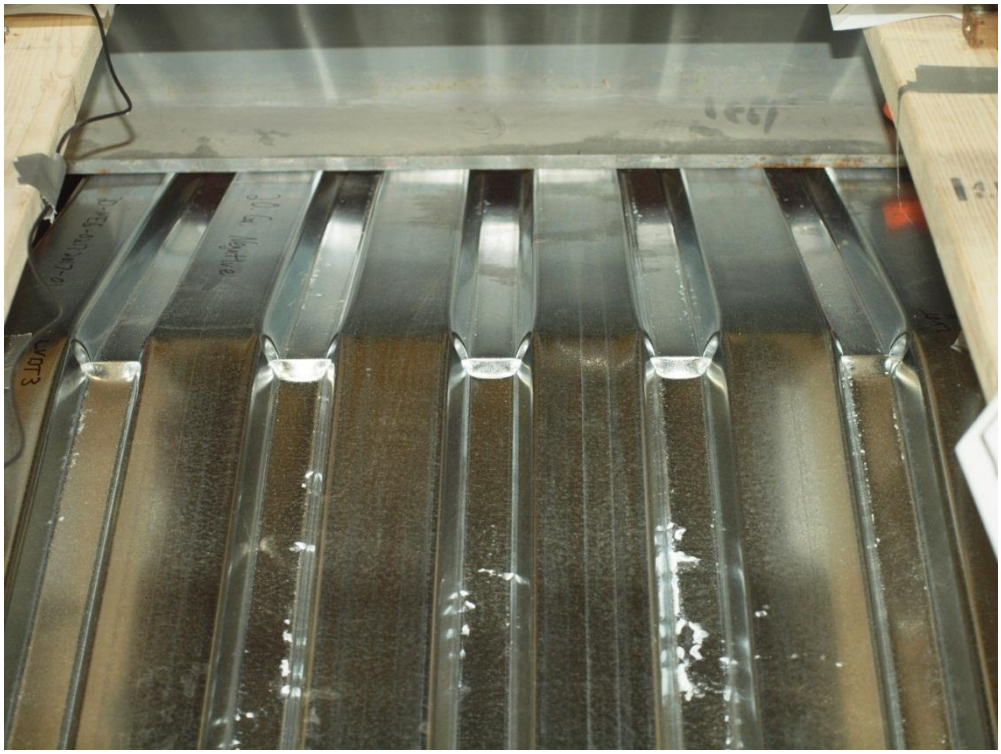

Figure 54: 20 Gage Deck Negative Bending - Further Buckling.

Figure 55 shows the results of the first 20 gage steel roof deck test for positive bending. This test had an issue with LVDT 3 and the signal conditioner returned fuzzy data. However, the maximum force at yielding is still useful as the load sensor was still reporting the data accurately. These data were still used in the average yielding force to compare with the analytical values.

Figures 56 through 58 show the results of the second through fourth 20 gage tests in the positive bending position, respectively. One additional test was conducted with this configuration.

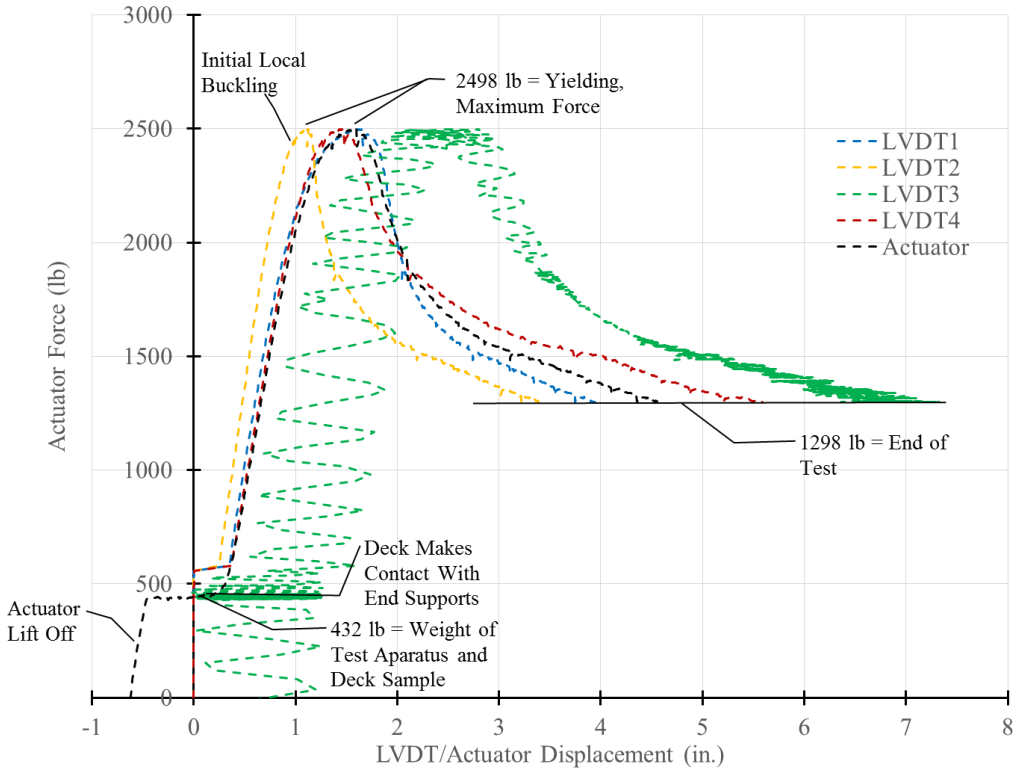

Figure 55: Results for Test 20-POS-01202017-01.

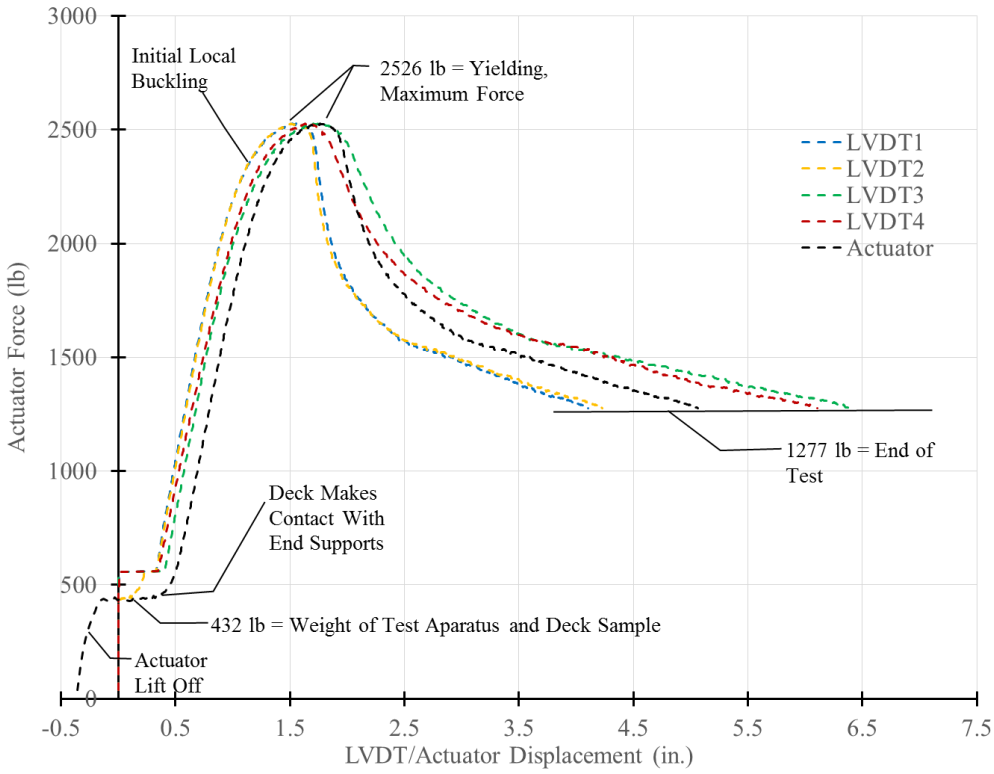

Figure 56: Results for Test 20-POS-02172017-02.

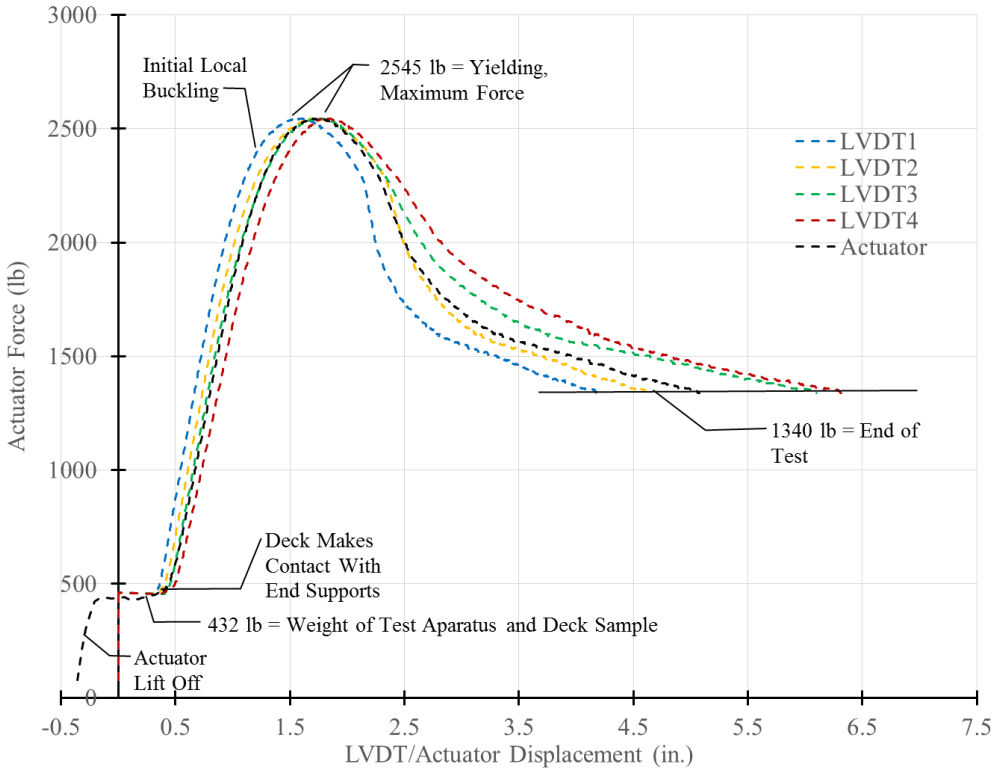

Figure 57: Results for Test 20-POS-02172017-03.

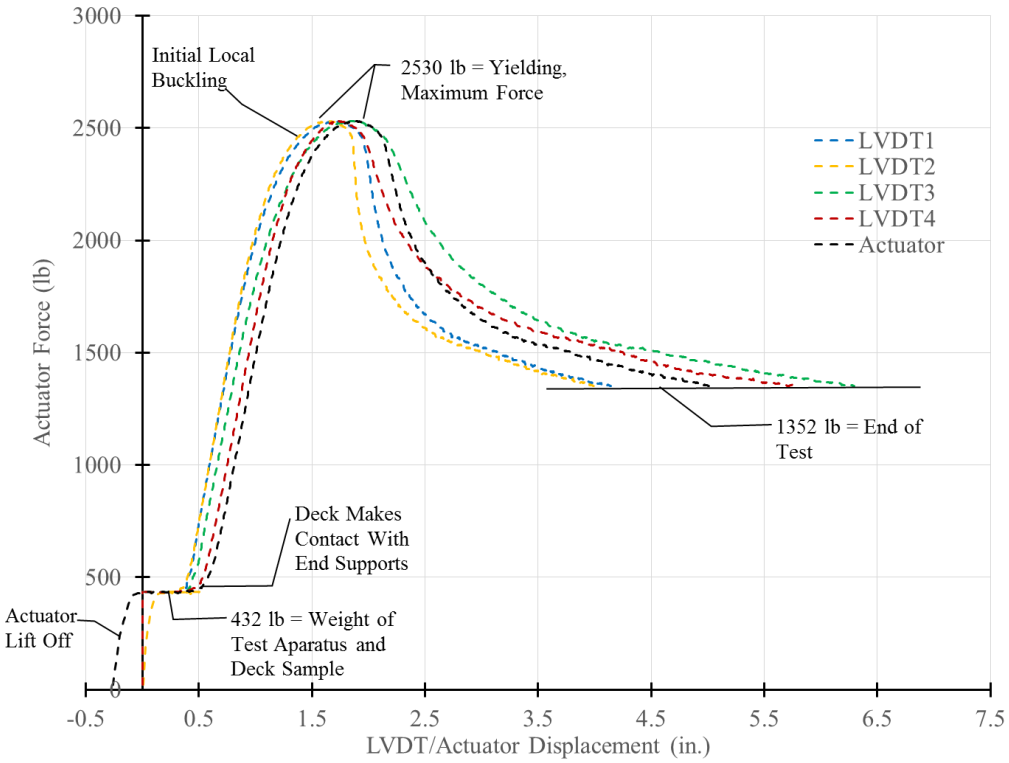

Figure 58: Results for Test 20-POS-03172017-04.

Figure 59 shows each of the 20 gage positive tests overlaid on one another. As with the tests of other gages, the 20 gage positive bending tests show consistent data.

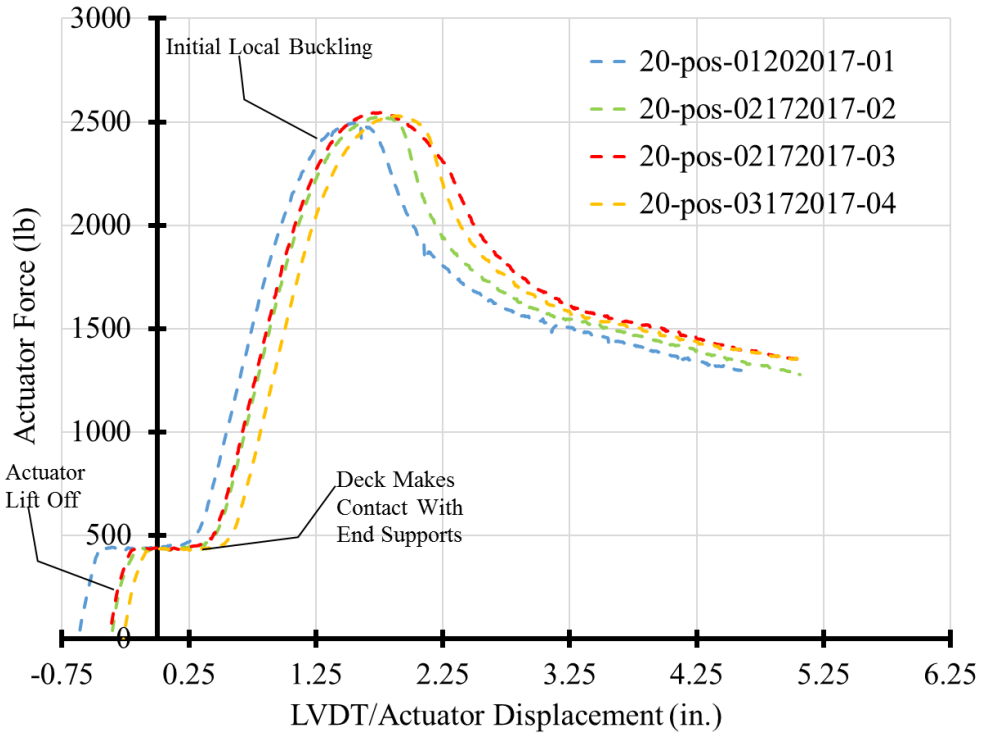

Figure 59: Overlay of 20 Gage Positive Test Results.

Figure 60 is a photograph of 20 gage deck in positive bending showing the early signs of local buckling. Notice the ripples in the ribs between the load points. This photograph was taken near the point of highest applied load during a test.

Figure 60: 20 Gage Deck Positive Bending - Initial Buckling.

Figure 61 is a photograph of 20 gage deck in positive bending with further local buckling. This would be typically seen just after maximum load.

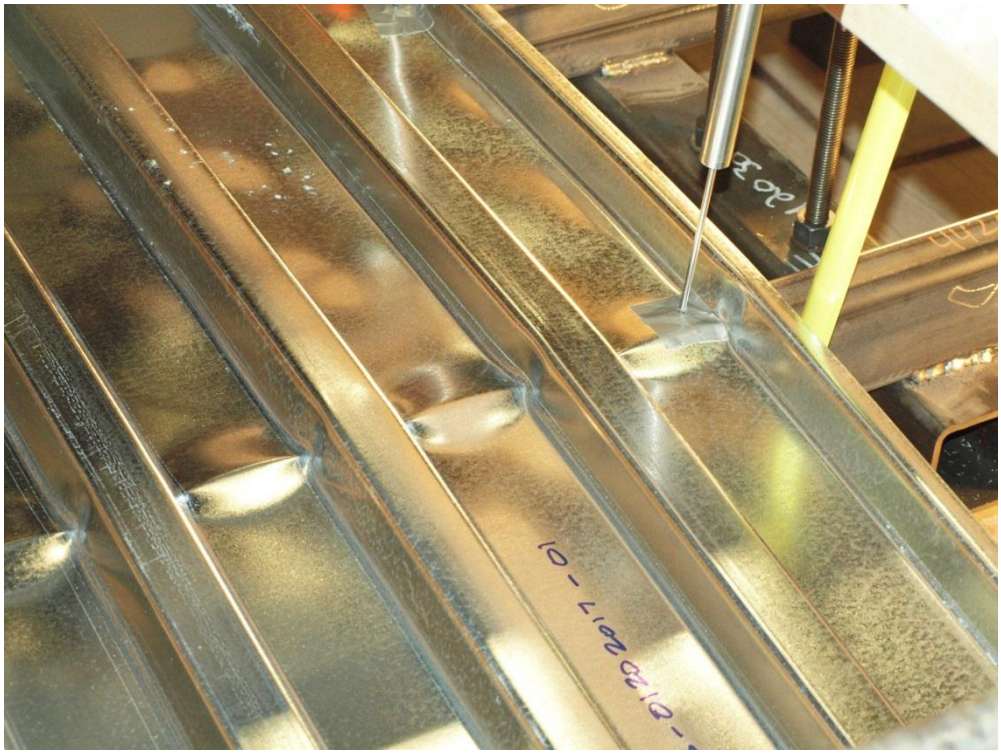

Figure 61: 20 Gage Deck Positive Bending - Further Buckling.

Figure 62 is a photograph of 20 gage deck in positive bending nearing the end of the test with significant local buckling.

Figure 62: 20 Gage Deck Positive Bending - Final State.

Figures 63, 64 and 65 show the results for the 22 gage roof deck tests for negative bending

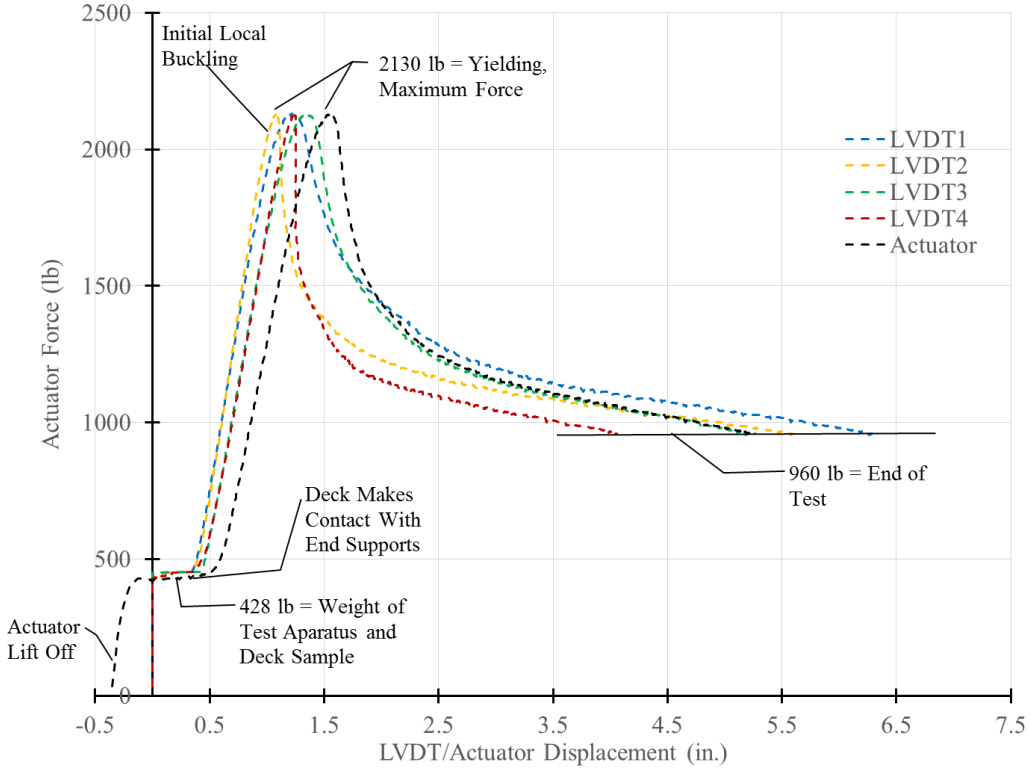

Figure 63: Results for Test 22-NEG-02172017-01.

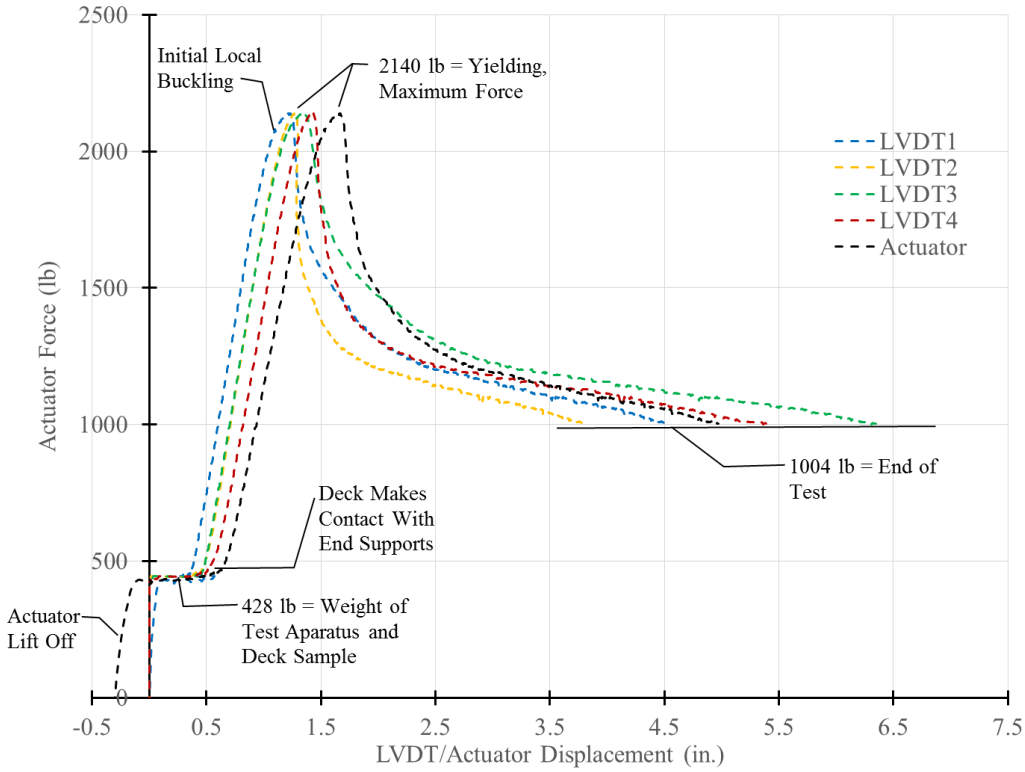

Figure 64: Results for Test 22-NEG-02222017-02.

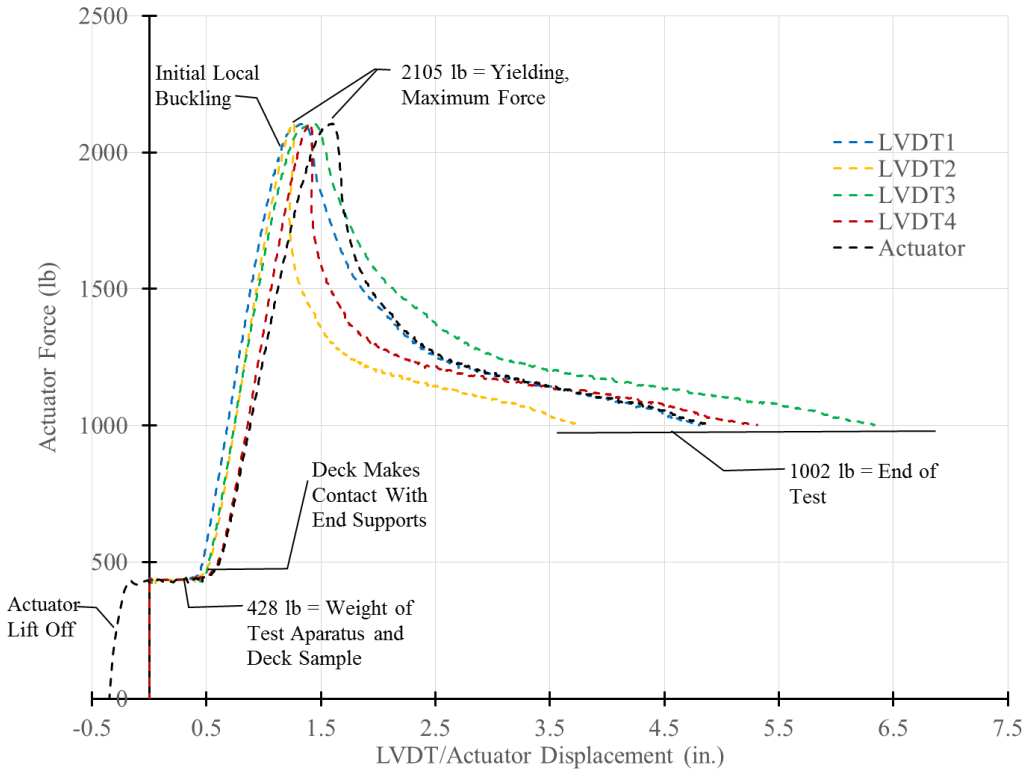

Figure 65: Results for Test 22-NEG-02222017-03.

Figure 66 shows each of the three 22 gage negative tests overlaid on one another. As with other sets of tests, results are very consistent.

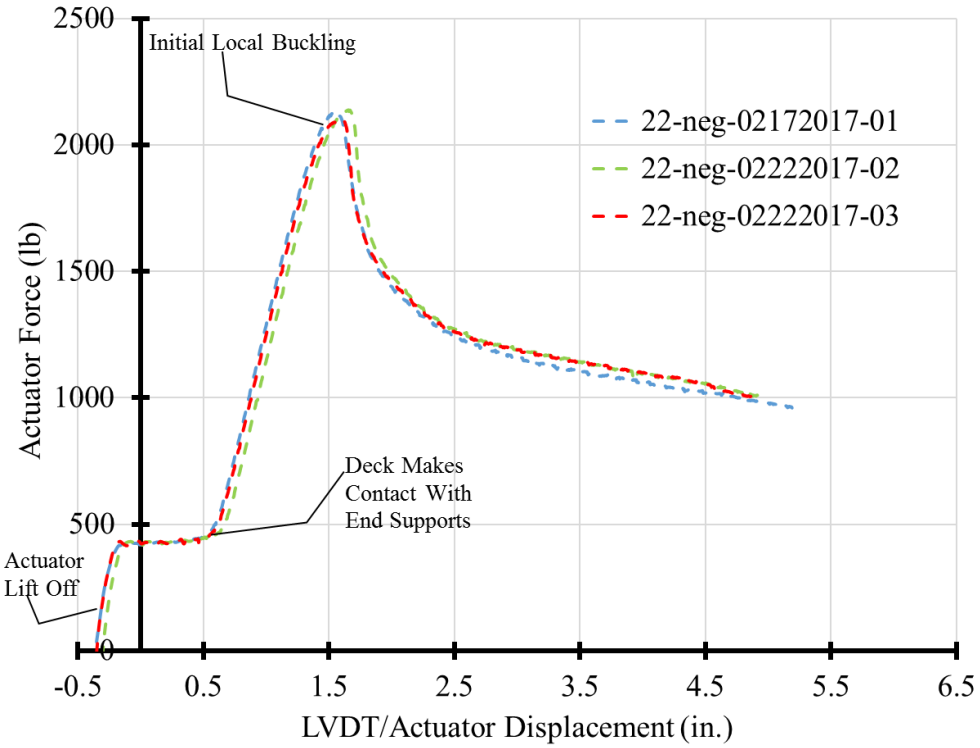

Figure 66: Overlay of 22 Gage Negative Test Results.

Figure 67 is a photograph of 22 gage deck in negative bending in the early stages of local buckling. Notice the webs and ribs buckling near the application of load as well as the exterior web starting to buckle outward.

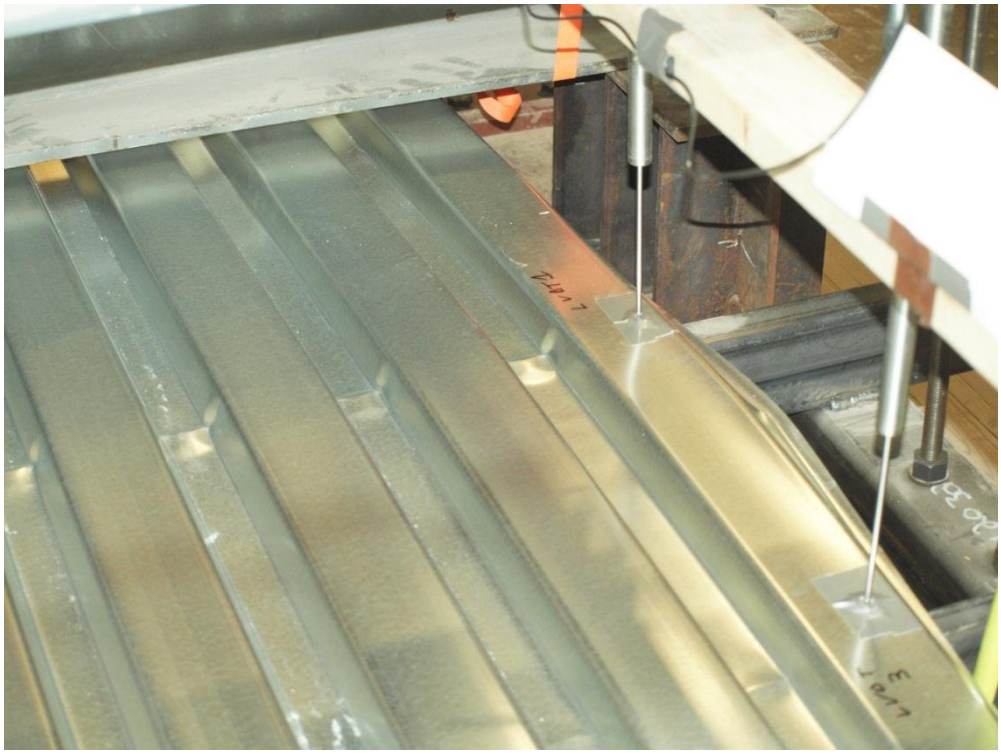

Figure 67: 22 Gage Deck Negative Bending - Initial Buckling.

Figure 68 is a photograph of 22 gage deck in negative bending in the test frame in its final state. Notice the severe buckling of the exterior unsupported web.

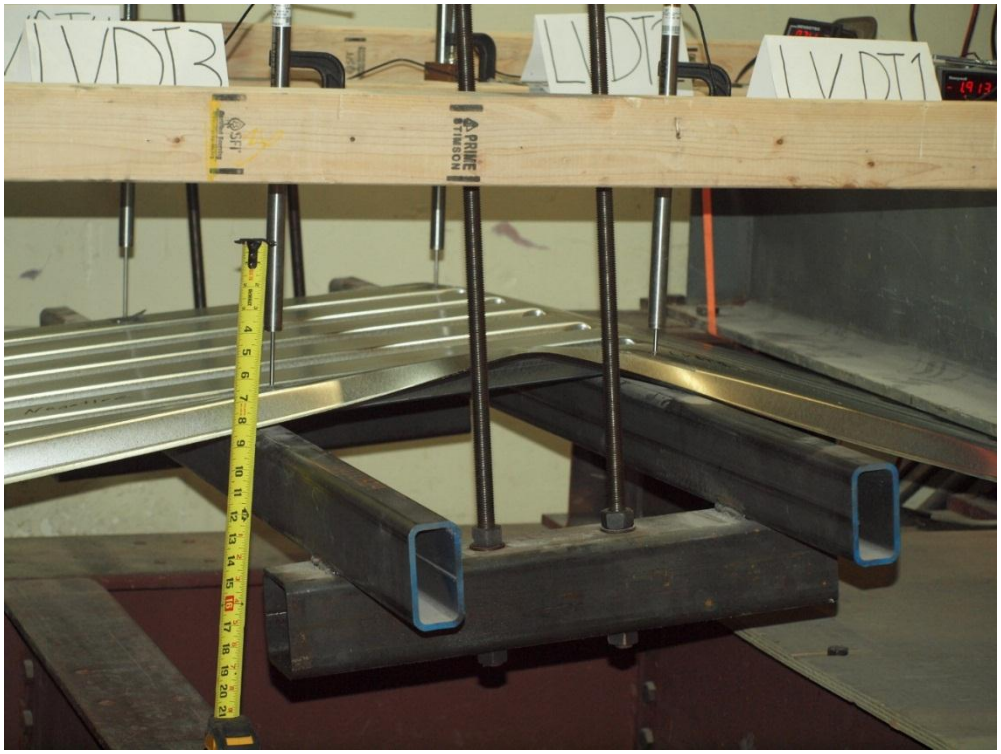

Figure 68: 22 Gage Deck Negative Bending - Final State.

Figure 69 shows the first 22 gage steel roof deck test results for positive bending. This test had an issue with LVDT 3 and the signal conditioner reported fuzzy data. However, the maximum force at yielding is still useful as the load sensor was still reporting the data accurately. These data were still used in the average yielding force to compare with the analytical values.

Figures 70 through 72 show load versus displacement plots for 22 gage roof deck in positive bending. Four tests were conducted with 22 gage deck to ensure enough tests were conducted after the first test returned questionable data for LVDT 3.

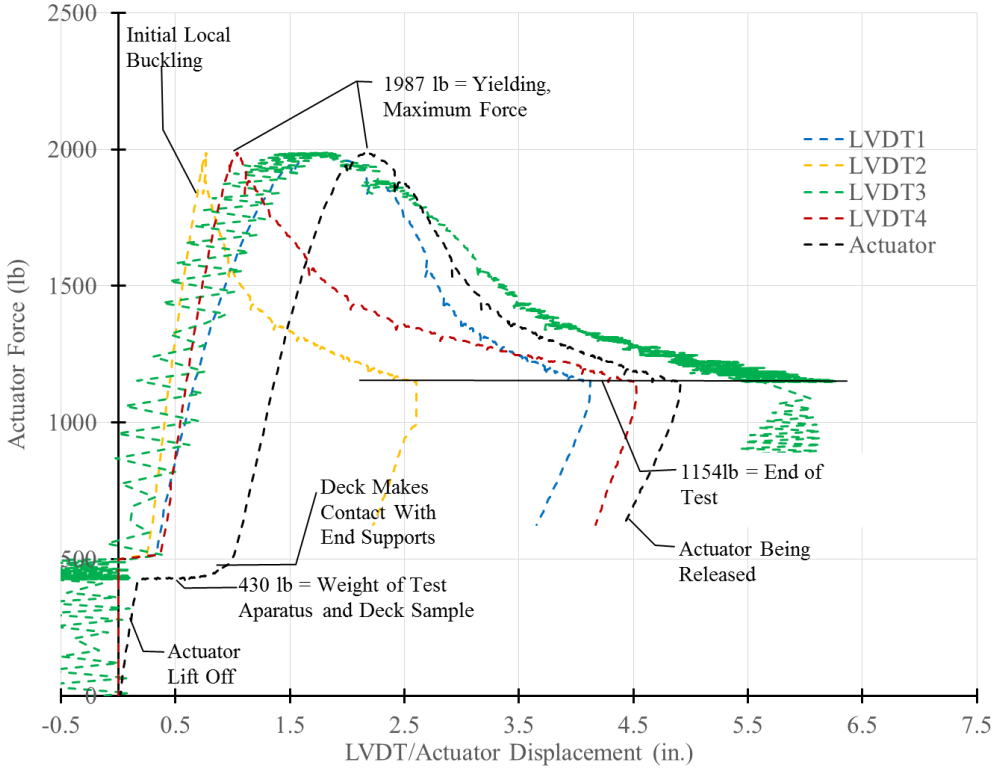

Figure 69: Results for Test 22-POS-01202017-01.

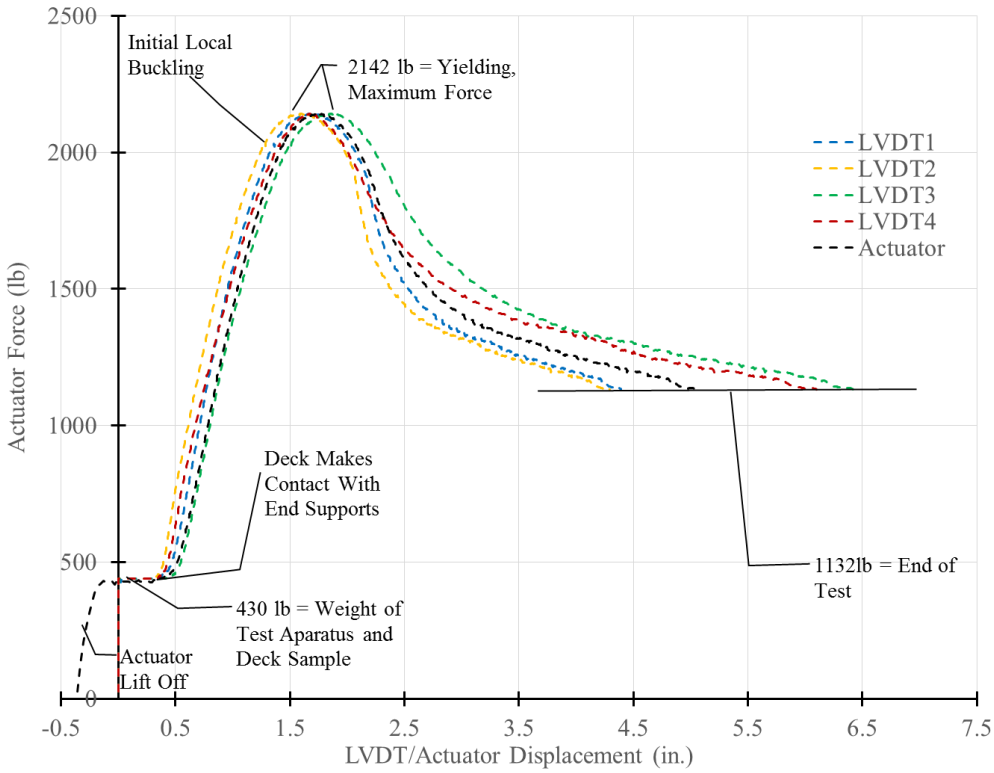

Figure 70: Results for Test 22-POS-02172017-02.

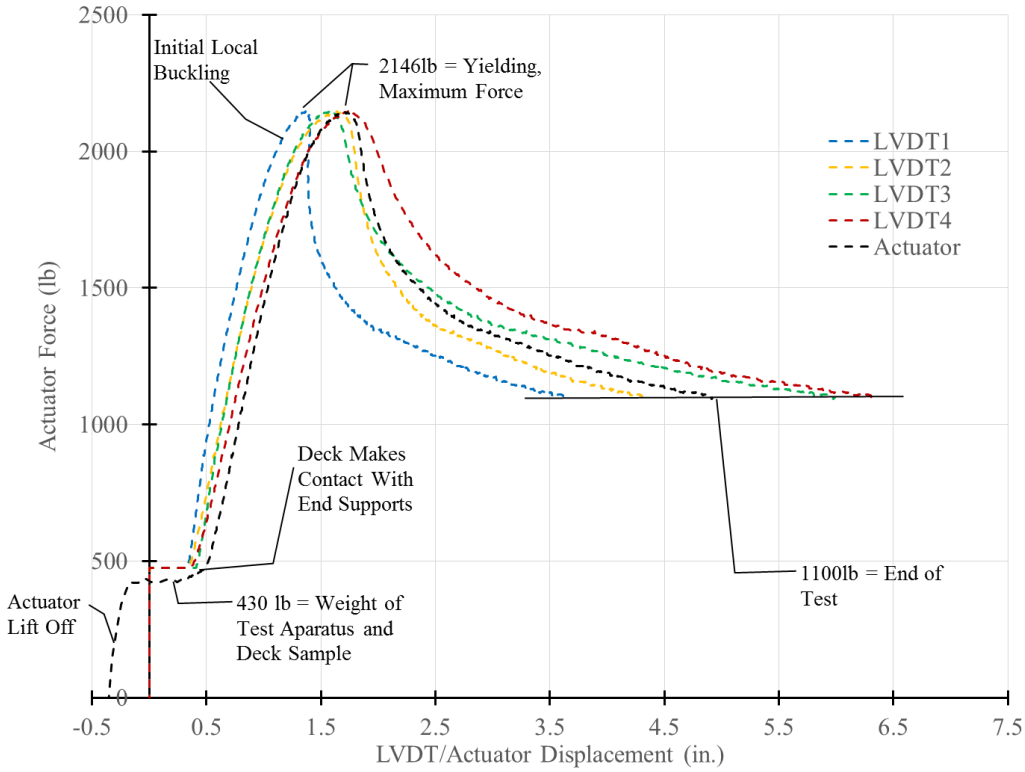

Figure 71: Results for Test 22-POS-02172017-03.

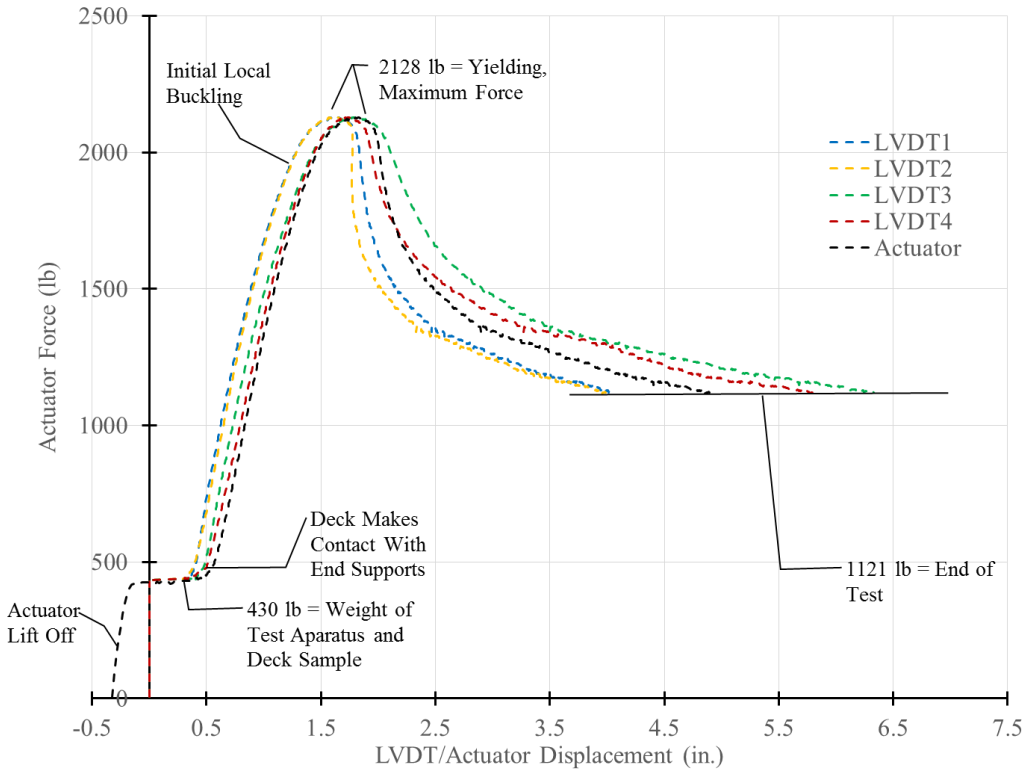

Figure 72: Results for Test 22-POS-03172017-04.

Figure 73 shows each of the 22 gage positive tests overlaid on one another. Tests 02, 03 and 04 are very consistent, but test 01 shows a lower maximum force and a somewhat shifted force versus displacement trace. However, the general trend is similar to the other tests.

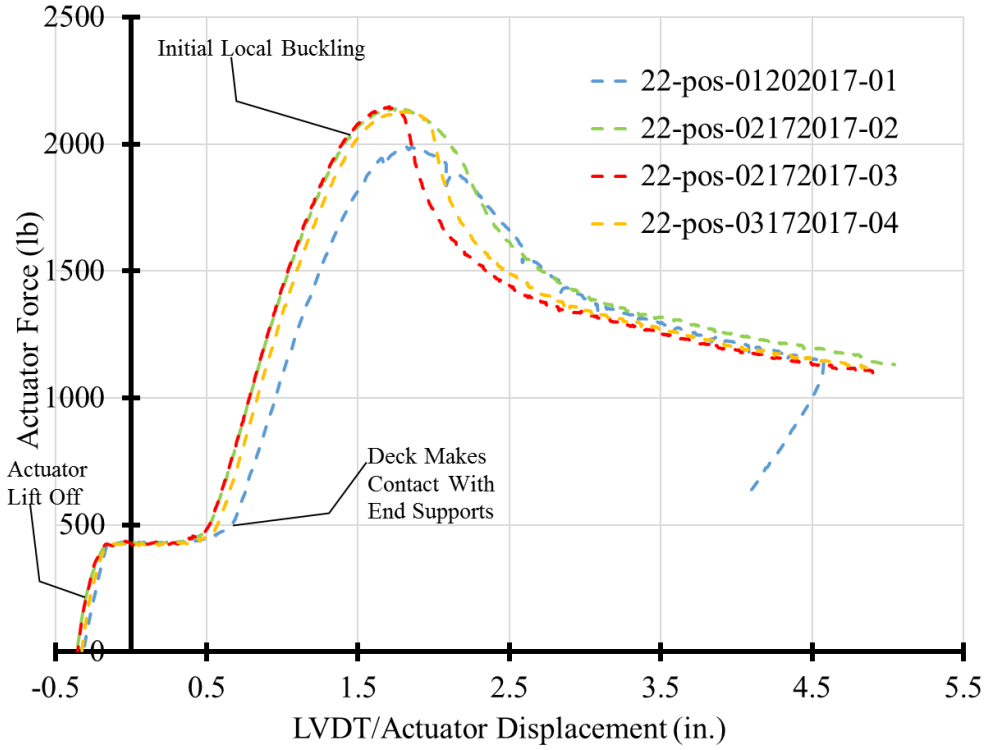

Figure 73: Overlay of 22 Gage Positive Test Results.

Figure 74 is a photograph of 22 gage deck in positive bending showing the signs of initial local buckling. Notice the bottom ribs buckling in the constant moment region between the load points. This photograph was taken just before maximum applied load was reached.

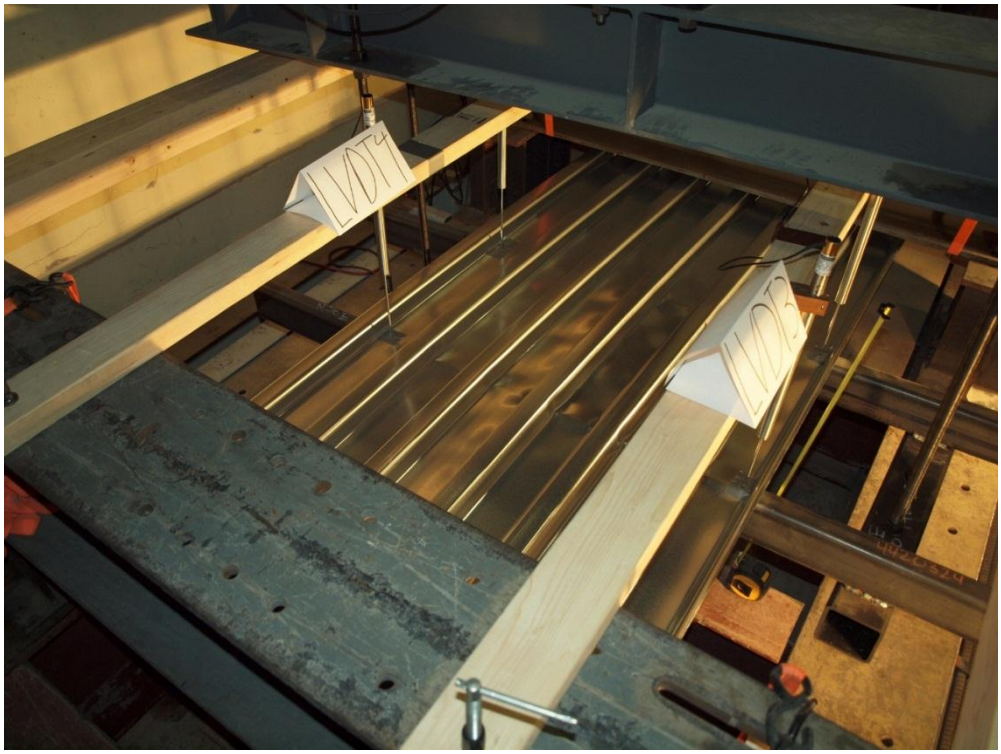

Figure 74: 22 Gage Deck Positive Bending - Initial Buckling.

Figure 75 is a photograph of 22 gage deck in positive bending showing more pronounced local buckling in the webs and ribs.

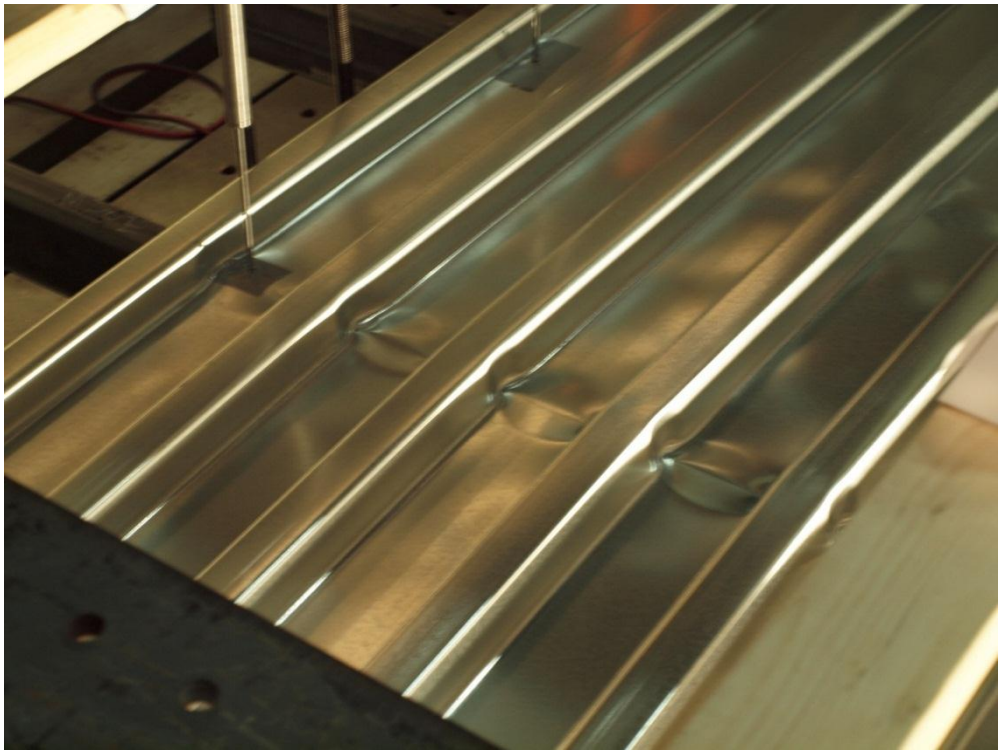

Figure 75: 22 Gage Deck Positive Bending - Further Buckling.

Figure 76 is a photograph of 22 gage deck in positive bending after being removed from the test frame and in its final state.

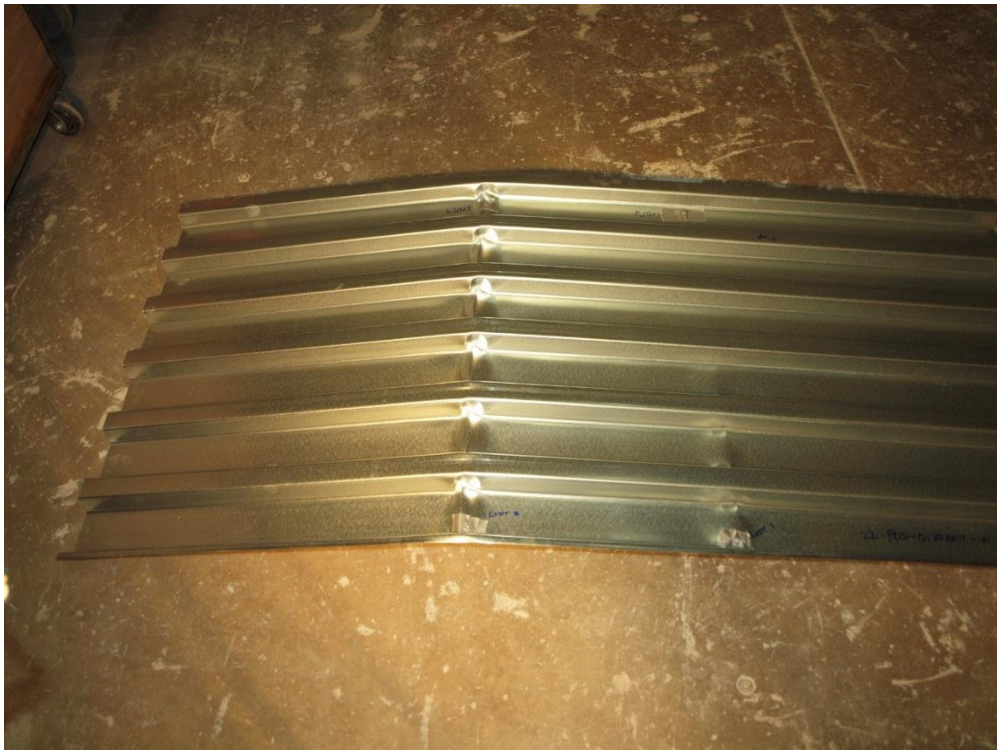

Figure 76: 22 Gage Deck Positive Bending - Final State.

3.1.2 Summary of Key Data Points

Several key points were extracted from the data and summarized in the Table 20. Note that even though test 01 was reported for both the 22 gage and 20 gage deck under positive bending, these data were not used in calculating the maximum moment capacity because of the LVDT malfunction mentioned previously.

Table 20: Summary of Key Data Points.

Deck	Orientation	DL (lb)*	T1 Yield (lb)	T2 Yield (lb)	T3 Yield (lb)	T4 Yield (lb)
1.5WR22	Positive	430	1987	2142	2146	2128
1.5WR20	Positive	432	2498	2526	2545	2530
1.5WR18	Positive	454	3699	3690	3720	-
1.5WR16	Positive	464	4915	4914	4901	-
1.5WR22	Negative	428	2130	2140	2105	-
1.5WR20	Negative	434	2543	2530	2562	-
1.5WR18	Negative	448	3828	3700	3845	-
1.5WR16	Negative	459	4938	5052	5049	-

**DL is the weight of the test frame pieces, deck and actuator clevis*

The test data were averaged and used for comparison to the EWM results and the DSM results. Table 21 summarizes the average nominal moment capacity as well as the corresponding load applied to produce that moment magnitude.

Table 21: Average Nominal Moment Capacity.

Deck	Orientation	Ave. Yield (lb)	Applied Load Ave. (lb)	Applied Mn (kip-in.)
1.5WR22	Positive	2101	1671	22.56
1.5WR20	Positive	2525	2093	28.25
1.5WR18	Positive	3703	3249	43.86
1.5WR16	Positive	4910	4446	60.02
1.5WR22	Negative	2125	1697	22.91
1.5WR20	Negative	2545	2111	28.50
1.5WR18	Negative	3791	3343	45.13
1.5WR16	Negative	5013	4554	61.48

3.2 Discussion

3.2.1 Comparison of Effective Width Method Results and Experimental Results

Figure 77 illustrates the average nominal moment capacities as determined from test data as compared to the nominal moment capacity as calculated using the Effective Width Method.

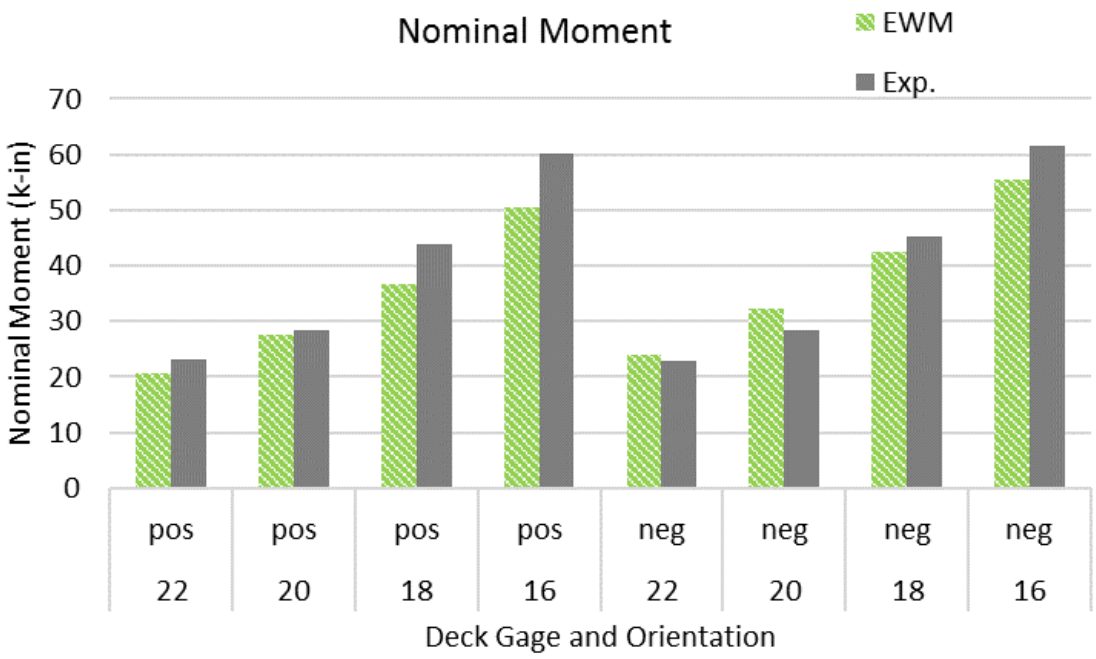

Figure 77: EWM Nominal Moment versus Experimental Nominal Moment.

The EWM results compare well with the experimental results. For positive bending, as the deck thickness increases, the nominal moment magnitude that the EWM predicts separates from the magnitude calculated using experimental results. For negative bending, the EWM over predicted nominal moment capacity for both the 22 gage and 20 gage decks, but underestimated the moment capacity for the heavier decks. The underestimation is similar in magnitude to that observed with the positive bending results. There are a few possible explanations for this discrepancy. First, as the deck started to buckle locally, the effective section decreased leading to a lower effective section in the experiment, thus leading to a lower nominal moment. Since the EWM assumes the effective section remains the same throughout the test up to the point of first failure, this is a viable theory as it would lead to a higher nominal moment capacity. Furthermore, the possibility of the section flattening out due to the effects of buckling

could be considered as a mechanism for reducing the depth of the section, resulting in decreased the maximum moment capacity.

The typical installation method for these steel roof decks differs from that in the experimental setup. Typical installation includes panels laying side by side and usually being attached along their length, known as "sidelap" connections. Without the sidelap connections, the steel roof deck in the laboratory experiments was free to deform at its sides. This may have contributed to a "flattening" effect and a reduction in the effective section modulus, whereas the typical in situ installation would restrain such movement.

3.2.2 Comparison of Direct Strength Method Results and Experimental Results

Figure 78 compares the average nominal moment capacities as calculated using the DSM against the nominal moment capacities as calculated using experimental results.

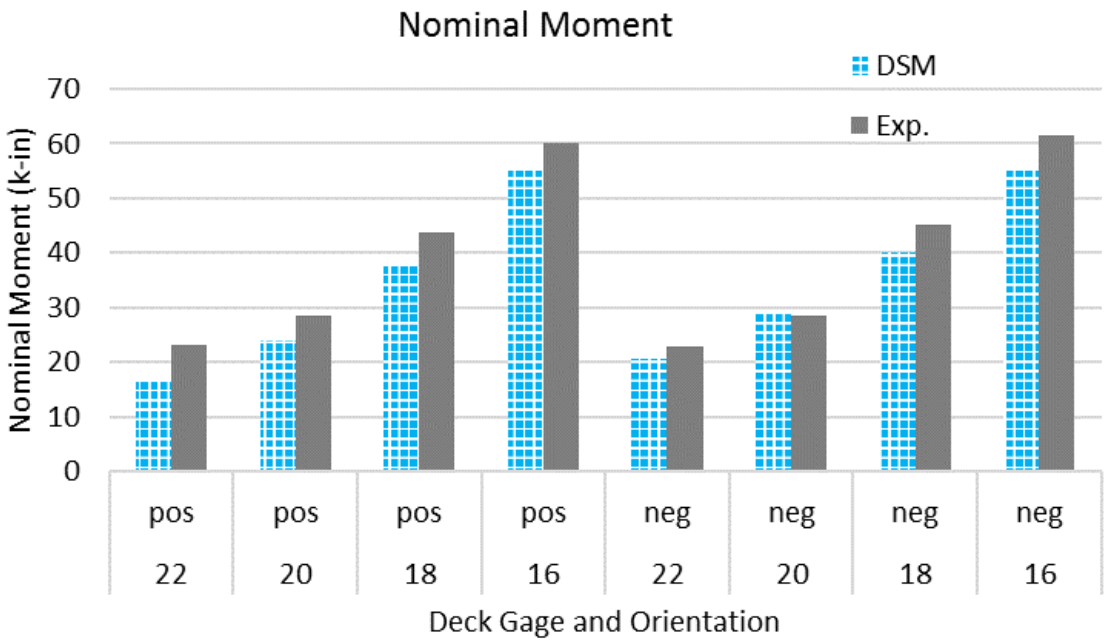

Figure 78: DSM Nominal Moment versus Experimental Nominal Moment.

Similar to that of the EWM, the results under predicted the nominal moment capacity as compared to the experimental nominal moment capacity. One observation is that the difference between the DSM and experimental value stays more consistent as deck thickness increases. The DSM results for 20 gage deck in negative bending slightly overestimated the moment capacity as compared to the experimental. Similar reasoning as that used in the EWM comparison section can be made.

Figure 79 compares the nominal moment capacities using the EWM, DSM and the experimental results.

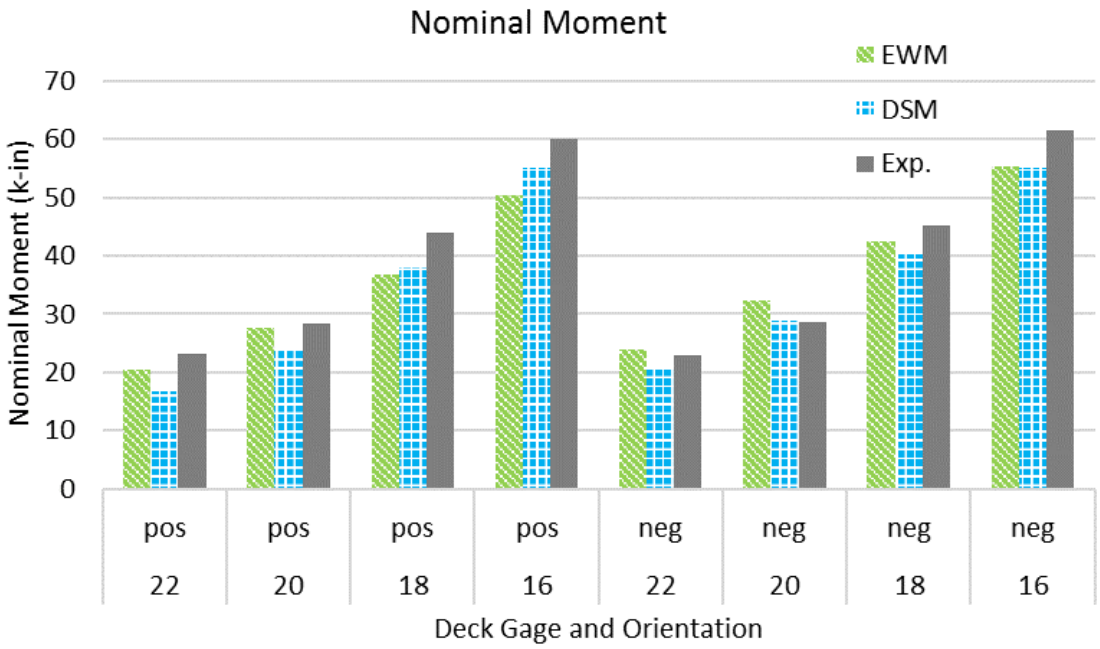

Figure 79: Nominal Moment Capacities: EWM versus DSM versus Experimental.

Table 22 compares the nominal moment capacities as calculated using the EWM, the DSM and experimental data. Also included in this table is the theoretical yield

moment as calculated using basic mechanics. The percent differences calculated use the experimental magnitude as a basis.

Table 22: Summary of Nominal Moment Results (Experimental as Base Value).

Deck	Exp Mn (kip-in.)	EWM Mn (kip-in.)	SR	DSM Mn (kip-in.)	SR	Yield My (kip-in.)	SR
1.5WR22 (Pos)	23.07	20.53	0.89	16.67	0.72	25.37	1.10
1.5WR20 (Pos)	28.38	27.66	0.97	23.98	0.84	34.02	1.20
1.5WR18 (Pos)	43.86	36.81	0.84	37.93	0.86	41.71	0.95
1.5WR16 (Pos)	60.02	50.38	0.84	54.98	0.92	54.98	0.92
1.5WR22 (Neg)	22.91	23.96	1.05	20.53	0.90	25.37	1.11
1.5WR20 (Neg)	28.50	32.29	1.13	28.91	1.01	34.02	1.19
1.5WR18 (Neg)	45.13	42.53	0.94	40.22	0.89	41.71	0.92
1.5WR16 (Neg)	61.48	55.41	0.90	54.98	0.89	54.98	1.10

A trend between the DSM and the EWM was noticed that is consistent with Dudenbostel's study [1]. The ratio of DSM to EWM typically starts out with the EWM results being higher than the DSM for the thinner gage decks. As the deck thickness increases, the DSM begins to increase and surpasses the EWM at thicker gages.

Chapter 4: Conclusions and Recommendations

4.0 Conclusions

4.0.1 Effective Width Method Conclusions

The effective width method was observed to provide more comparable results to the experimental data for the thinner gage decks. As deck thickness increased, the effective width method separated from the experimental results and under predicted the nominal moment capacity.

An observation was made regarding the computation time necessary to produce EWM results. One must investigate each unique element of a given shape's cross-section. One must also consider the geometric properties of the element and an effective width for that element is calculated given an assumed centroidal location. Furthermore, this is an iterative process so multiple iterations are necessary in a software program to generate a solution that converges.

4.0.2 Direct Strength Conclusion

The direct strength method was observed as typically under predicting the capacity of the thinner decks as compared to the effective width method. However, once the thicker decks were being analyzed, the DSM eclipsed that of the EWM and in some cases surpassed it. The main benefit observed in the DSM is the ease of using the CUFSM program and coming up with capacities for a given cross-section with all failure modes (local, distortional and global buckling) assessed and a graphical read-out of the first failure. Once the user had a shape drawn in the program, adjusting the thickness was a simple input change. Multiple shapes could be run in a short amount of time.

4.1 Recommendations

4.1.1 Analysis Method

The analysis of steel roof deck without stiffeners is one where different methods may be necessary to produce an accurate solution. The EWM is most appropriate for analyzing thinner roof deck (e.g., 20 or 22 gage).

The DSM is more suitable to thicker roof decks (e.g., 18 and 16 gages).

A general recommendation can be made to the use of these two analysis methods. The DSM may be used for all roof deck gages and produce reasonable results, albeit somewhat conservative as compared to EWM results for thinner deck. Although the EWM could also be used for any analysis its overestimation of nominal moment capacity for thinner deck in negative bending causes concern.

4.2 Suggestions for Future Research

Further research is necessary. An obvious next step is to study steel floor deck with stiffeners in the flanges of the deck. The impact of these stiffeners would be interesting to observe in the lab in full scale testing and comparing the results to both the EWM and the DSM. Additional tests could be run where the loading is altered with a single line load perpendicular to the span of the deck sample instead of a constant moment region. Also, tests could then include a uniform pressure applied to the deck sample as opposed to a line load. Both of these could be run in the laboratory with full scale specimens and observations and data collected could be compared to the EWM and the DSM results. These tests could prove valuable as a constant moment region is not as common as a uniform pressure or point load on roof deck.

References

[1] Dudenbostel, Randall. 2015. *Direct Strength Method For Steel Deck.* Master's thesis, University of Florida, Gainesville.

[2] Li, Z and Schafer, B. "Buckling Analysis of Cold-Formed Steel Members with General Boundary Conditions using CUFSM: Conventional and Constrained Finite Strip Methods." In American Iron and Steel Institute *et al.* 3-4 November 2010. *Twentieth International Specialty Conference on Cold-Formed Steel Structures -- Recent Research and Developments in Cold-Formed Steel Design and Construction*. University of Missouri-Rolla, pp. 17-31.

[3] Ping, Kee (Steven). 20 April 2006. *Influence of Steel Deck Properties and Attachment on Wind Uplift Resistance.* National Research Council Canada. Canada.

[4] Schafer, B W and Adany, S. "Buckling Analysis of Cold-Formed Steel Members Using CUFSM: Conventional and Constrained Finite Strip Methods." In *Eighteenth International Specialty Conference on Cold-Formed Steel Structures: Recent Research and Developments in Cold-Formed Steel Design and Construction*, 26-27 October 2006. University of Missouri-Rolla, pp. 39-54.

[5] Yu, C and Lokie, T. "Effective Width Method Based Design for Distortional Buckling of Cold Formed Steel Beams." In *Eighteenth International Specialty Conference on Cold-Formed Steel Structures: Recent Research and Developments in Cold-Formed Steel Design and Construction*, 26-27 October 2006. University of Missouri-Rolla, pp. 105-118.

[6] American Iron and Steel Institute (AISI S100). 2012. *North American Specification for the Design of Cold-Formed Steel Structural Members.*

[7] CANAM Solutions + Service. 2010. *Steel Deck Manual*. Point of Rocks, MD: CANAM. *1.5 Type B Roof Deck Data Base.* [Internet, WWW, PDF]. ADDRESS: https://www.canam-construction.com/wp-content/uploads/2014/11/canam-steel-deck.pdf

Appendix A: Hand Calculations

A.1 Effective Width Method

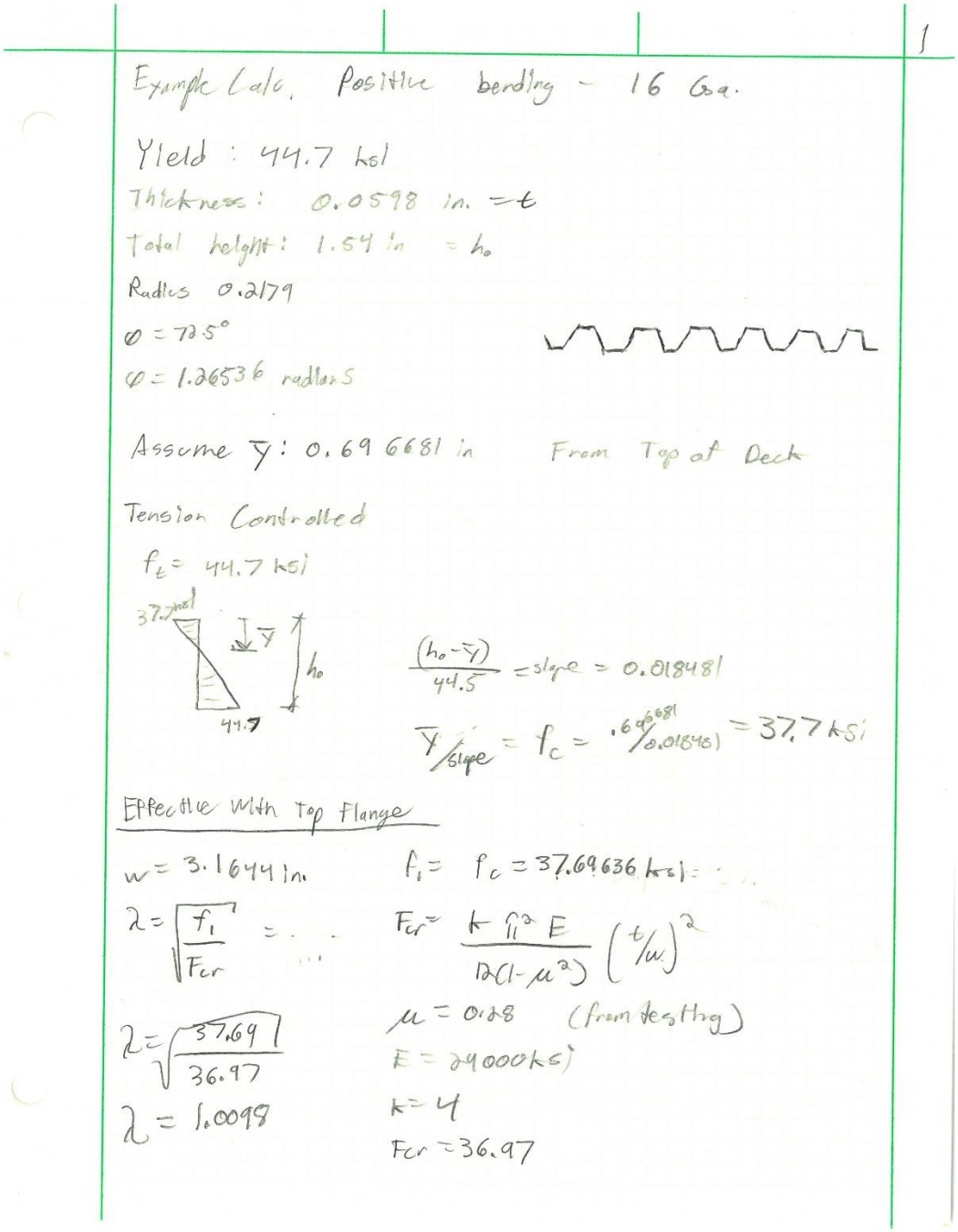

Figure A1: 16 Gage EWM Example Calculations.

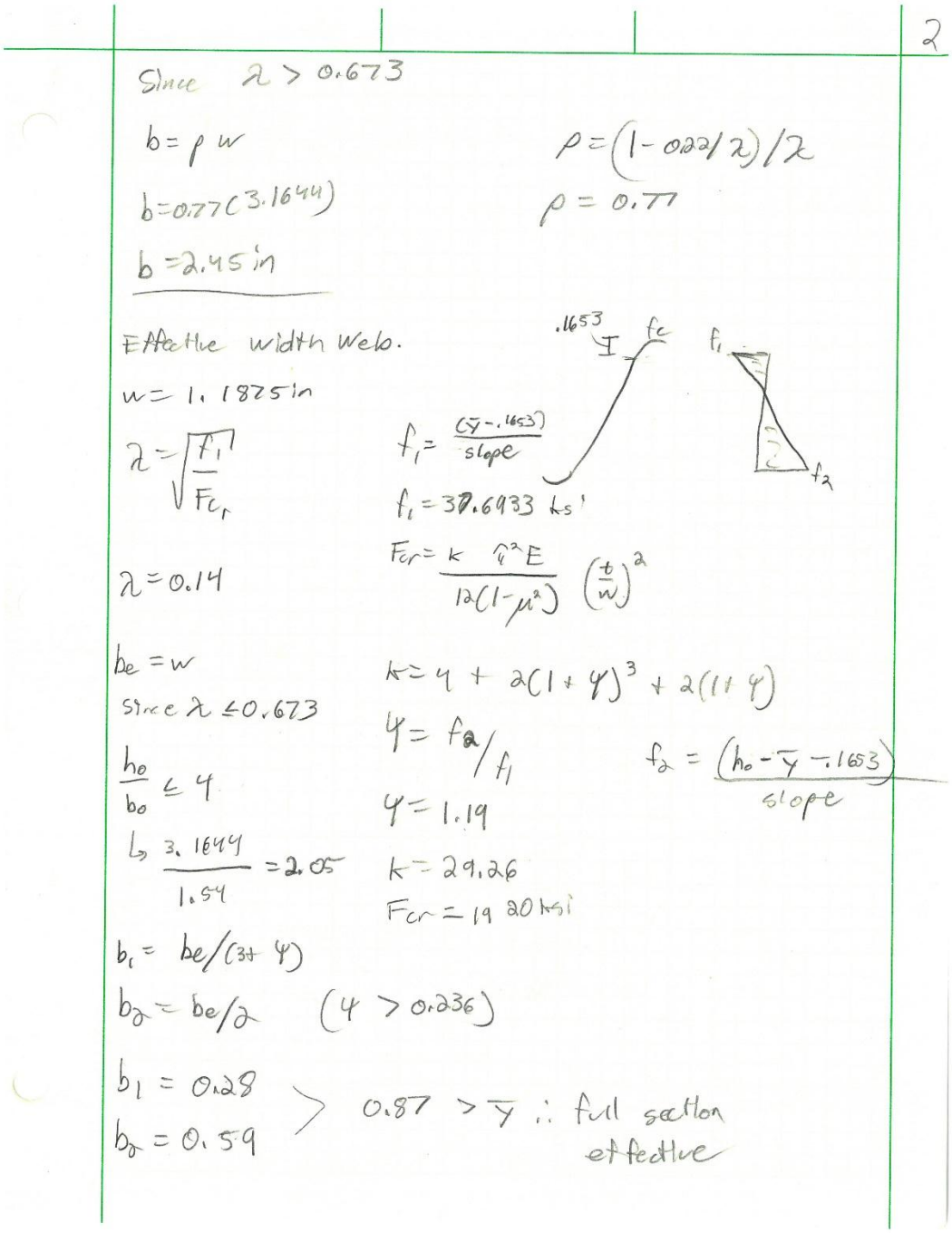

Figure A2: 16 Gage EWM Example Calculations.

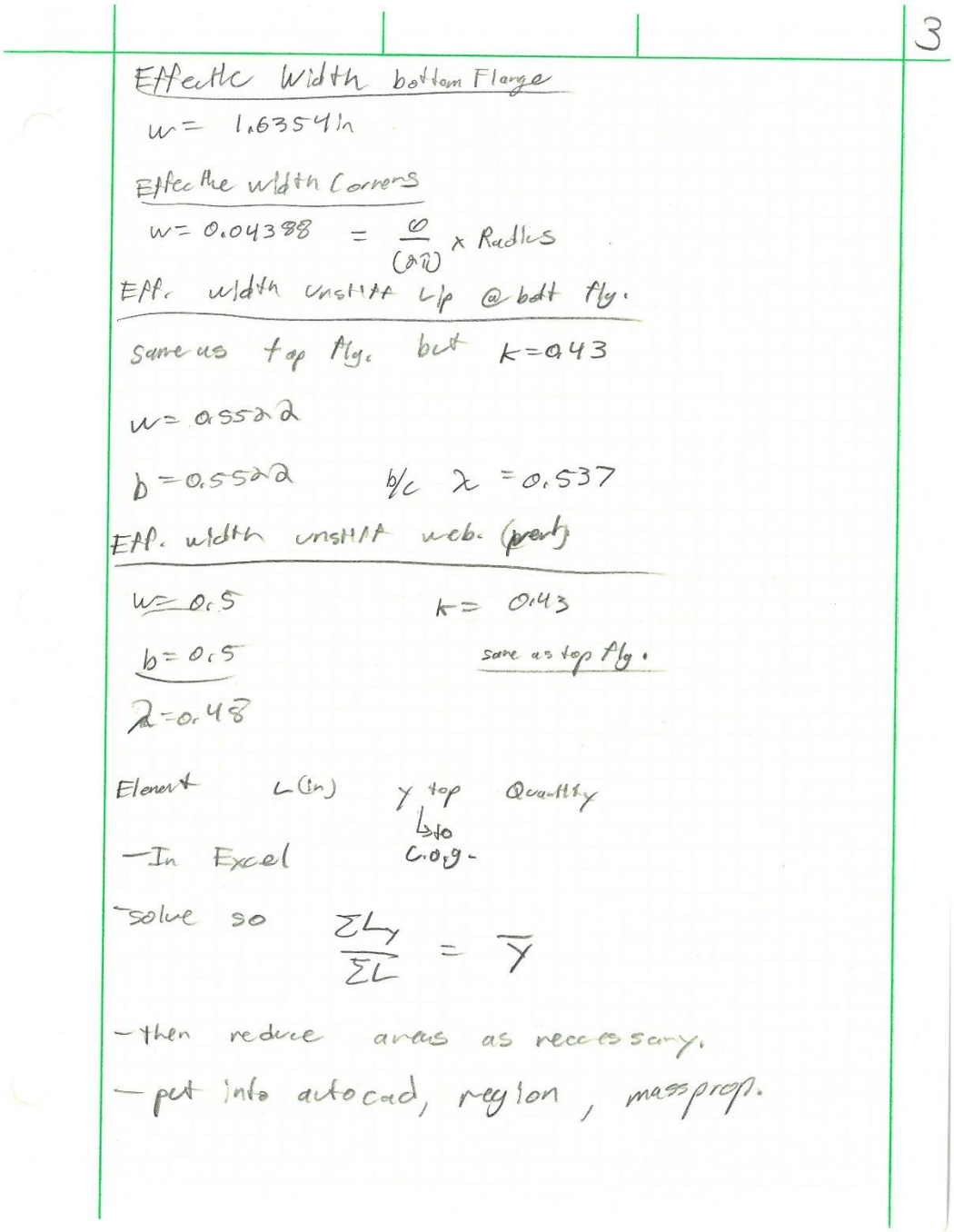

Figure A3: 16 Gage EWM Example Calculations.

Deck	1.5B	pos bend
Gage	16	GA
Yield	44.7	ksi
Thickness	0.0598	in
Total Height	1.54	in
Radius	0.2179	in
θ	72.5	degrees
θ	1.265363708	radian
Curve I'x	0.000592	in^3

Effective Width Top Flange		
w	3.1644	
b	2.45101949	
λ	1.009771019	0.713381
ρ	0.774560577	0.35669
f	37.69636234	
k	4	-
E	29000	ksi
μ	0.28	-
t	0.0598	in
Fcr	36.97035653	ksi

Tension Controlled							
			y bar	0.696681	in		
			fc	37.69636			
			ft	44.7			
			slope	0.018481			
Element	L (in)	y from top (in.)	Quantity	ΣL	ΣLy	$ΣLy^2$	
Lip	0.5522	1.5101	1	0.5522	0.833877	1.259238	
T, Corners	0.043883	0.0878	12	0.526592	0.046235	0.004059	
B, Corners	0.043883	1.4522	13	0.570474	0.828443	1.203065	
Top Flg.	2.451019	0.0299	6	14.70612	0.439713	0.013147	
Web, b1	0	0	12	0	0	0	
Web, b2	0	0	12	0	0	0	
lip up	0.5	1.136270762	1	0.5	0.568135	0.645556	
Web, Ten	0	0	12	0	0	0	
Web	1.1875	0.77	12	14.25	10.9725	8.448825	
Bot. Flg.	1.6354	1.5101	6	9.8124	14.81771	22.37622	
				40.91778	28.50661	33.95011	
0.69668							
7.54E-07							

Comp Controlled		
y bar	0.696681	in
fc	44.7	
ft	54.1085	
slope	0.015586	

Effective Width Web		
w	1.1875	in
be	1.1875	
λ	0.14010535	
ρ	-4.07012977	
f1	37.69330737	
f2	44.69694503	
k	29.25806784	-
E	29000	ksi
μ	0.28	-
t	0.0598	in
Fcr	1920.236874	ksi
ψ	1.185805867	
b1	0.283696865	
b2	0.59375	
w in comp	0.557168384	
Check	0.877446865	
ho/bo	2.054805195	-

Effective Width Bottom Flange		
w	1.6354	in

Effective Width Corners		
w	0.043882639	in

Effective Width Unstiff. Lip Horiz.		
w	0.5522	in
b	0.5522	
λ	0.537432216	
ρ	1.09901497	
f	37.69636234	
k	0.43	-
E	29000	ksi
μ	0.28	-
t	0.0598	in
Fcr	130.5124824	ksi

Effective Width Unstiff. Lip Vert.		
w	0.5	in
b	0.5	
λ	0.486628	
ρ	1.12593	
f	37.69636	
k	0.43	-
E	29000	ksi
μ	0.28	-
t	0.0598	in
Fcr	159.186	ksi

Figure A4: 16 Gage Positive EWM Example Calculation.

Deck	1.5B	pos bend
Gage	18	GA
Yield	43.45	ksi
Thickness	0.0474	in
Total Height	1.54	in
Radius	0.2179	in
θ	72.5	degrees
θ	1.265363708	radian
Curve I'x	0.000592	in^3

Effective Width Top Flange		
w	3.1644	
b	2.112538049	
λ	1.229992711	1.051862
ρ	0.667595136	0.525931
f	35.14091212	
k	4	-
E	29000	ksi
μ	0.28	-
t	0.0474	in
Fcr	23.22779338	ksi

Tension Controlled						
Element	L (in)	y from top (in.)	Quantity	ΣL	ΣLy	$ΣLy^2$
Lip	0.5522	1.5163	1	0.5522	0.837301	1.269599
T, Corners	0.043883	0.0878	12	0.526592	0.046235	0.004059
B, Corners	0.043883	1.4522	13	0.570474	0.828443	1.203065
Top Flg.	2.112538	0.0237	6	12.67523	0.300403	0.00712
Web, b1	0	0	12	0	0	0
Web, b2	0	0	12	0	0	0
lip up	0.5	1.136270762	1	0.5	0.568135	0.645556
Web, Ten	0	0	12	0	0	0
Web	1.1875	0.77	12	14.25	10.9725	8.448825
Bot. Flg.	1.6354	1.5163	6	9.8124	14.87854	22.56033
				38.88689	28.43156	34.13856

0.731135
9.86E-05

Tension Controlled		
y bar	0.731233	in
fc	35.14091	
ft	43.45	
slope	0.020809	

Comp Controlled		
y bar	0.731233	in
fc	43.45	
ft	48.05704	
slope	0.016829	

Effective Width Web		
w	1.1875	in
be	1.1875	
λ	0.461555069	
ρ	1.13388525	
f1	35.13747246	
f2	43.44656034	
k	4	-
E	29000	ksi
μ	0.28	-
t	0.0474	in
Fcr	164.9390426	ksi
ψ	1.236473693	
b1	0.280303877	
b2	0.59375	
w in comp	0.593397572	
Check	0.874053877	

Effective Width Bottom Flange		
w	1.6354	in

Effective Width Corners		
w	0.043882639	in

Effective Width Unstiff. Lip		
w	0.5522	in
b	0.5522	
λ	0.654641197	
ρ	1.014201442	
f	35.14091212	
k	0.43	-
E	29000	ksi
μ	0.28	-
t	0.0474	in
Fcr	81.9985864	ksi

Effective Width Unstiff. Lip		
w	0.5	in
b	0.5	
λ	0.592757	
ρ	1.060895	
f	35.14091	
k	0.43	-
E	29000	ksi
μ	0.28	-
t	0.0474	in
Fcr	100.0136	ksi

Figure A5: 18 Gage Positive EWM Example Calculation.

Deck	1.5B	pos bend
Gage	20	GA
Yield	47.25	ksi
Thickness	0.0358	in
Total Height	1.54	in
Radius	0.2179	in
θ	72.5	degrees
θ	1.265363708	radian
Curve I'x	0.000592	in^3

Effective Width Top Flange		
w	3.1644	
b	1.667057613	
λ	1.644211016	1.497342
ρ	0.526816336	0.748671
f	35.82056497	
k	4	-
E	29000	ksi
μ	0.28	-
t	0.0358	in
Fcr	13.25004411	ksi

Tension Controlled							
			y bar	0.781893	in		
			fc	35.82056			
			ft	47.25			
			slope	0.021828			
Element	L (in)	y from top (in.)	Quantity	ΣL	ΣLy	$ΣLy^2$	
Lip	0.472376	1.5221	1	0.472376	0.719004	1.094396	
T, Corners	0.043883	0.0878	12	0.526592	0.046235	0.004059	
B, Corners	0.043883	1.4522	13	0.570474	0.828443	1.203065	
Top Flg.	1.667058	0.0179	6	10.00235	0.179042	0.003205	
Web, b1	0	0	12	0	0	0	
Web, b2	0	0	12	0	0	0	
lip up	0.455815	1.15734086	1	0.455815	0.527533	0.610536	
Web, Ten	0	0	12	0	0	0	
Web	1.1875	0.77	12	14.25	10.9725	8.448825	
Bot. Flg.	1.6354	1.5221	6	9.8124	14.93545	22.73325	
				36.09	28.20821	34.09734	
0.781607							
0.000285							

Comp Controlled		
y bar	0.781893	in
fc	47.25	
ft	45.81263	
slope	0.016548	

Effective Width Web		
w	1.1875	in
be	1.1875	
λ	0.616989711	
ρ	1.042853751	
f1	35.81695679	
f2	47.24639182	
k	4	-
E	29000	ksi
μ	0.28	-
t	0.0358	in
Fcr	94.08769718	ksi
ψ	1.319106816	
b1	0.274941105	
b2	0.59375	
w in comp	0.646515514	
Check	0.868691105	

Effective Width Bottom Flange		
w	1.6354	in

Effective Width Corners		
w	0.043882639	in

Effective Width Unstiff. Lip			0.079824
w	0.5522	in	
b	0.472376401		
λ	0.875101338		
ρ	0.855444406		
f	35.82056497		
k	0.43	-	
E	29000	ksi	
μ	0.28	-	
t	0.0358	in	
Fcr	46.77520886	ksi	

Effective Width Unstiff. Lip			0.044185
w	0.5	in	
b	0.455815		
λ	0.792377		
ρ	0.91163		
f	35.82056		
k	0.43	-	
E	29000	ksi	
μ	0.28	-	
t	0.0358	in	
Fcr	57.05169	ksi	

Figure A6: 20 Gage Positive EWM Example Calculation.

Deck	1.5B	pos bend
Gage	22	GA
Yield	44.5	ksi
Thickness	0.0295	in
Total Height	1.54	in
Radius	0.2179	in
θ	72.5	degrees
θ	1.265363708	radian
Curve I'x	0.000592	in^3

Effective Width Top Flange		
w	3.1644	
b	1.47004269	
λ	1.903846842	1.694357
ρ	0.464556532	0.847179
f	32.61063973	
k	4	-
E	29000	ksi
μ	0.28	-
t	0.0295	in
Fcr	8.996949914	ksi

Tension Controlled							
			y bar	0.807177	in		
			fc	32.61064			
			ft	44.5			
			slope	0.024752			
Element	L (in)	y from top (in.)	Quantity	ΣL	ΣLy	$ΣLy^2$	
Lip	0.42664	1.52525	1	0.42664	0.650733	0.99253	
T, Corners	0.043883	0.0878	12	0.526592	0.046235	0.004059	
B, Corners	0.043883	1.4522	13	0.570474	0.828443	1.203065	
Top Flg.	1.470043	0.01475	6	8.820256	0.130099	0.001919	
Web, b1	0	0	12	0	0	0	
Web, b2	0	0	12	0	0	0	
lip up	0.414288	1.177143488	1	0.414288	0.487676	0.574064	
Web, Ten	0	0	12	0	0	0	
Web	1.1875	0.77	12	14.25	10.9725	8.448825	
Bot. Flg.	1.6354	1.52525	6	9.8124	14.96636	22.82745	
				34.82065	28.08205	34.05191	
0.806477							
0.0007							

Comp Controlled		
y bar	0.807177	in
fc	44.5	
ft	40.40087	
slope	0.018139	

Effective Width Web		
w	1.1875	in
be	1.150339688	
λ	0.714409143	
ρ	0.968707106	
f1	32.60654823	
f2	44.4959085	
k	4	-
E	29000	ksi
μ	0.28	-
t	0.0295	in
Fcr	63.88675328	ksi
ψ	1.364631061	
b1	0.263559433	
b2	0.575169844	
w in comp	0.673026347	
Check	0.838729277	

Effective Width Bottom Flange		
w	1.6354	in

Effective Width Corners		
w	0.043882639	in

Effective Width Unstiff. Lip			
w	0.5522	in	0.12556
b	0.426639988		
λ	1.013287773		
ρ	0.772618595		
f	32.61063973		
k	0.43	-	
E	29000	ksi	
μ	0.28	-	
t	0.0295	in	
Fcr	31.76096682	ksi	

Effective Width Unstiff. Lip			
w	0.5	in	0.085712
b	0.414288		
λ	0.917501		
ρ	0.828575		
f	32.61064		
k	0.43	-	
E	29000	ksi	
μ	0.28	-	
t	0.0295	in	
Fcr	38.73883	ksi	

Figure A7: 22 Gage Positive EWM Example Calculation.

Deck	1.5B	neg bend
Gage	16	GA
Yield	44.7	ksi
Thickness	0.0598	in
Total Height	1.54	in
Radius	0.2179	in
θ	72.5	degrees
θ	1.265363708	radian
Curve I'x	0.000592	in^3

Effective Width Top Flange		
w	1.6354	
b	1.6354	
λ	0.549196292	0
ρ	1.091439688	0
f	41.74876149	
k	4	-
E	29000	ksi
μ	0.28	-
t	0.0598	in
Fcr	138.4166722	ksi

Tension Controlled								Tension Controlled				Comp Controlled		
								y bar	0.606023	in		y bar	0.606023	in
								fc	41.74876			fc	44.7	
								ft	44.7			ft	68.8897	
								slope	0.014516			slope	0.013558	
Element	L (in)	y from top (in.)	y for neg	Quantity	ΣL	ΣLy	ΣLy^2							
Lip	0.5522	1.5101	0.0299	1	0.5522	0.016511	1.259238							
T, Corners	0.043883	0.0878	1.4522	12	0.526592	0.764716	0.004059							
B, Corners	0.043883	1.4522	0.0878	13	0.570474	0.050088	1.203065							
Top Flg.	1.6354	0.0299	1.5101	6	9.8124	14.81771	0.008772							
Web, b1	0	0	1.54	12	0	0	0							
Web, b2	0	0	1.54	12	0	0	0							
lip up	0.5	1.136270762	0.403729	1	0.5	0.201865	0.645556							
Web, Ten	0	0	1.54	12	0	0	0							
Web	1.1875	0.77	0.77	12	14.25	10.9725	8.448825							
Bot. Flg.	3.1644	1.5101	0.0299	6	18.9864	0.567693	43.29662							
					45.19807	27.39108	54.86614							

0.606023
0

Effective Width Web		
w	1.1875	in
be	1.1875	
λ	0.398772077	
ρ	1.124217147	
f1	41.746362	
f2	44.69760051	
k	4	-
E	29000	ksi
μ	0.28	-
t	0.0598	in
Fcr	262.5240852	ksi
ψ	1.070694508	
b1	0.291719263	
b2	0.59375	
w in comp	0.462111146	
Check	0.885469263	
Effective Width Bottom Flange		
w	3.1644	in

Effective Width Corners		
w	0.043882639	in

Effective Width Unstiff. Lip			
w	0.5522	in	0
b	0.5522		
λ	0.565582252		
ρ	1.080338578		
f	41.74876149		
k	0.43	-	
E	29000	ksi	
μ	0.28	-	
t	0.0598	in	
Fcr	130.5124824	ksi	

Effective Width Unstiff. Lip			
w	0.5	in	0
b	0.5		
λ	0.512117		
ρ	1.113829		
f	41.74876		
k	0.43	-	
E	29000	ksi	
μ	0.28	-	
t	0.0598	in	
Fcr	159.186	ksi	

Figure A8: 16 Gage Negative EWM Example Calculation.

Deck	1.5B	neg bend
Gage	18	GA
Yield	43.45	ksi
Thickness	0.0474	in
Total Height	1.54	in
Radius	0.2179	in
θ	72.5	degrees
θ	1.265363708	radian
Curve I'x	0.000592	in^3

Effective Width Top Flange		
w	1.6354	
b	1.62174408	
λ	0.684142107	0.013656
ρ	0.991649798	0.006828
f	40.70383796	
k	4	-
E	29000	ksi
μ	0.28	-
t	0.0474	in
Fcr	86.96464311	ksi

Tension Controlled			Tension Controlled					Comp Controlled		
			y bar	0.603203	in			y bar	0.603203	in
			fc	40.70384				fc	43.45	
			ft	43.45				ft	67.47952	
			slope	0.014819				slope	0.013883	
Element	L (in)	y from top (in.)	y for neg	Quantity	ΣL	ΣLy	ΣLy^2			
Lip	0.539026	1.5163	0.0237	1	0.539026	0.012775	1.239311			
T, Corners	0.043883	0.0878	1.4522	12	0.526592	0.764716	0.004059			
B, Corners	0.043883	1.4522	0.0878	13	0.570474	0.050088	1.203065			
Top Flg.	1.621744	0.0237	1.5163	6	9.730464	14.7543	0.005466			
Web, b1	0	0	1.54	12	0	0	0			
Web, b2	0	0	1.54	12	0	0	0			
lip up	0.5	1.136270762	0.403729	1	0.5	0.201865	0.645556			
Web, Ten	0	0	1.54	12	0	0	0			
Web	1.1875	0.77	0.77	12	14.25	10.9725	8.448825			
Bot. Flg.	3.1644	1.5163	0.0237	6	18.9864	0.449978	43.65288			
					45.10296	27.20622	55.19916			

0.603203
1.24E-07

Effective Width Web		
w	1.1875	in
be	1.1875	
λ	0.49675572	
ρ	1.12152989	
f1	40.70138833	
f2	43.44755037	
k	4	-
E	29000	ksi
μ	0.28	-
t	0.0474	in
Fcr	164.9390426	ksi
ψ	1.067470967	
b1	0.291950455	
b2	0.59375	
w in comp	0.459153849	
Check	0.885700455	
Effective Width Bottom Flange		
w	3.1644	in

Effective Width Corners		
w	0.043882639	in

Effective Width Unstiff. Lip				Effective Width Unstiff. Lip			
w	0.5522	in	0.013174	w	0.5	in	0
b	0.53902623			b	0.5		
λ	0.704554345			λ	0.637952		
ρ	0.976143119			ρ	1.026952		
f	40.70383796			f	40.70384		
k	0.43	-		k	0.43	-	
E	29000	ksi		E	29000	ksi	
μ	0.28	-		μ	0.28	-	
t	0.0474	in		t	0.0474	in	
Fcr	81.9985864	ksi		Fcr	100.0136	ksi	

Figure A9: 18 Gage Negative EWM Example Calculation.

Deck	1.5B	neg bend		Tension Controlled			Tension Controlled					Comp Controlled		
Gage	20	GA					y bar	0.563185	in			y bar	0.563185	in
Yield	47.25	ksi					fc	46.15451				fc	47.25	
Thickness	0.0358	in					ft	47.25				ft	81.95266	
Total Height	1.54	in					slope	0.012202				slope	0.011919	
Radius	0.2179	in		Element	L (in)	y from top (in.)	y for neg	Quantity	ΣL	ΣLy	ΣLy^2			
θ	72.5	degrees		Lip	0.432783	1.5221	0.0179	1	0.432783	0.007747	1.002666			
θ	1.265363708	radian		T, Corners	0.043883	0.0878	1.4522	12	0.526592	0.764716	0.004059			
Curve I'x	0.000592	in^3		B, Corners	0.043883	1.4522	0.0878	13	0.570474	0.050088	1.203065			
				Top Flg.	1.308772	0.0179	1.5221	6	7.852631	11.95249	0.002516			
Effective Width Top Flange				Web, b1	0	0	1.54	12	0	0	0			
w	1.6354			Web, b2	0	0	1.54	12	0	0	0			
b	1.308771855			lip up	0.419929	1.174453093	0.365547	1	0.419929	0.153504	0.579225			
λ	0.964563946	0.326628		Web, Ten	0	0	1.54	12	0	0	0			
ρ	0.800276296	0.163314		Web	1.1875	0.77	0.77	12	14.25	10.9725	8.448825			
f	46.15450929			Bot. Flg.	3.1644	1.5221	0.0179	6	18.9864	0.339857	43.98747			
k	4	-							43.03881	24.2409	55.22783			
E	29000	ksi		0.563234										
μ	0.28	-		-4.9E-05										
t	0.0358	in												
Fcr	49.60804233	ksi												

Effective Width Web			
w	1.1875	in	
be	1.1875		
λ	0.282304064		
ρ	0.78177561		
f1	46.15249227		
f2	47.24798298		
k	24.62	-	24.62393
E	29000	ksi	
μ	0.28	-	
t	0.0358	in	
Fcr	579.1097761	ksi	
ψ	1.023736328		
b1	0.295123712		
b2	0.59375		
w in comp	0.417193999		
Check	0.888873712		
Effective Width Bottom Flange			
w	3.1644	in	
Effective Width Corners			
w	0.043882639	in	

Effective Width Unstiff. Lip				Effective Width Unstiff. Lip			
w	0.5522	in	0.119417	w	0.5	in	0.080071
b	0.432782922			b	0.419929		
λ	0.993342921			λ	0.899441		
ρ	0.783743067			ρ	0.839859		
f	46.15450929			f	46.15451		
k	0.43	-		k	0.43	-	
E	29000	ksi		E	29000	ksi	
μ	0.28	-		μ	0.28	-	
t	0.0358	in		t	0.0358	in	
Fcr	46.77520886	ksi		Fcr	57.05169	ksi	

Figure A10: 20 Gage Negative EWM Example Calculation.

Deck	1.5B	neg bend
Gage	22	GA
Yield	44.5	ksi
Thickness	0.0295	in
Total Height	1.54	in
Radius	0.2179	in
θ	72.5	degrees
θ	1.265363708	radian
Curve I'x	0.000592	in^3

Effective Width Top Flange		
w	1.6354	
b	1.151064906	
λ	1.148652806	0.484335
ρ	0.703843039	0.242168
f	44.44343556	
k	4	-
E	29000	ksi
μ	0.28	-
t	0.0295	in
Fcr	33.68449708	ksi

Tension Controlled							
			y bar	0.541271	in		
			fc	44.44344			
			ft	44.5			
			slope	0.012179			
Element	L (in)	y from top (in.)	y for neg	Quantity	ΣL	ΣLy	$ΣLy^2$
Lip	0.379992	1.52525	0.01475	1	0.379992	0.005605	0.884009
T, Corners	0.043883	0.0878	1.4522	12	0.526592	0.764716	0.004059
B, Corners	0.043883	1.4522	0.0878	13	0.570474	0.050088	1.203065
Top Flg.	1.151065	0.01475	1.52525	6	6.906389	10.53397	0.001503
Web, b1	0	0	1.54	12	0	0	0
Web, b2	0	0	1.54	12	0	0	0
lip up	0.370928	1.19781962	0.34218	1	0.370928	0.126924	0.532198
Web, Ten	0	0	1.54	12	0	0	0
Web	1.1875	0.77	0.77	12	14.25	10.9725	8.448825
Bot. Flg.	3.1644	1.52525	0.01475	6	18.9864	0.280049	44.16972
					41.99078	22.73385	55.24338

0.541401
-0.00013

Tension Controlled		
y bar	0.541271	in
fc	44.44344	
ft	44.5	
slope	0.012179	

Comp Controlled		
y bar	0.541271	in
fc	44.5	
ft	82.10938	
slope	0.012163	

Effective Width Web		
w	1.1875	in
be	1.048227236	
λ	0.834043239	
ρ	0.882717672	
f1	44.44142239	
f2	44.49798683	
k	4	-
E	29000	ksi
μ	0.28	-
t	0.0295	in
Fcr	63.88675328	ksi
ψ	1.001272786	
b1	0.26197345	
b2	0.524113618	
w in comp	0.39421666	
Check	0.786087068	
Effective Width Bottom Flange		
w	3.1644	in

Effective Width Corners		
w	0.043882639	in

Effective Width Unstiff. Lip			
w	0.5522	in	0.172208
b	0.379992164		
λ	1.182924304		
ρ	0.688142275		
f	44.44343556		
k	0.43	-	
E	29000	ksi	
μ	0.28	-	
t	0.0295	in	
Fcr	31.76096682	ksi	

Effective Width Unstiff. Lip			
w	0.5	in	0.129072
b	0.370928		
λ	1.071101		
ρ	0.741857		
f	44.44344		
k	0.43	-	
E	29000	ksi	
μ	0.28	-	
t	0.0295	in	
Fcr	38.73883	ksi	

Figure A11: 22 Gage Negative EWM Example Calculation.

From AutoCAD				
Gage	Orientation	Se	Fy	Mn
22	pos	0.4614	44.5	20.5323
20	pos	0.5853	47.25	27.65543
18	pos	0.8471	43.45	36.8065
16	pos	1.1271	44.7	50.38137
22	neg	0.5384	44.5	23.9588
20	neg	0.6834	47.25	32.29065
18	neg	0.9788	43.45	42.52886
16	neg	1.2396	44.7	55.41012

Figure A12: EWM Effective Section Modulus.

A.2 Direct Strength Method

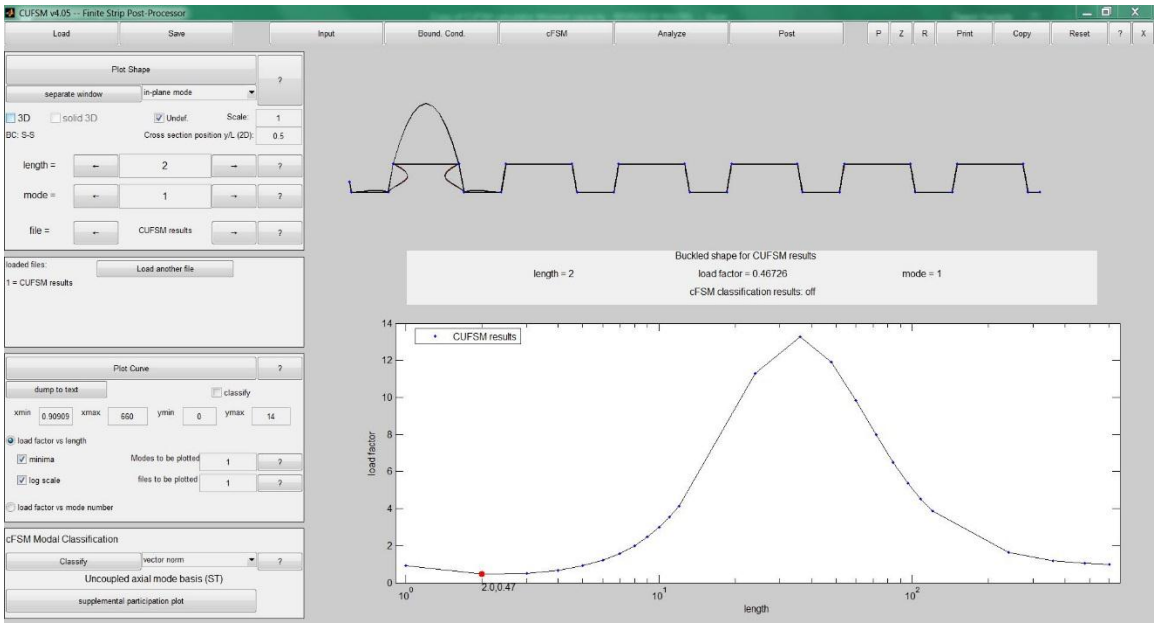

Figure A13: 22 Gage Positive DSM Output.

Section Prop.		
Sn	0.57	in^3
Fy	44.5	ksi
My	25.365	k-in

Sn used	0.19	
Snp	0.19	
Snn	0.19	
Fy flute	47.1	
Fy flange	41.9	

Local		
Mcrl/My	0.47	-
Mcrl	11.9216	k-in

Distortional		
Mcrd/My	11.2779	-
Mcrd	286.064	k-in

LTB		
Mcrlt/My	11.2779	-
Mcrle	286.064	k-in

Mne		
Mne	25.365	k-in

Local Buck. 1.3.2		
λ1	1.45865	-
Limit	0.776	-
Mnl	16.6734	k-in

Dist. Buck 1.3.3		
λd	0.29777	-
Limit	0.673	-
Mnd	25.365	k-in

Nominal Moment		
Mn	16.6734	k-in

My	
Positive	25.365
Negative	25.365

Figure A14: 22 Gage Positive DSM Example Calculation.

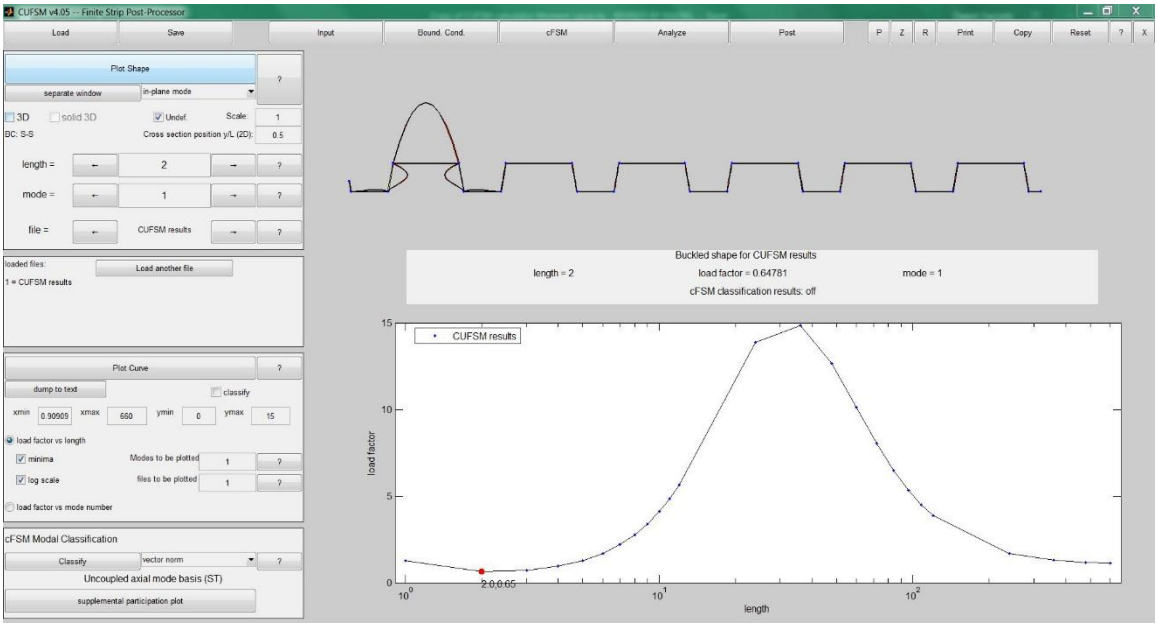

Figure A15: 20 Gage Positive DSM Output.

Section Prop.		
Sn	0.72	in^3
Fy	47.25	ksi
My	34.02	k-in

Sn used	0.24	
Snp	0.23	
Snn	0.24	
Fy flute	48.6	
Fy flange	45.9	

Local		
Mcrl/My	0.65	-
Mcrl	22.113	k-in

Distortional		
Mcrd/My	13.8554	-
Mcrd	471.361	k-in

LTB		
Mcrlt/My	13.8554	-
Mcrle	471.361	k-in

Mne		
Mne	34.02	k-in

Local Buck. 1.3.2		
λ1	1.24035	-
Limit	0.776	-
Mnl	25.0198	k-in

Dist. Buck 1.3.3		
λd	0.26865	-
Limit	0.673	-
Mnd	34.02	k-in

Nominal Moment		
Mn	25.0198	k-in

My	
Positive	32.6025
Negative	34.02

Figure A16: 20 Gage Positive DSM Example Calculation.

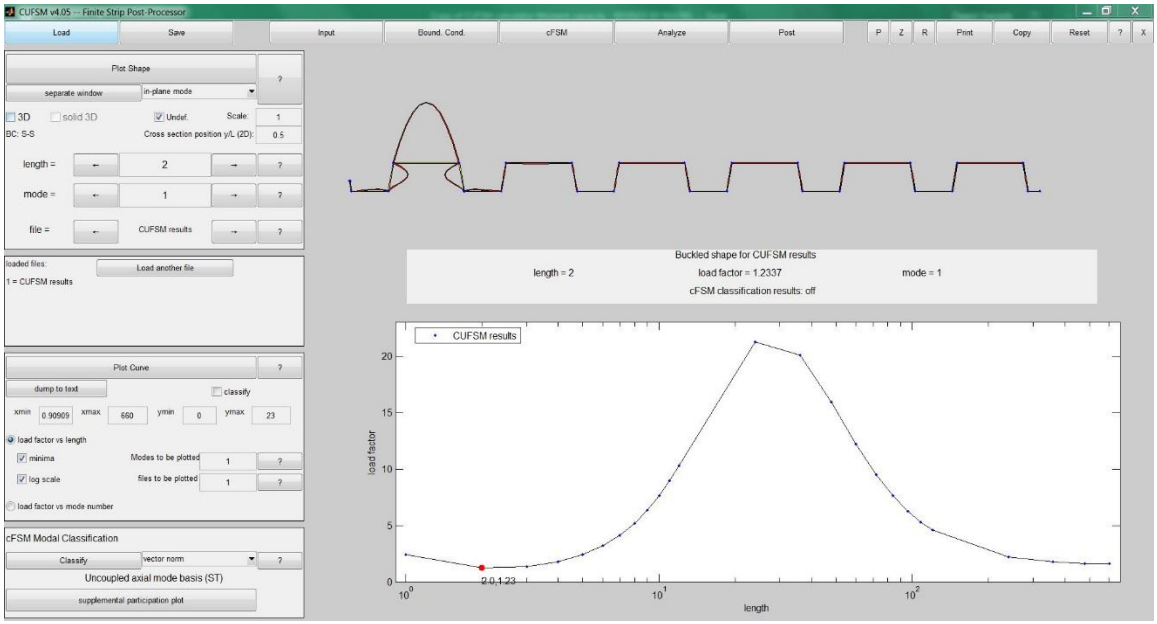

Figure A17: 18 Gage Positive DSM Output.

Section Prop.		
Sn	0.96	in^3
Fy	43.45	ksi
My	41.712	k-in

Sn used	0.32	
Snp	0.32	
Snn	0.32	
Fy flute	42.6	
Fy flange	44.3	

Local		
Mcrl/My	1.23	-
Mcrl	51.3058	k-in

Distortional		
Mcrd/My	21.2747	-
Mcrd	887.41	k-in

LTB		
Mcrlt/My	21.2747	-
Mcrle	887.41	k-in

Mne		
Mne	41.712	k-in

Local Buck. 1.3.2		
λ1	0.90167	-
Limit	0.776	-
Mnl	37.9293	k-in

Dist. Buck 1.3.3		
λd	0.2168	-
Limit	0.673	-
Mnd	41.712	k-in

Nominal Moment		
Mn	37.9293	k-in

My	
Positive	41.712
Negative	41.712

Figure A18: 18 Gage Positive DSM Example Calculation.

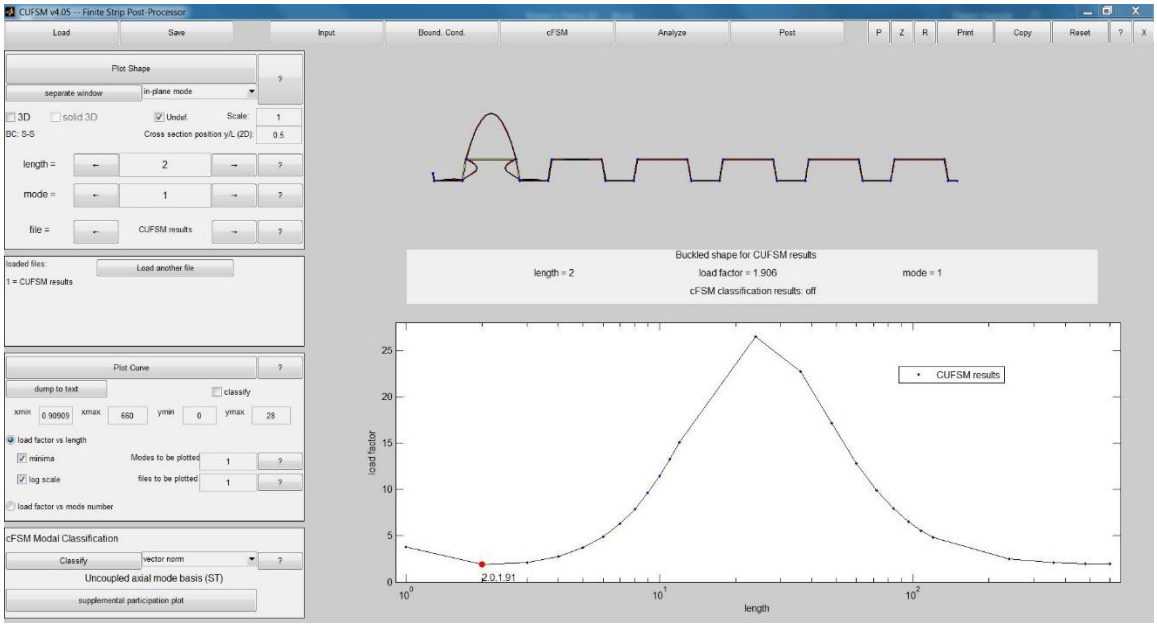

Figure A19: 16 Gage Positive DSM Output.

Section Prop.		
Sn	1.23	in^3
Fy	44.7	ksi
My	54.981	k-in

Sn used	0.41	
Snp	0.41	
Snn	0.41	
Fy flute	44.9	
Fy flange	44.5	

My	
Positive	54.981
Negative	54.981

Local		
Mcrl/My	1.91	-
Mcrl	105.014	k-in

Distortional		
Mcrd/My	26.464	-
Mcrd	1455.02	k-in

LTB		
Mcrlt/My	26.464	-
Mcrle	1455.02	k-in

Mne		
Mne	54.981	k-in

Local Buck. 1.3.2		
λ1	0.72357	-
Limit	0.776	-
Mnl	54.981	k-in

Dist. Buck 1.3.3		
λd	0.19439	-
Limit	0.673	-
Mnd	54.981	k-in

Nominal Moment		
Mn	54.981	k-in

Figure A20: 16 Gage Positive DSM Example Calculation.

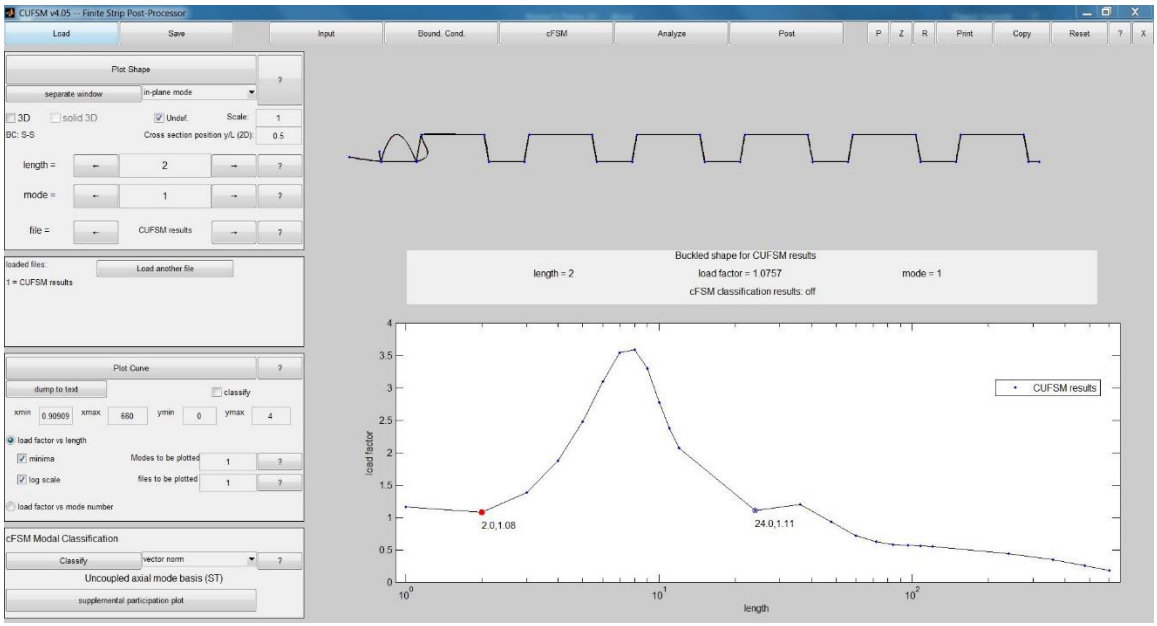

Figure A21: 22 Gage Negative DSM Output.

Section Prop.		
Sn	0.57	in^3
Fy	44.5	ksi
My	25.365	k-in

Sn used	0.19	
Snp	0.19	
Snn	0.19	
Fy flute	47.1	
Fy flange	41.9	

Local		
Mcrl/My	1.08	-
Mcrl	27.3942	k-in

Distortional		
Mcrd/My	1.11	-
Mcrd	28.1552	k-in

LTB		
Mcrlt/My	10	-
Mcrle	253.65	k-in

Mne		
Mne	25.365	k-in

Local Buck. 1.3.2		
λ1	0.96225	-
Limit	0.776	-
Mnl	22.1116	k-in

Dist. Buck 1.3.3		
λd	0.94916	-
Limit	0.673	-
Mnd	20.5296	k-in

Nominal Moment		
Mn	20.5296	k-in

My	
Positive	25.365
Negative	25.365

Figure A22: 22 Gage Negative DSM Example Calculation.

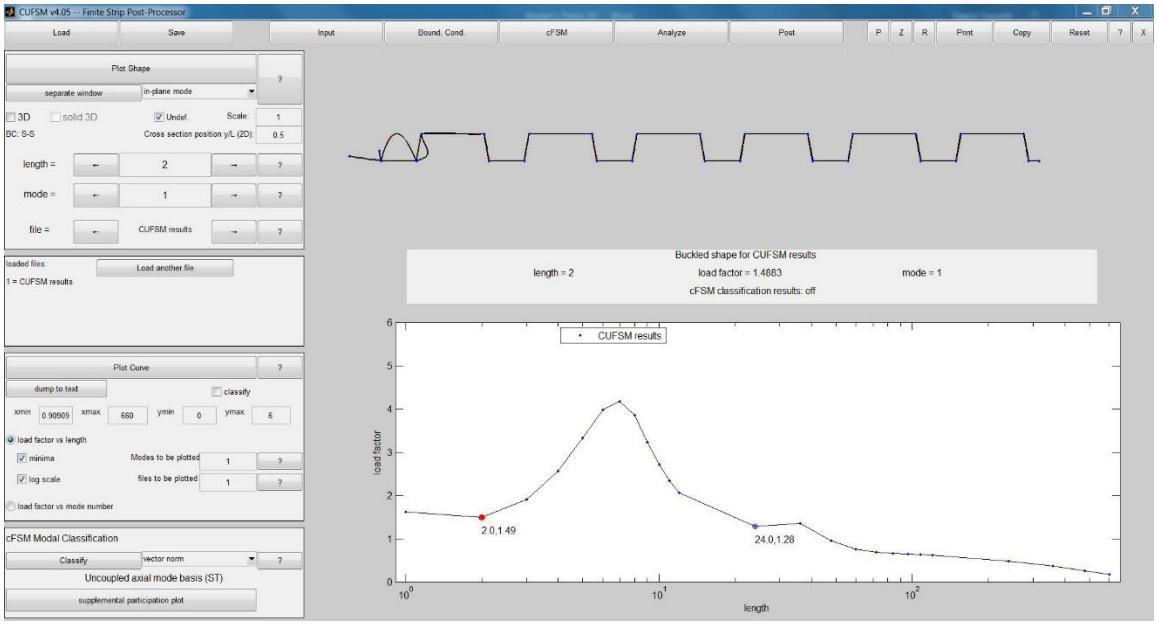

Figure A23: 20 Gage Negative DSM Output.

Section Prop.		
Sn	0.72	in^3
Fy	47.25	ksi
My	34.02	k-in

Sn used	0.24	
Snp	0.23	
Snn	0.24	
Fy flute	48.6	
Fy flange	45.9	

Local		
Mcrl/My	1.49	-
Mcrl	50.6898	k-in

Distortional		
Mcrd/My	1.28	-
Mcrd	43.5456	k-in

LTB		
Mcrlt/My	10	-
Mcrle	340.2	k-in

Mne		
Mne	34.02	k-in

Local Buck. 1.3.2		
λ1	0.81923	-
Limit	0.776	-
Mnl	32.8827	k-in

Dist. Buck 1.3.3		
λd	0.88388	-
Limit	0.673	-
Mnd	28.9092	k-in

Nominal Moment		
Mn	28.9092	k-in

My	
Positive	32.6025
Negative	34.02

Figure A24: 20 Gage Negative DSM Example Calculation.

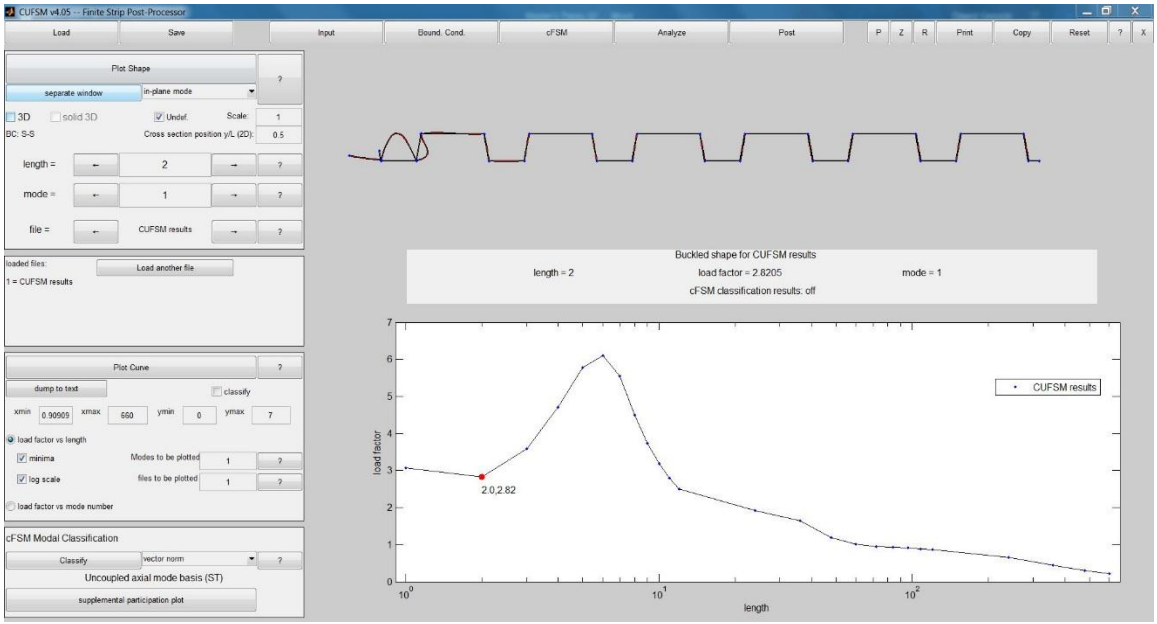

Figure A25: 18 Gage Negative DSM Output.

Section Prop.		
Sn	0.96	in^3
Fy	43.45	ksi
My	41.712	k-in

Sn used	0.32	
Snp	0.32	
Snn	0.32	
Fy flute	42.6	
Fy flange	44.3	

Local		
Mcrl/My	2.82	-
Mcrl	117.628	k-in

Distortional		
Mcrd/My	1.9266	-
Mcrd	80.3623	k-in

LTB		
Mcrlt/My	10	-
Mcrle	417.12	k-in

Mne		
Mne	41.712	k-in

Local Buck. 1.3.2		
λ1	0.59549	-
Limit	0.776	-
Mnl	41.712	k-in

Dist. Buck 1.3.3		
λd	0.72045	-
Limit	0.673	-
Mnd	40.2174	k-in

Nominal Moment		
Mn	40.2174	k-in

My	
Positive	41.712
Negative	41.712

Figure A26: 18 Gage Negative DSM Example Calculation.

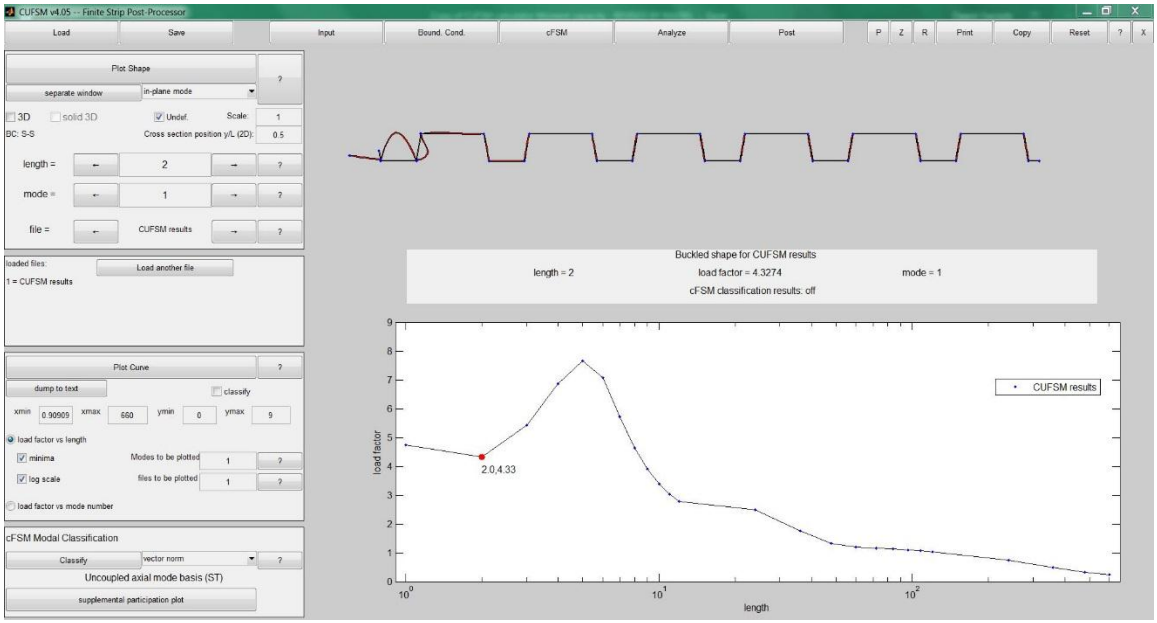

Figure A27: 16 Gage Negative DSM Output.

Section Prop.		
Sn	1.23	in^3
Fy	44.7	ksi
My	54.981	k-in

Sn used	0.41	
Snp	0.41	
Snn	0.41	
Fy flute	44.9	
Fy flange	44.5	

Local		
Mcrl/My	4.33	-
Mcrl	238.068	k-in

Distortional		
Mcrd/My	2.4852	-
Mcrd	136.639	k-in

LTB		
Mcrlt/My	10	-
Mcrle	549.81	k-in

Mne		
Mne	54.981	k-in

Local Buck. 1.3.2		
λ1	0.48057	-
Limit	0.776	-
Mnl	54.981	k-in

Dist. Buck 1.3.3		
λd	0.63434	-
Limit	0.673	-
Mnd	54.981	k-in

Nominal Moment		
Mn	54.981	k-in

My	
Positive	54.981
Negative	54.981

Figure A28: 16 Gage Negative DSM Example Calculation.

Appendix B: Initial Project Synthesis Documents

I have attached a spreadsheet that shows 16 tests Perhaps we could delete the 20 and 18 gage and only test the limits at 22 and 16 gage, and do multiple tests. I am suggesting also testing floor deck in order to capture the effect of flange stiffeners ... adding flange stiffeners back to WR roof deck may be a possibility, but FM would have to be brought on board.
The tested strength would have to be compared to the predicted strength by Direct Strength and Effective Width at the actual Fy of the deck that is tested. You could get the mill test reports on the coils used, but it would be good to pull standard ASTM coupons to verify.
Let me know what you think. As soon as the SDI sees the proposal, we can get a check over to MSOE. We would need to know how to make the check out, etc.

MSOE Testing

For the testing, the Excel Spreadsheet shows the following:

1. 1.5WR roof deck in 22, 20, 18, 16 gage, which is the range of deck thickness that are used. WR deck produced currently does not have a flange stiffener. In the past, WR deck did have a flange stiffener, however around 25-30 years ago, at the insistence of Factory Mutual, the industry removed the flange stiffener because it was felt that the stiffener created a "channel" that held the asphalt that was used to adhere the insulation boards to the deck, and weakened the bond. Currently, insulation board is attached with screws, so potentially the flange stiffener could be reintroduced.
2. 2C and 3C composite floor deck, which does have a flange stiffener; 22, 20, 18, and 16 gage. These tests would show if the presence of the flange stiffener does increase deck flexural strength to the extend that the DSM method predicts.
3. The table shows deck with a nominal yield of 50 ksi. This is pretty common for the deck that is currently produced, so it was used in the table to get a feel for what loads would be required.
4. The testing would be done with a single 36 inch wide deck panel, in 4 point loading. The spreadsheet is showing a 6 foot span and 18 inches between the center load points. The load could be applied as a single load, with a spreader bar.

$$M = P(L-S)/4$$

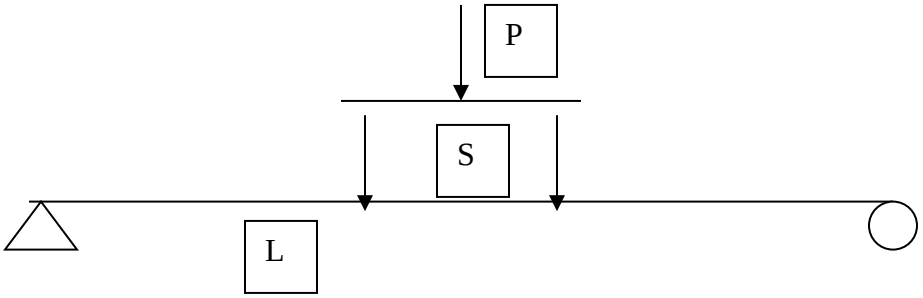

Figure B1: Proposed Testing Diagram.

Appendix C: Material Sources and Testing Documents

MAI METALLURGICAL ASSOCIATES, INC.

Test Report (Page 1 of 1)

MAI Report No:	217-1-177	**Date:**	March 23, 2017
Client:	Milwaukee School of Engineering	**Contact:**	Dr. Christopher Rabel
P.O. No:	Verbal	**Date Rec'd.:**	March 8, 2017
Description:	16, 18, 20, and 22 gage Corrugated Steel Sheets		
Specified Material:	ASTM A1008	**Actual Material:**	See Notes

Tensile Properties

Property	16 gage		18 gage		ASTM A1008, SS Grade 40
	Flange	Flute	Flange	Flute	
Test Bar Dimensions					
Width, inch	0.511	0.512	0.510	0.508	0.500
Thickness, inch	0.060	0.060	0.050	0.048	Mat'l Thickness
Gage Length, inches	2.0	2.0	2.0	2.0	2.0
Tensile Strength, psi	51,500	57,500	52,000	52,500	52,000 min.
Yield Strength, psi (1)	44,500	44,900	44,300	42,600	40,000 min.
Elongation, %	27	29	27	29	20 min.

Property	20 gage		22 gage		ASTM A1008, SS Grade 40
	Flange	Flute	Flange	Flute	
Test Bar Dimensions					
Width, inch	0.507	0.517	0.513	0.507	0.500
Thickness, inch	0.038	0.036	0.034	0.030	Mat'l Thickness
Gage Length, inches	2.0	2.0	2.0	2.0	2.0
Tensile Strength, psi	52,000	56,500	53,000	61,000	52,000 min.
Yield Strength, psi (1)	45,900	48,600	41,900	47,100	40,000 min.
Elongation, %	29	29	29	26	20 min.

(1): At 0.2% offset.

Notes: Standard flat tensile bars were machined from each of the submitted corrugated sheets. The tensile properties of all eight samples are in conformance with structural steel (SS) Grade 40 as included in ASTM A1008, " Standard Specification for Steel, Sheet, Cold-Rolled, Carbon, Structural, High-Strength Low-Alloy and High-Strength Low-Alloy with Improved Formability."

Respectfully submitted,

Thomas C. Tefelske

Thomas C. Tefelske
President

MAI ▪ 20900 Swenson Drive - Suite 800 ▪ Waukesha, WI 53186
Phone: 262-798-8098 ▪ 800-798-4966 ▪ FAX: 262-798-8099 ▪ e-mail: info@metassoc.com
www.metassoc.com

Figure C1: Material Testing Summary.

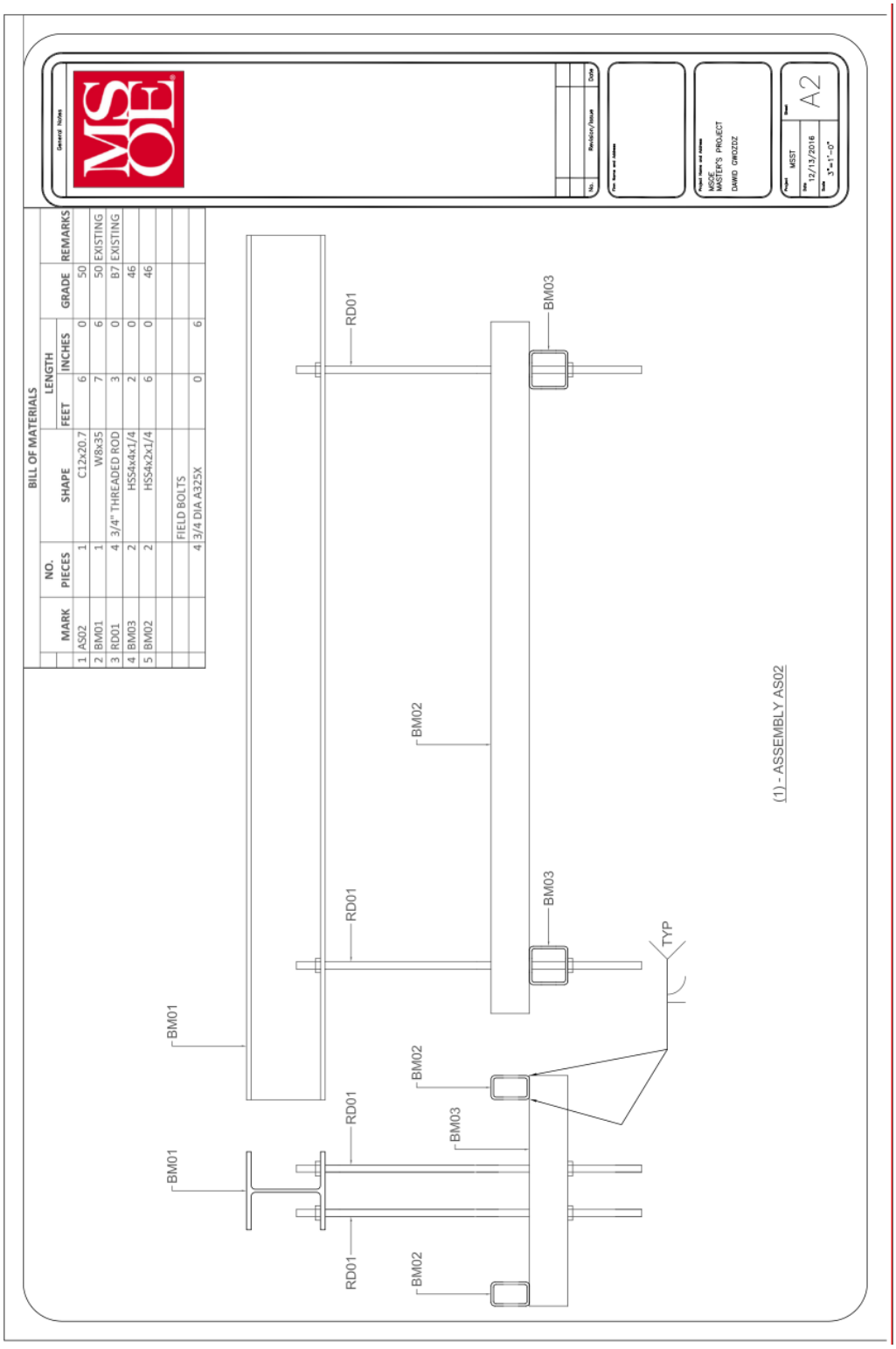

Figure C2: Test Frame Assembly Shop Drawing.

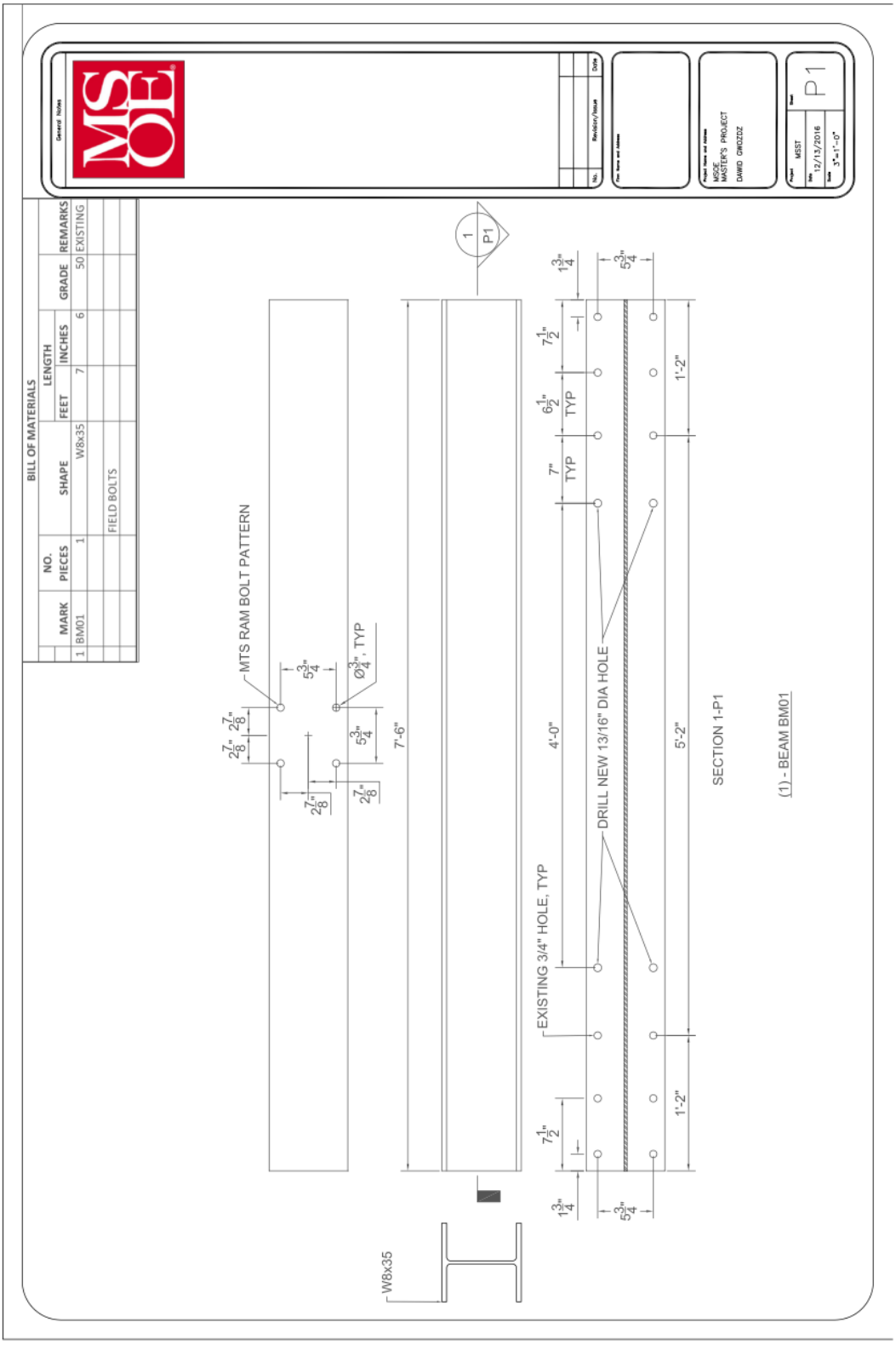

Figure C3: Cross Beam Shop Drawing.

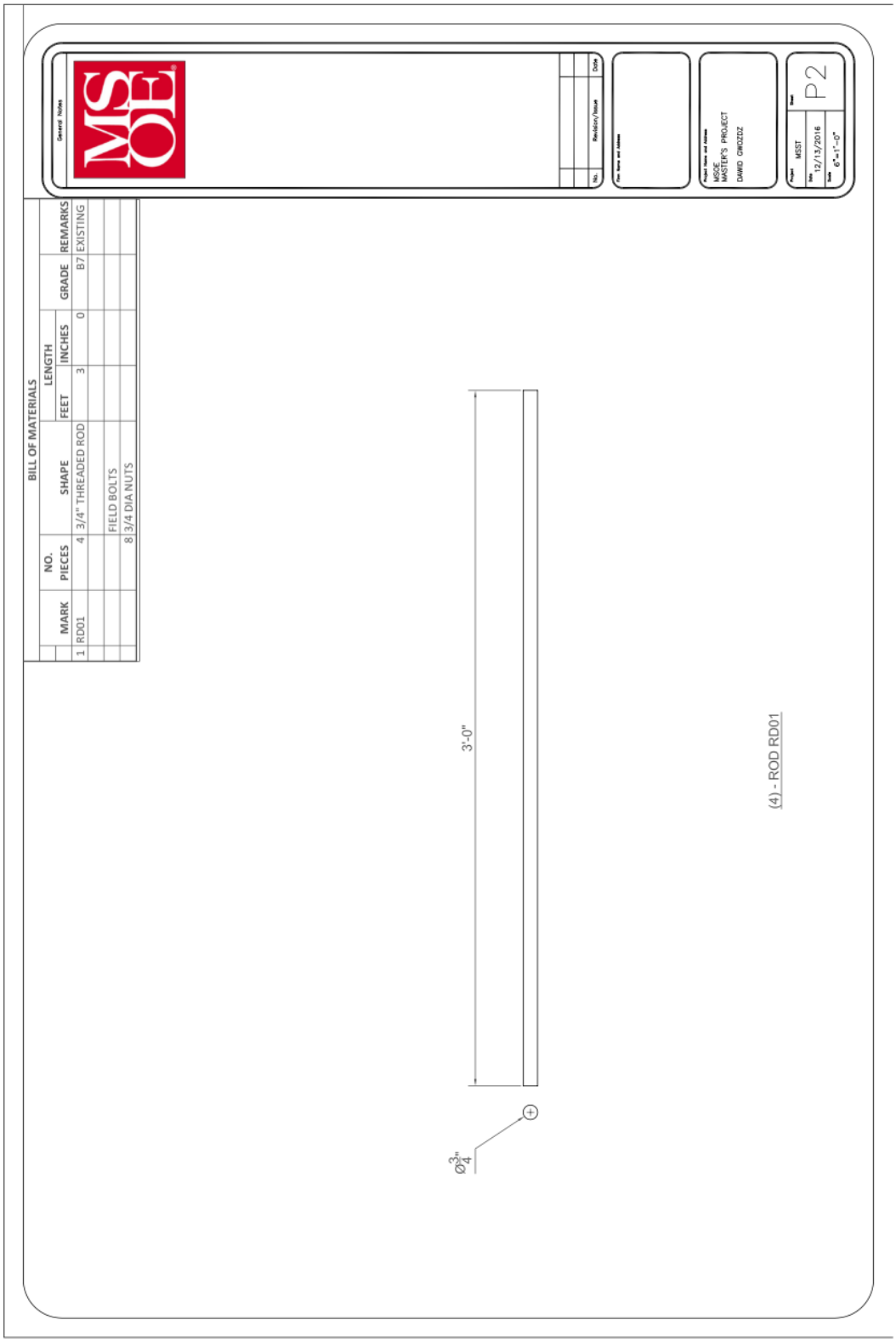

Figure C4: Threaded Rod Shop Drawing.

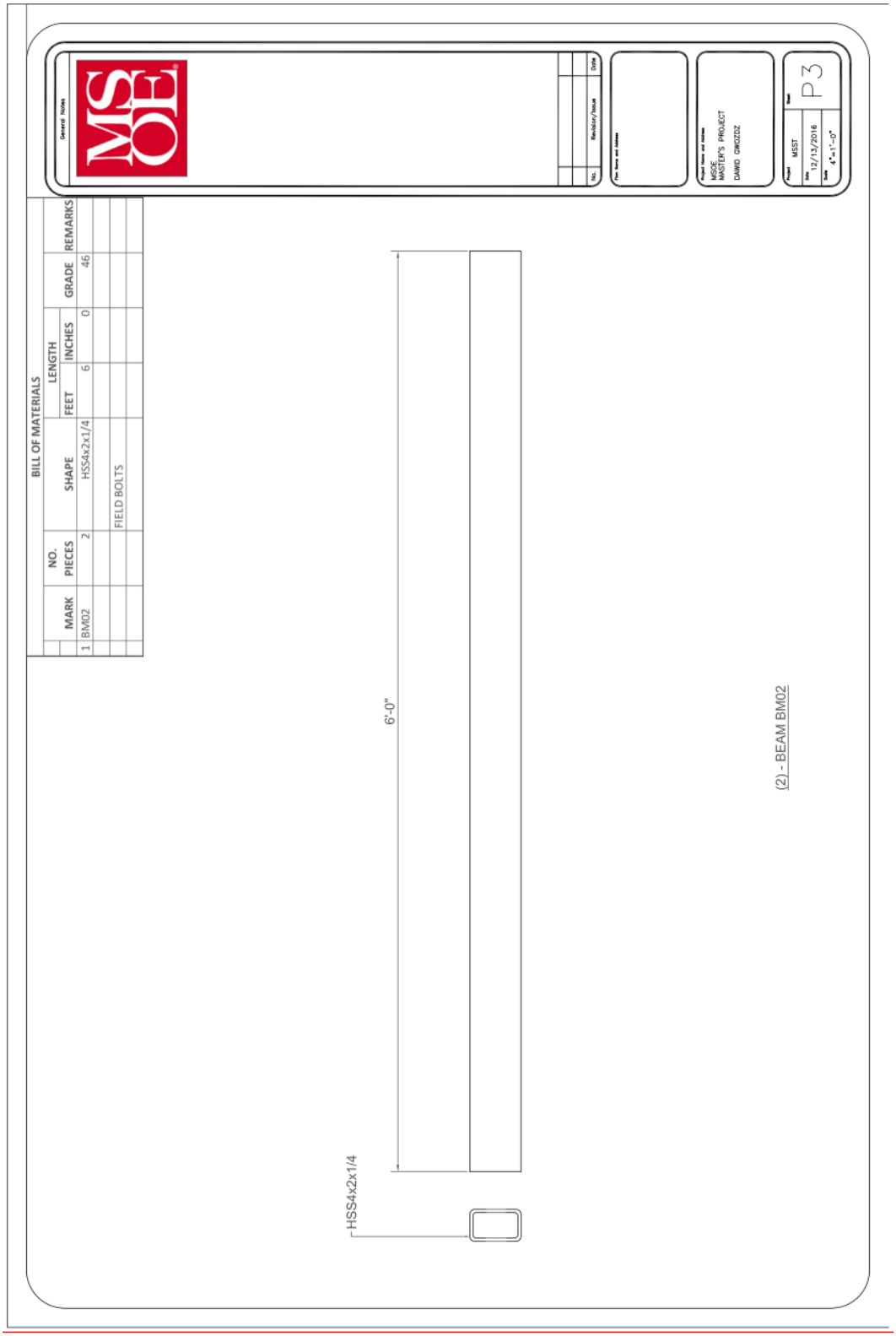

Figure C5: Line Load HSS Shop Drawing.

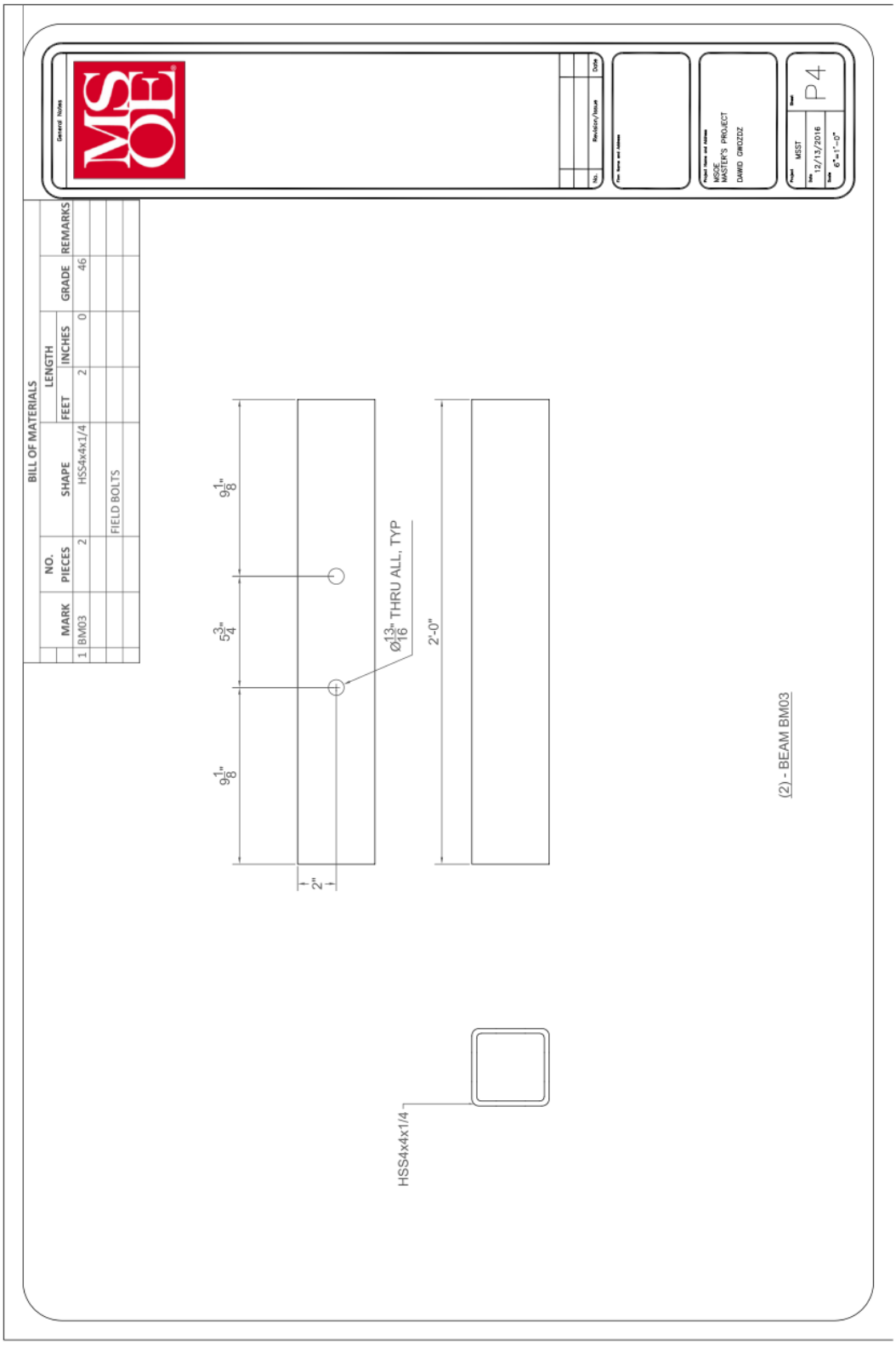

Figure C6: Girder HSS Shop Drawing.

Civil Engineering

Capstone Report Approval Form

Master of Science in Civil Engineering -- MSCVE

Milwaukee School of Engineering

This capstone report, entitled "Experimental and Numerical Comparison of Flexural Capacity of Light Gage Cold Formed Steel Roof Deck," submitted by the student Dawid M. Gwozdz, has been approved by the following committee:

Faculty Advisor: _____ Date: _____

Dr. Christopher Raebel

Faculty Member: _____ Date:_____

Dr. Richard DeVries

Faculty Member: _____ Date: _____

Dr. Hans-Peter Huttelmaier